

Supporting Information

**Secondary-Sphere Preorganization Enables
Nickel-Catalyzed Nitrile Hydroboration**

Medina Afandiyeva[†], Xijue Wu[†], William W. Brennessel, Abhishek A. Kadam, C. Rose Kennedy*

Department of Chemistry, University of Rochester

Rochester, New York 14627, United States

* c.r.kennedy@rochester.edu

Table of Contents for the Supporting Information

1.	Procedures, Materials, and Instrumentation	S4
1.1	General Considerations	S4
1.2	Materials	S4
1.3	Instrumentation	S4
1.4	Abbreviations	S5
2.	Ligand Synthesis	S6
3.	Catalytic Procedures and Product Characterization	S9
3.1	General Procedure for Nitrile Hydroboration	S9
3.2	Testing for Sensitivity to Air	S9
3.3	Product Characterization Data	S10
4.	Mechanistic Experiments	S60
4.1	Synthesis and Characterization of Nitrile Adducts 5a–c	S60
4.2	Experiments with Nickel Complex 5c and HBpin	S64
4.3	Synthesis and Characterization of Imine Adduct 8	S67
4.4	Experiments with Nickel Complex 8 and HBpin	S69
4.5	Evaluating Homogeneity	S73
4.6	Excluding Hidden Borane Generation	S74
5.	SC-XRD Data	S76
5.1	General Procedure for SC-XRD Data Collection	S76
5.2	SC-XRD Data for [K(18-crown-6)][(^h IMesPyO)Ni(PhCN)] (5a)	S78
5.3	SC-XRD Data for [K(18-crown-6)][(^h IMesPyO)Ni(1k)] (5b)	S83
5.4	SC-XRD Data for [K(18-crown-6)][(^h IMesPyO)Ni(CyCN)] (5c)	S86
5.5	SC-XRD Data for [(^h IMesPyO)Ni(CyHCN(Bpin) ₂)] (6)	S89

5.6 SC-XRD Data for [K(18-crown-6)][(^hIMesPyO)Ni(7)] (8)	S92
6. Computational Analyses	S95
6.1 Computational Methods	S95
6.2 Anionic Model	S96
6.3 Neutral Model	S99
7. References	S101

1. Procedures, Materials, and Instrumentation

1.1 General Considerations

All air- and moisture-sensitive techniques were carried out using standard Schlenk technique on a Schlenk line or a high-vacuum line¹ or in an M. Braun glovebox containing an atmosphere of N₂. The glovebox was equipped with vacuum feed-throughs, a cold well, and a freezer for storing samples at –30 °C. Colors are described in comparison to the complete list of Prismacolor colored pencils.² Column chromatography was performed on SiliaFlash P60 (230–400 mesh) silica gel from SiliCycle using standard glass columns. Thin-layer chromatography (TLC) was performed using aluminum-backed plates pre-coated with silica gel and a fluorescent indicator for visualization upon UV irradiation.

1.2 Materials

Reagents were purchased in reagent grade from commercial suppliers and used without further purification unless described otherwise. Bis(cyclooctadiene) nickel [Ni(cod)₂] was prepared according to a literature procedure³ or purchased from Strem and stored at –30 °C in the glovebox. 1-Arylimidazoles were prepared according to a reported literature procedure.^{4,5} Ligands **L1–L3** and nickel complexes thereof were prepared as reported previously.⁶ Solvents (acetonitrile, diethyl ether, *n*-pentane, tetrahydrofuran, and toluene) used for air- and moisture-sensitive manipulations were dried and deoxygenated by passage through an activated alumina column⁷ and stored over activated molecular sieves. Deuterated solvents used for NMR spectroscopy of air- and moisture-sensitive compounds were stirred over sodium (C₆D₆, THF-*d*₈) or calcium hydride (CD₃CN) and distilled prior to storage in the glovebox. 18-Crown-6 was recrystallized from acetonitrile at –30 °C before use.

1.3 Instrumentation and Software

Proton nuclear magnetic resonance (¹H NMR) spectra were recorded at 25 °C on Bruker 400 or 500 Avance I spectrometer operating at 400.13 or 500.20 MHz. Proton-decoupled ¹³C NMR spectra were recorded at 25 °C on Bruker 400 or 500 Avance I spectrometer operating at 100.25 or 125.78 MHz. All experiments were performed at the University of Rochester, Department of Chemistry, Nuclear Magnetic Resonance Facility. Chemical shifts are reported in parts per million downfield from tetramethylsilane (SiMe₄) and are referenced in ppm relative to the NMR solvent according to literature values:⁸ δ(¹H) = 7.16, δ(¹³C) = 128.1 for C₆D₆; δ(¹H) = 1.94, δ(¹³C) = 118.3 for CD₃CN; δ(¹H) = 1.72, 3.58, δ(¹³C) = 67.2, 25.3 for THF-*d*₈; δ(¹H) = 7.26, δ(¹³C) = 77.2 for CDCl₃; δ(¹H) = 3.31, δ(¹³C) = 49.0 for CD₃OD. ¹H NMR data for diamagnetic substances are

reported as follows: chemical shift, (multiplicity, coupling constant in Hz, integration) where s = singlet, d = doublet, t = triplet, q = quartet, m = multiplet, and br = broad. ^{13}C NMR data for diamagnetic substances are reported as a list of chemical shifts. NMR spectra were processed using the MestReNova software suite. Low resolution mass spectra (LRMS) were recorded using an LC (Agilent Technology 1260 Infinity II)-MS (Advion Expression CMS) system. Infrared (FT-IR, ATR) spectra were recorded on a Shimadzu IR Affinity Fourier Transform Infrared Spectrophotometer.

1.4 Abbreviations

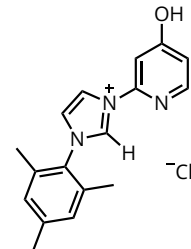
Ar = aryl; ATR = attenuated total reflectance; Bpin = pinacolboryl = 4,4,5,5-tetramethyl-1,3-dioxaboryl; cod = 1,5-cyclooctadiene; DFT = density functional theory; dmso = dimethylsulfoxide; ESI = electrospray ionization; FT-IR = Fourier transform infrared spectroscopy; $^{\text{h}}\text{IMesPyO}$ = 1-(2,4,6-trimethylphenyl)-3-(6-oxidopyridin-2-yl)-imidazol-2-ylidene); $^{\text{h}}\text{IEtPyO}$ = 1-(2,6-diethylphenyl)-3-(6-oxidopyridin-2-yl)-imidazol-2-ylidene; $^{\text{h}}\text{IPrPyO}$ = 1-(2,6-diisopropylphenyl)-3-(6-oxidopyridin-2-yl)-imidazol-2-ylidene; LRMS = low-resolution mass spectrometry; NHC = N-heterocyclic carbene; NMR = nuclear magnetic resonance spectroscopy; PTFE = poly(tetrafluoroethylene); Py = pyridine; SC-XRD = single-crystal X-ray diffraction; THF = tetrahydrofuran

2. Ligand Synthesis

Ligands **L1–L3** and nickel complexes thereof were prepared as reported previously.⁶ Ligand **L4** was prepared as reported previously.⁹ Ligands **L5** and **L6** were generated in situ as their potassium salts using KO^tBu and 18-crown-6. Imidazolium precursor **L5•HCl** was prepared through a procedure analogous to that reported previously.⁶

3-(4-hydroxypyridin-2-yl)-1-mesityl-1*H*-imidazol-3-ium chloride (**L5•HCl**)

To a 100 mL pressure tube equipped with a PTFE-coated stir bar, 1-arylimidazole (8.9 mmol, 1.0 equiv.) and 6-chloro-4-hydroxypyridine (8.9 mmol, 1.0 equiv.) were added. The pressure vessel was flushed with N₂ and quickly sealed with a Teflon cap. The reaction mixture was stirred vigorously at 160 °C. (Note: The pressure vessel should be fully immersed in silicone oil up to the neck of the vessel to make sure the starting materials do not condense on the walls). The reaction was stopped once the reaction mixture turned solid (typically 3 days). The reaction mixture was allowed to cool to room temperature, transferred to a 500 mL round-bottom flask using chloroform, and concentrated in vacuo to give brown-colored semi-solid material. The crude mixture was triturated overnight in dichloromethane to afford **L5•HCl** as a putty beige solid.



- ¹H NMR (500 MHz, CD₃OD) δ 8.61 (d, *J* = 2.1 Hz, 1H), 8.32 (d, *J* = 5.7 Hz, 1H), 7.94 (d, *J* = 2.0 Hz, 1H), 7.41 (d, *J* = 2.1 Hz, 1H), 7.17 (s, 2H), 7.00 (dd, *J* = 5.8, 2.0 Hz, 1H), 5.49 (s, 1H), 2.39 (s, 3H), 2.16 (s, 6H), 2.02 (s, 1H).
- ¹³C NMR (126 MHz, CD₃OD): δ 169.1, 151.6, 149.5, 142.8, 135.8, 132.5, 130.8, 130.3, 126.3, 121.5, 114.3, 103.1, 54.8, 21.1, 17.4.
- LRMS (ESI): Calculated for C₁₇H₁₈N₃O⁺ ([M-Cl]⁺): 280.1; found: m/z = 280.1

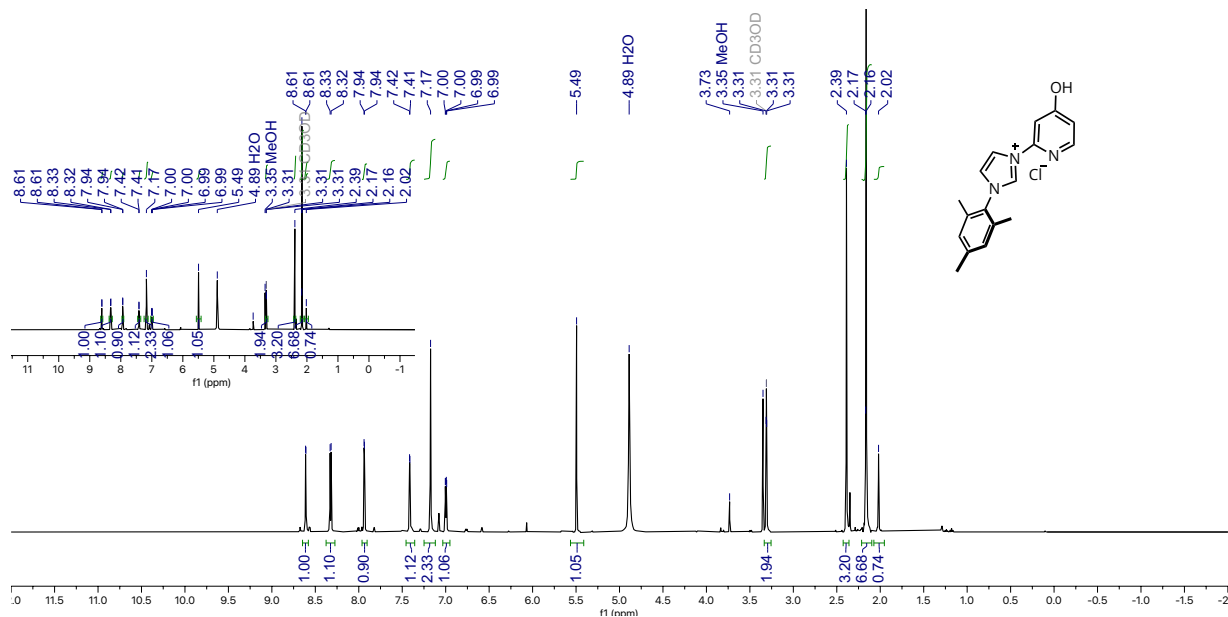


Figure S1. ^1H NMR (500 MHz, CD_3OD) spectrum of $\text{L5}\bullet\text{HCl}$

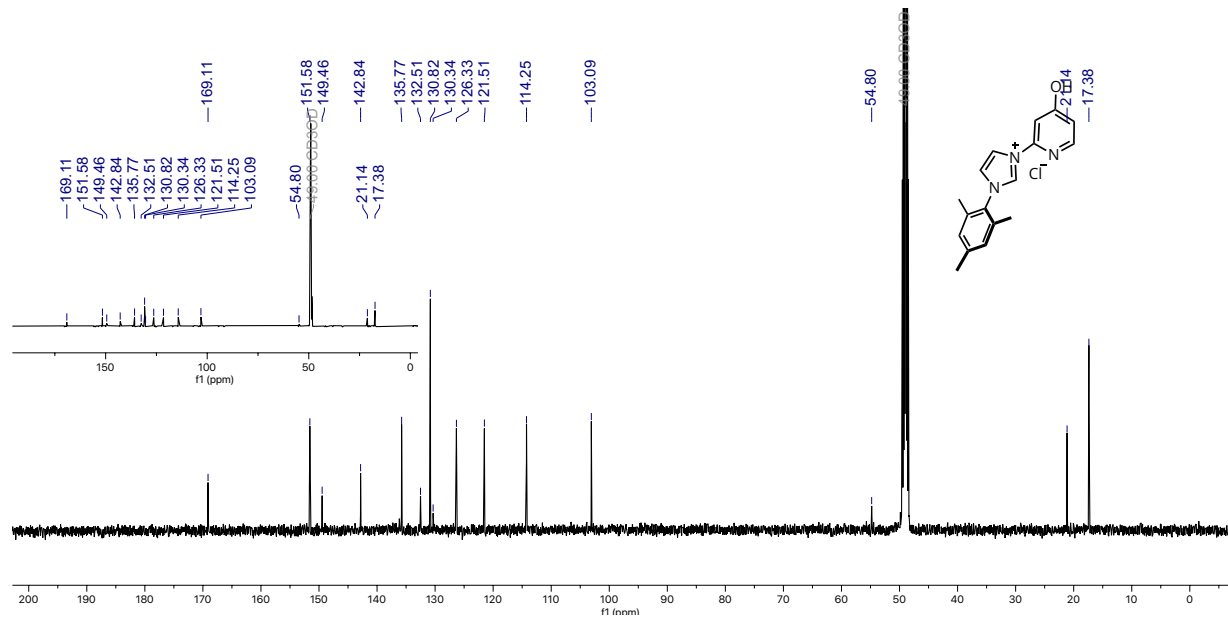
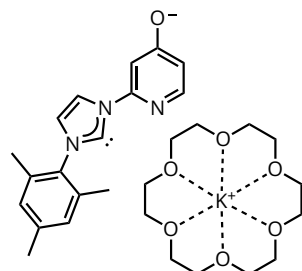


Figure S2. ^{13}C NMR (126 MHz, CD_3OD) spectrum $\text{L5}\bullet\text{HCl}$

*Potassium 1-(2,4,6-trimethylphenyl)-3-(4-oxidopyridin-2-yl)-1*H*-imidazol-2-ylidene (1,4,7,10,13,16-hexaoxacyclooctadecane) ([K(18-crown-6)][L5])*

In an N₂-filled glovebox, a 20 mL scintillation flask equipped with a PTFE-coated stir bar was charged with **L5•HCl** (1.00 equiv.) and potassium tert-butoxide (2.00 equiv.). Toluene (2 mL) was added to the reaction vessel, and the resulting mixture was stirred at room temperature for 1.5 hours. The reaction mixture was then passed through a short plug of Celite and eluted with THF. The filtrate was concentrated to give the potassium salt of the free carbene as a sienna brown solid. To the crude material, 18-crown-6 (384 mg, 1.45 mmol) and THF (10 mL) were added, swirled to mix, and concentrated in vacuo. The crude material was used with no further purification.



- ^1H NMR (400 MHz, C_6D_6): δ 8.76 (d, J = 1.7 Hz, 1H), 8.39 (d, J = 6.0 Hz, 1H), 7.89 (d, J = 2.3 Hz, 1H), 6.83 (s, 2H), 6.76 (dd, J = 5.9, 2.3 Hz, 1H), 6.51 (d, J = 1.7 Hz, 1H), 2.16 (s, 3H), 2.13 (s, 6H).

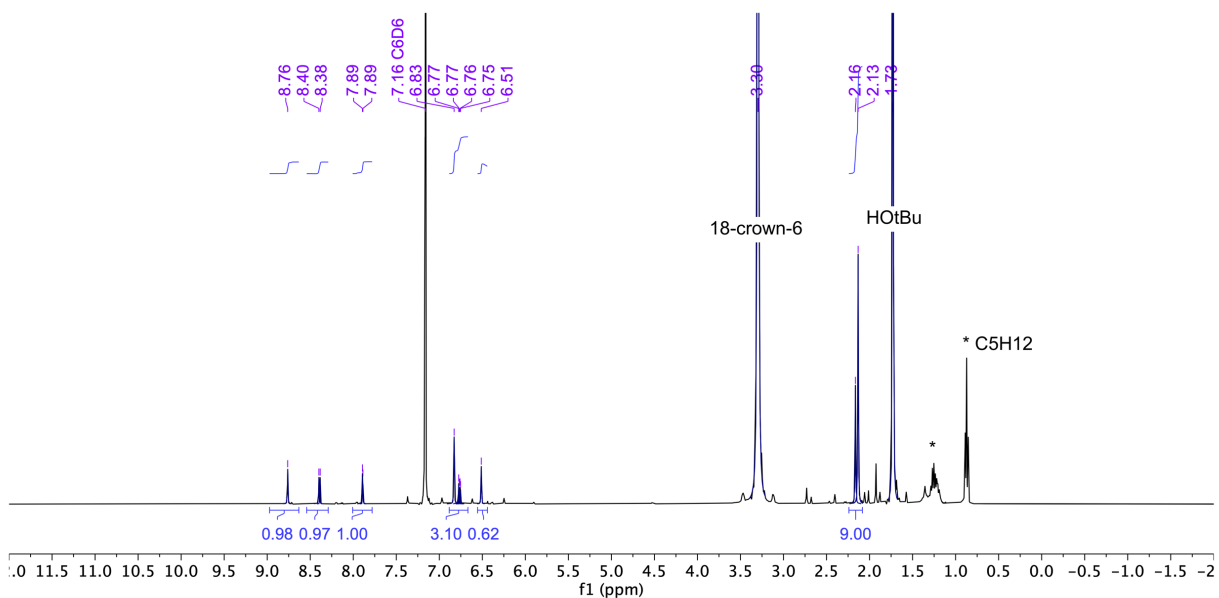


Figure S3. ^1H NMR (500 MHz, C_6D_6) spectrum of crude $[\text{K}(18\text{-crown-6})]\text{L5}$ generated in situ.

3. Catalytic Procedures and Product Characterization

3.1 General Procedure for Nitrile Hydroboration

In a glovebox, a 3.7 mL vial was charged with of $[K(18\text{-crown}\text{-}6)][(L1)\text{Ni}(\text{cod})]$ (7.5 mg, 0.01 mmol, 5.0 mol%) and a PTFE-coated magnetic stir bar. The nitrile substrate (0.2 mmol, 1.0 equiv) was added, followed by HBPin (0.8 mmol, 4.0 equiv) and toluene (0.50 mL, 0.4 M). The vial was sealed with a PTFE-lined screw cap and maintained with stirring at ambient temperature ($\sim 22^\circ\text{C}$) in the glovebox. After 6 hours, the reaction mixture was concentrated in vacuo and analyzed by ^1H and ^{11}B NMR in C_6D_6 using 1,3,5-trimethoxybenzene (17 mg, 0.10 mmol) as an internal standard to obtain an analytical yield. The solution was then added to a 0.05 M aqueous HCl solution (3.0 mL, 0.05 M) outside the glovebox and stirred for two hours. The solution was passed through a short plug of Celite, which was subsequently rinsed with DI H_2O two more times. The filtrate was concentrated in vacuo to afford a white solid. The crude material was re-dissolved in minimal DI H_2O passed through a plug of reverse-phase C_{18} silica using water as an eluent. The crude product was obtained in the first three 3-mL fractions. The fractions were combined and concentrated to afford a white solid. The crude material was resuspended in ethyl acetate and passed through a plug of Celite, rinsing with additional ethyl acetate (5 mL). The ethyl acetate filtrate primarily contained boric acid-derived impurities and was discarded. The Celite plug was then rinsed with methanol (10 mL) and the methanol filtrate was collected and concentrated in vacuo to afford the indicated product as a white solid. The isolated yield was determined based on the mass of product isolated.

3.2 Testing for Sensitivity to Air

The Ni(0) precatalysts evaluated, including $[(L1)\text{Ni}(\text{cod})][K(18\text{-crown}\text{-}6)]$, are prone to decomposition when exposed to air as a solid or solution as evidenced by a rapid color change from purple to brown. However, in the presence of nitrile reagents, decomposition appeared qualitatively slower. To evaluate the air-sensitivity of the overall reaction set-up, two variations to standard conditions were tested.

In a glovebox, two 10-mL solvent pots were each charged with $[K(18\text{-crown}\text{-}6)][(L1)\text{Ni}(\text{cod})]$ (7.5 mg, 0.01 mmol, 5.0 mol%) and a PTFE-coated magnetic stir bar. Nitrile **1n** (0.2 mmol, 1.0 equiv) and trimethoxybenzene (17 mg, 0.10 mmol) were added, followed by HBPin (0.8 mmol, 4.0 equiv) and toluene (0.50 mL, 0.4 M). The flasks were sealed with a screw-in PTFE-plug, removed from the glovebox, and stirred at ambient temperature ($\sim 22^\circ\text{C}$). After 5 minutes of stirring, one of the flasks was opened to air for up to 5 minutes and then re-sealed. Both reaction

solutions were left stirring outside of the glovebox at ambient temperature (~22 °C). After 6 hours, both reaction mixtures were concentrated in vacuo by vacuum distillation of the solvent using a Schlenk line. The crude residue obtained in each case was then analyzed by ¹H and ¹¹B NMR in C₆D₆ to obtain an analytical yield. (Note: Diborylamine products such as **2n** are not stable to air, so all product manipulations required air-free handling until the hydrolysis step.) The isolated yields were obtained after performing a standard work-up procedure. Reactions set-up inside the glovebox and removed from the glovebox in a sealed vessel proceeded with no penalty to net product yield. However, exposing the reaction mixture to air for ≤5 minutes resulted in lower and inconsistent (but non-zero) yield of the diborylamine product. Taken together, these results suggest moderate air-sensitivity and support the benefit of a glovebox set-up (Table S1).

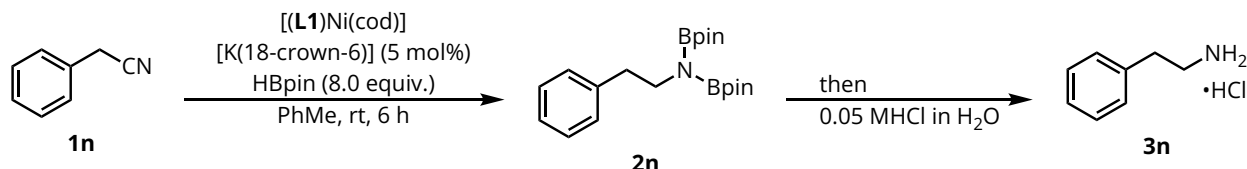


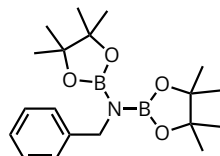
Table S1. Comparison of reaction yields upon exposure to air.

Entry	Modifications	NMR Yield of 2n
1	sealed	98%
2	exposed to air	82%
3	sealed	98%
4	exposed to air	22%

3.3 Product Characterization Data

N-benzyl-4,4,5,5-tetramethyl-N-(4,4,5,5-tetramethyl-1,3,2-dioxaborolan-2-yl)-1,3,2-dioxaborolan-2-amine (**2a**)

The general procedure was followed using benzonitrile, pinacolborane and toluene (¹H NMR yield: 84%). ¹H, ¹³C and ¹¹B spectroscopic data are consistent with literature values.¹⁰



- ¹H NMR (500 MHz, C₆D₆) δ 7.58 (d, *J* = 7.6 Hz, 2H), 7.25 (t, *J* = 7.6 Hz, 2H), 7.12 (t, *J* = 7.4 Hz, 1H), 4.60 (s, 2H), 1.03 (s, 24H).
- ¹³C NMR (126 MHz, C₆D₆): δ 143.8, 128.4, 126.7, 82.6, 47.9, 24.7.
- ¹¹B NMR (160 MHz, C₆D₆): δ 27.3

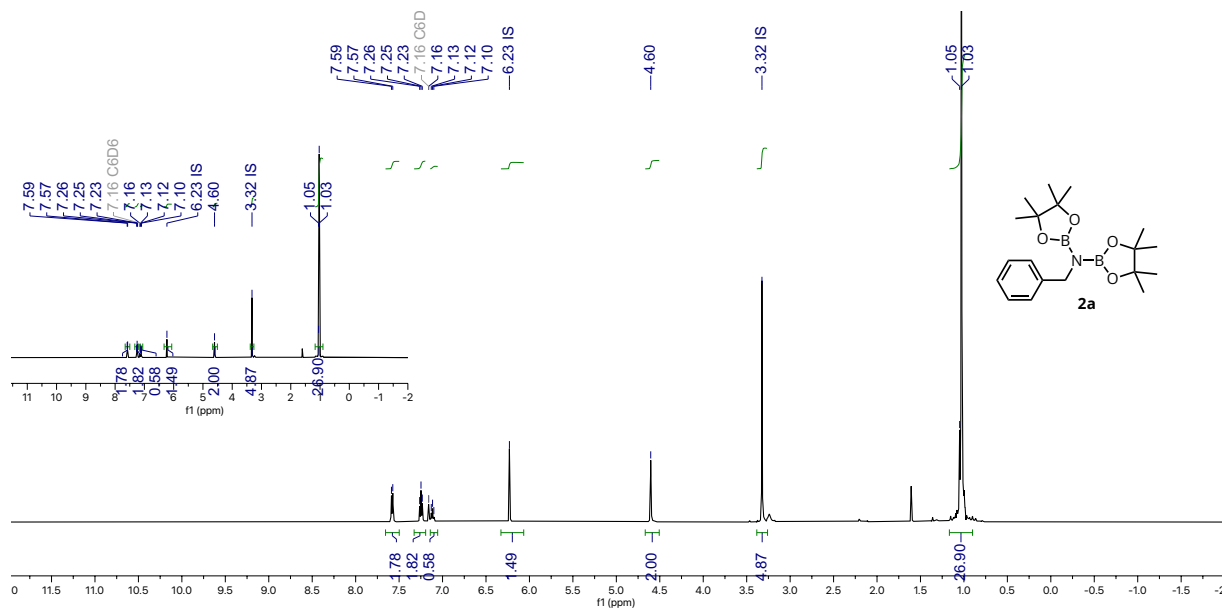


Figure S4. ^1H NMR (500 MHz, C_6D_6) spectrum of **2a**

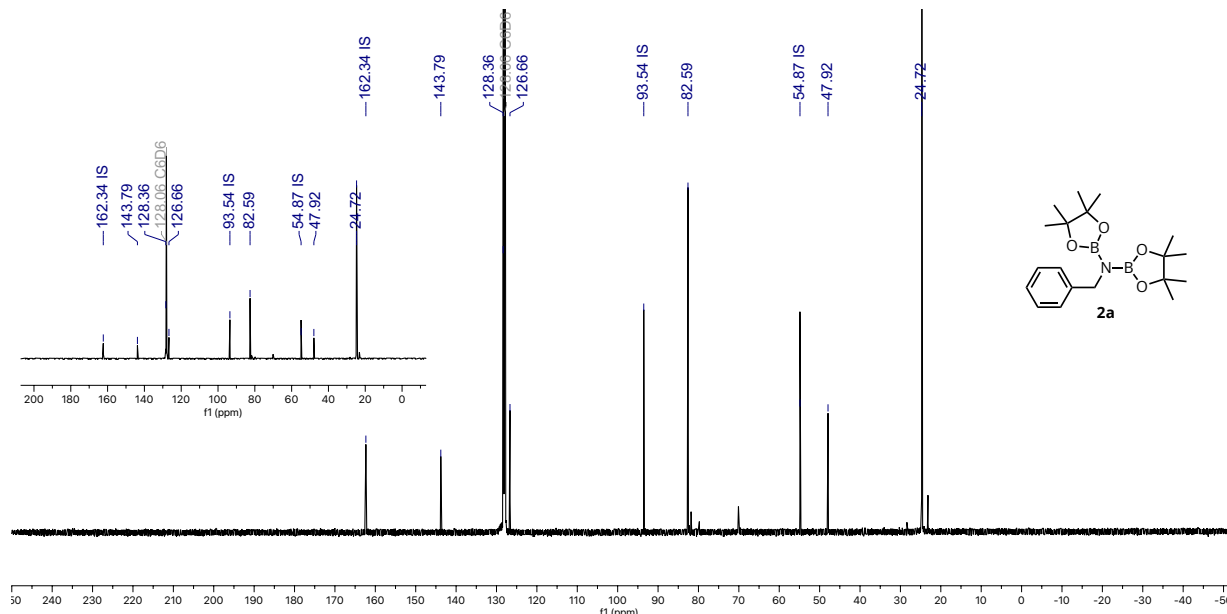


Figure S5. ^{13}C NMR (126 MHz, C_6D_6) spectrum of **2a**

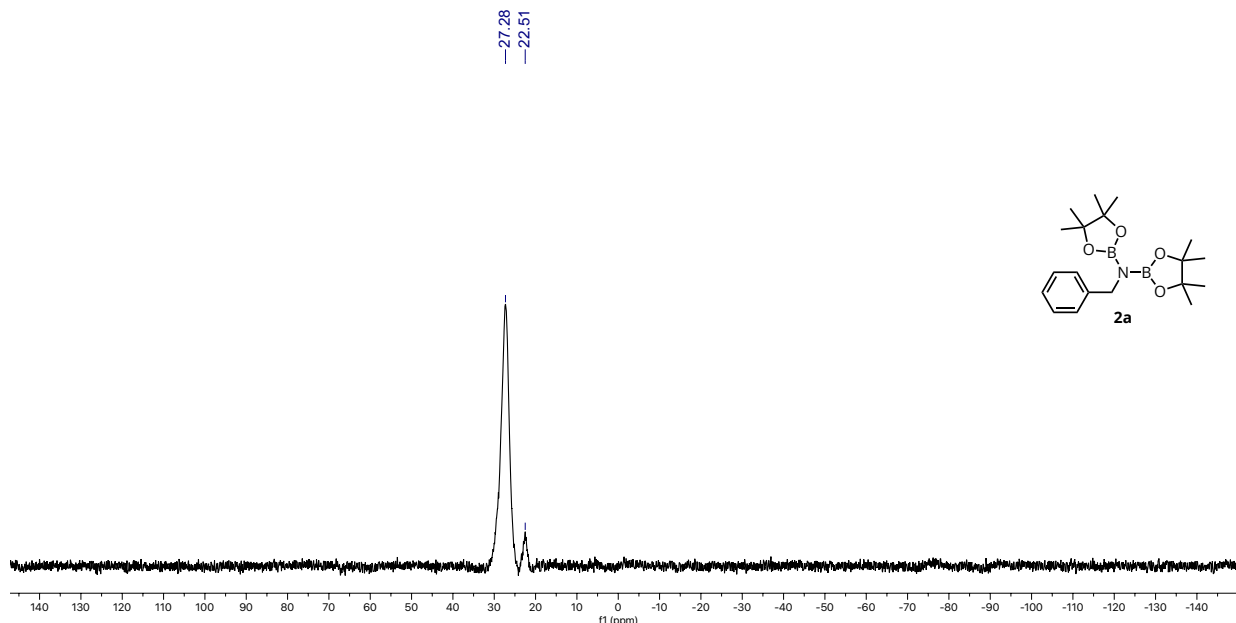
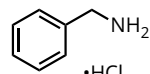


Figure S6. ^{11}B NMR (160 MHz, C_6D_6) spectrum of **2a**

Benzylamine hydrochloride (**3a**)

The isolation protocol was followed to yield **3a** as a white solid (20 mg, 70%). ^1H NMR spectroscopic data are consistent with literature values.¹¹



- ^1H NMR (500 MHz, D_2O) δ 7.42 (s, 5H), 4.13 (s, 2H)

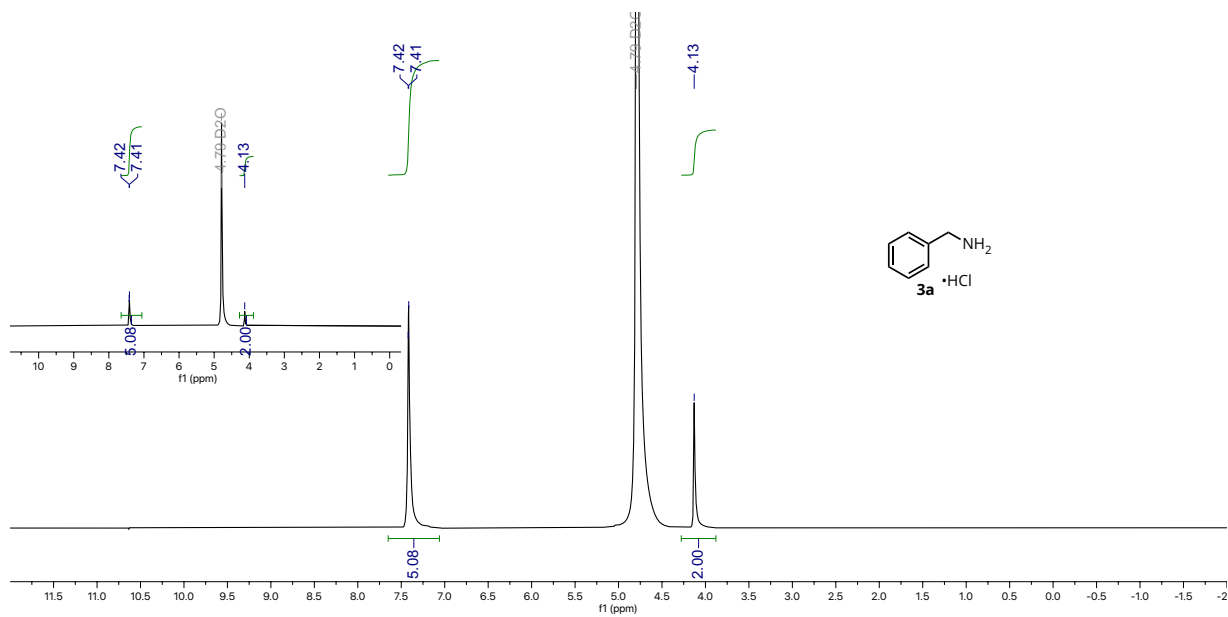
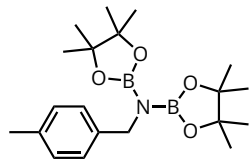


Figure S7. ^1H NMR (500 MHz, D_2O) spectrum of **3a**

4,4,5,5-tetramethyl-N-(4-methylbenzyl)-N-(4,4,5,5-tetramethyl-1,3,2-dioxaborolan-2-yl)-1,3,2-dioxaborolan-2-amine (2b)

The general procedure was followed using 4-methylbenzonitrile, pinacolborane and toluene (^1H NMR yield: 99%). ^1H , ^{13}C and ^{11}B spectroscopic data are consistent with literature values.¹²



- ^1H NMR (500 MHz, C_6D_6) δ 7.53 (d, $J = 7.8$ Hz, 2H), 7.08 (d, $J = 7.8$ Hz, 2H), 4.61 (s, 2H), 2.16 (s, 3H), 1.05 (s, 24H).
- ^{13}C NMR (125 MHz, C_6D_6): δ 140.9, 135.8, 129.1, 82.6, 47.6, 24.7, 21.1.
- ^{11}B NMR (160 MHz, C_6D_6): δ 27.4

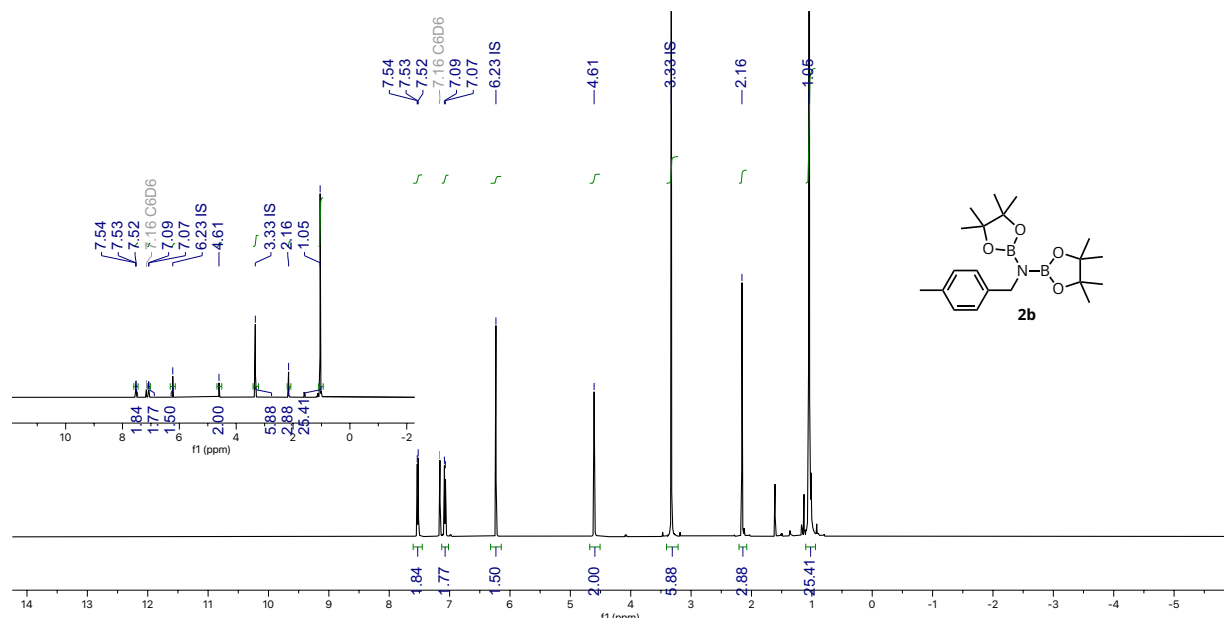
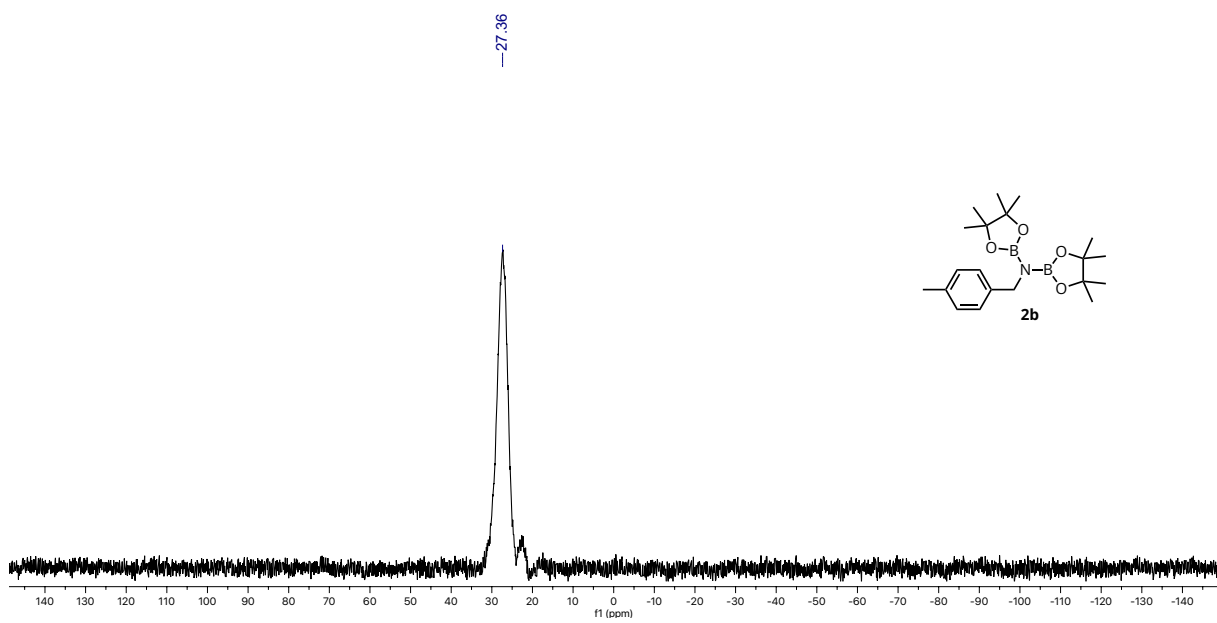
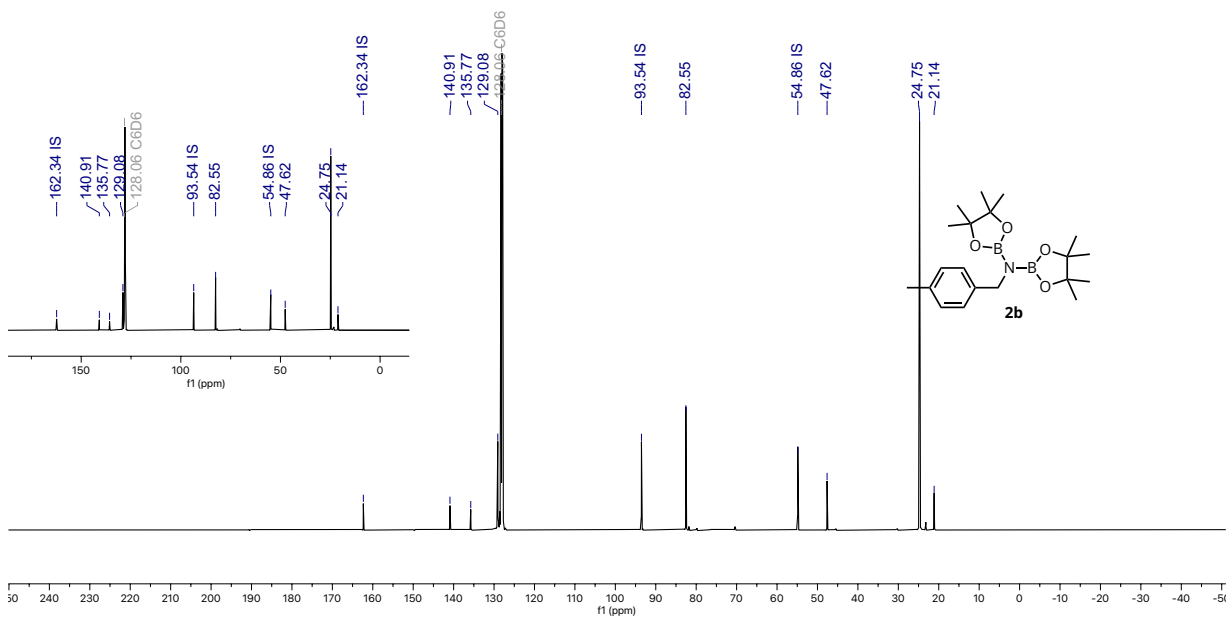
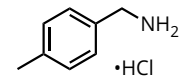


Figure S8. ^1H NMR (500 MHz, C_6D_6) spectrum of **2b**



p-tolylmethanamine hydrochloride (**3b**)

The isolation protocol was followed to yield **3b** as a white solid (10 mg, 32%). ¹H NMR spectroscopic data are consistent with literature values.¹³



- ¹H NMR (500 MHz, D₂O): δ 7.47 – 7.20 (m, 4H), 4.15 (s, 2H), 2.37 (s, 3H).

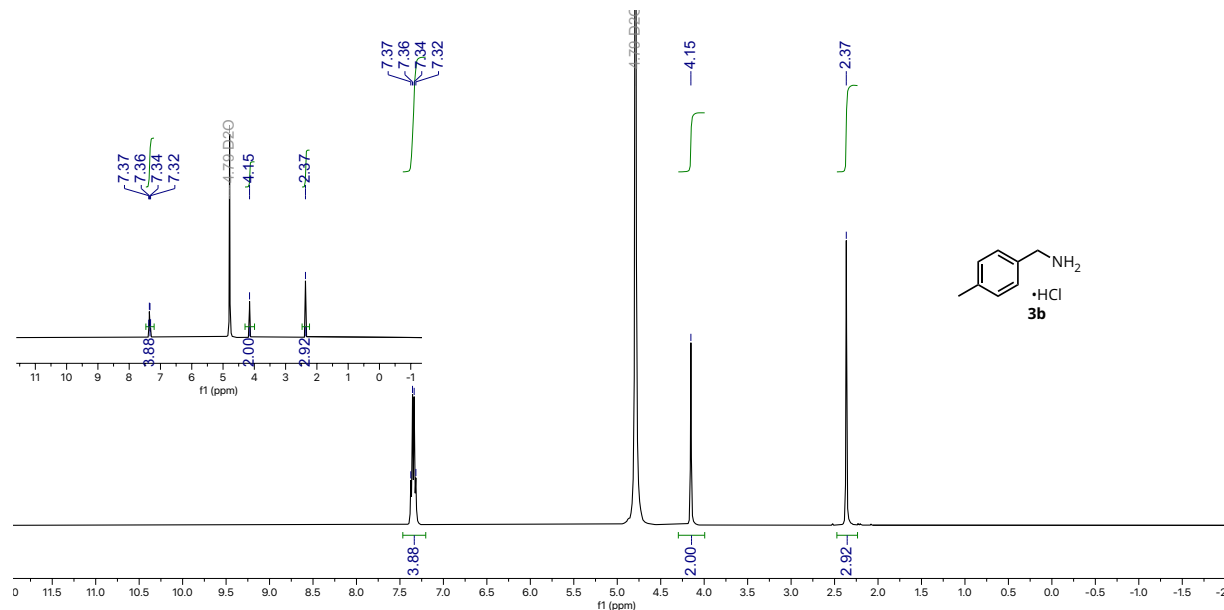
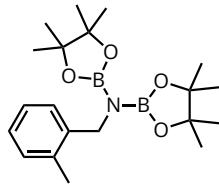


Figure S11. ¹H NMR (500 MHz, D₂O) spectrum of **3b**

4,4,5,5-tetramethyl-N-(2-methylbenzyl)-N-(4,4,5,5-tetramethyl-1,3,2-dioxaborolan-2-yl)-1,3,2-dioxaborolan-2-amine (2c)



The general procedure was followed using o-tolunitrile, pinacolborane and toluene (^1H NMR yield: 97%). ^1H , ^{13}C and ^{11}B spectroscopic data are consistent with literature values.¹⁴

- ^1H NMR (500 MHz, C_6D_6) δ 7.64 (d, J = 6.3 Hz, 1H), 7.24 (dd, J = 6.3, 7.3 Hz, 1H), 7.07 (dd, J = 7.3, 6.3 Hz, 1H), 6.99 (d, J = 7.3 Hz, 1H), 4.60 (s, 2H), 2.12 (s, 3H), 1.03 (s, 24H).
 - ^{13}C NMR (126 MHz, C_6D_6): δ 141.2, 135.3, 130.1, 126.2, 126.0, 125.7, 82.6, 45.4, 24.7, 19.0.
 - ^{11}B NMR (160 MHz, C_6D_6): δ 27.3.

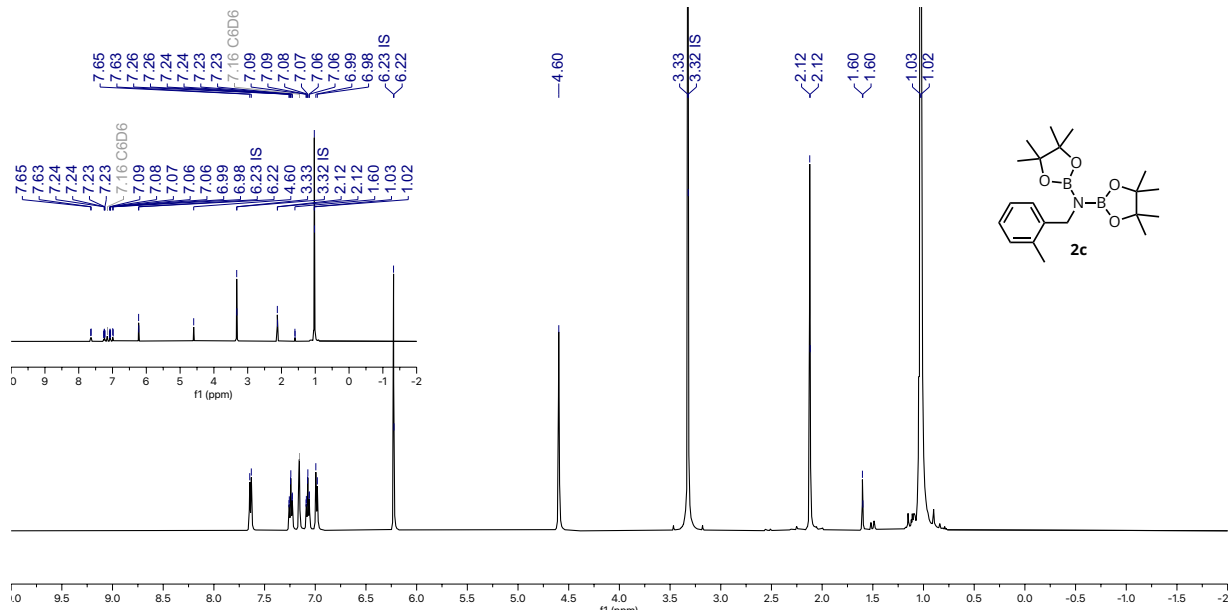


Figure S12. ^1H NMR (500 MHz, C_6D_6) spectrum of **2c**

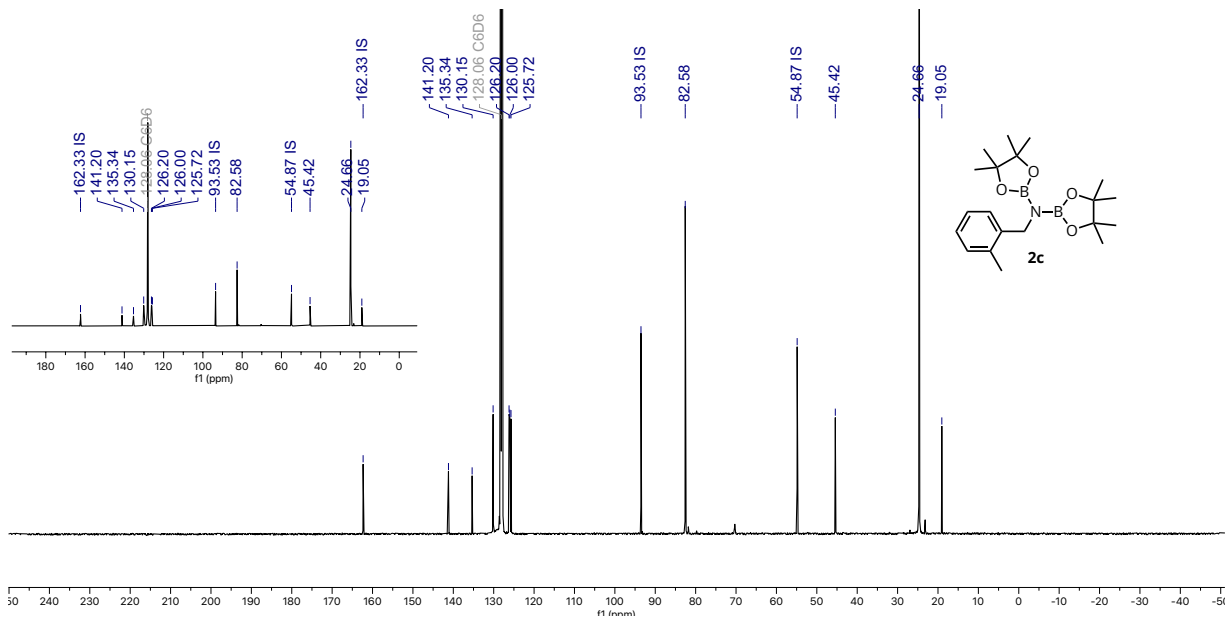


Figure S13. ^{13}C NMR (125 MHz, C_6D_6) spectrum of **2c**

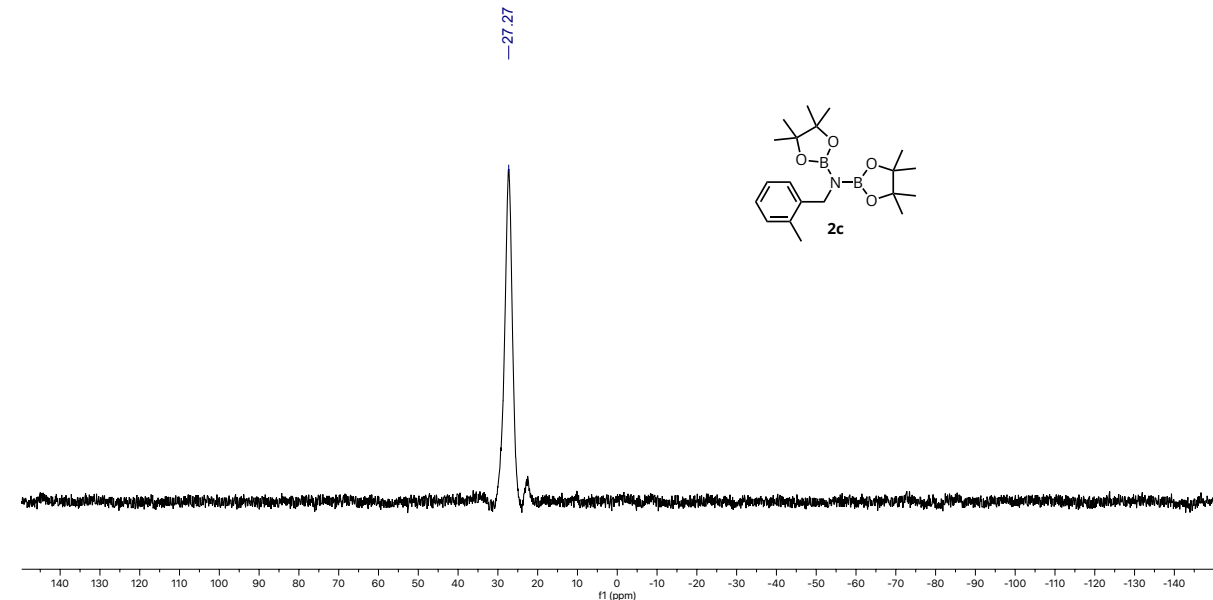
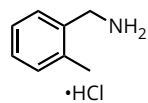


Figure S14. ^{11}B NMR (160 MHz, C_6D_6) spectrum of **2c**

o-tolylmethanamine hydrochloride (**3c**)

The isolation protocol was followed to yield **3c** as a white solid (18 mg, 54%). ¹H NMR spectroscopic data are consistent with literature values.¹⁵



- ¹H NMR (500 MHz, D₂O) δ 7.74-7.18 (m, 4H), 4.22 (s, 2H), 2.37 (s, 3H).

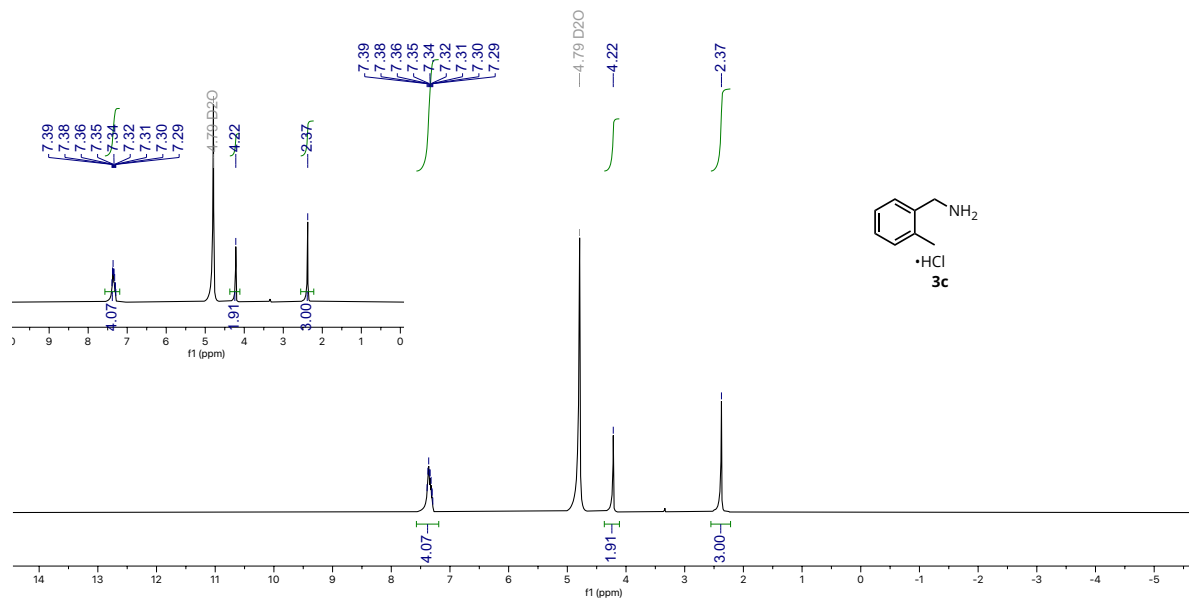
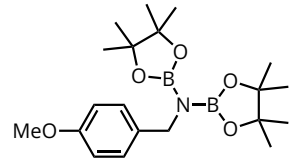


Figure S15. ¹H NMR (500 MHz, D₂O) spectrum of **3c**

*N-(4-methoxybenzyl)-4,4,5,5-tetramethyl-N-(4,4,5,5-tetramethyl-1,3,2-dioxaborolan-2-yl)-1,3,2-dioxaborolan-2-amine (**2d**)*

The general procedure was followed using 4-(methoxy)benzonitrile, pinacolborane and toluene (^1H NMR yield: 99%). ^1H , ^{13}C , ^{11}B and ^{19}F NMR spectroscopic data are consistent with literature values.¹²



- ^1H NMR (500 MHz, C_6D_6) δ 7.56 (d, J = 8.2 Hz, 2H), 6.87 (d, J = 8.2 Hz, 2H), 4.57 (s, 2H), 3.34 (s, 3H), 1.05 (s, 24H).
- ^{13}C NMR (125 MHz, C_6D_6): δ 159.0, 136.1, 129.5, 128.6, 113.9, 82.5, 47.3, 24.8.
- ^{11}B NMR (160 MHz, C_6D_6): δ 27.5

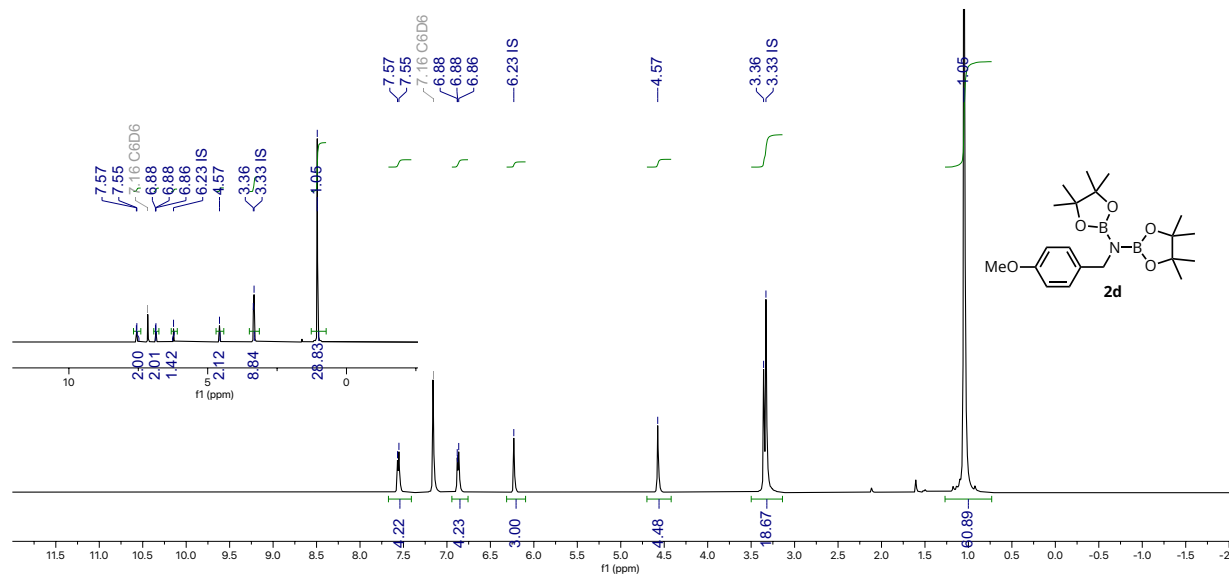


Figure S16. ^1H NMR (500 MHz, C_6D_6) spectrum of **2d**

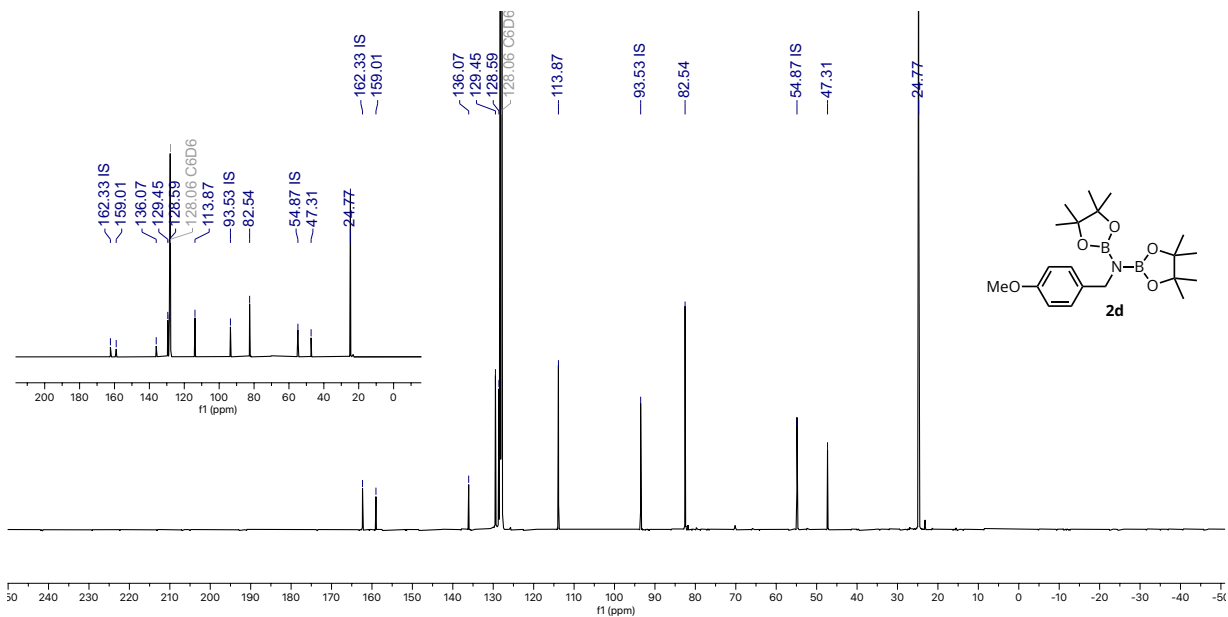


Figure S17. ^{13}C NMR (125 MHz, C₆D₆) spectrum of **2d**

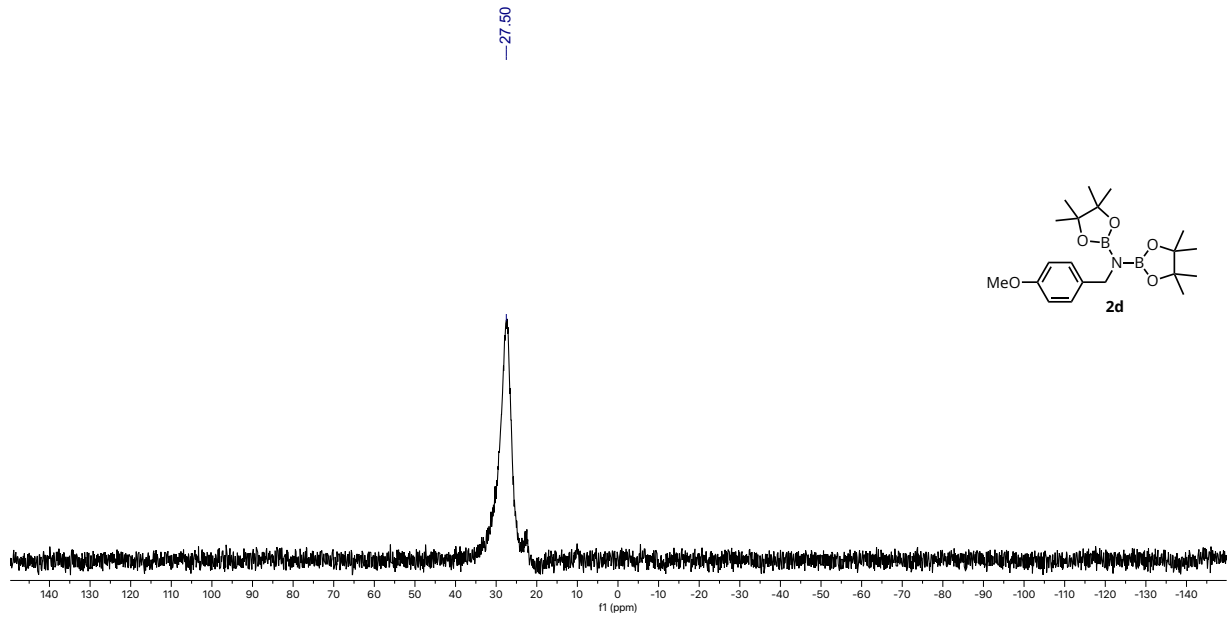
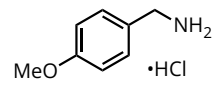


Figure S18. ^{11}B NMR (160 MHz, C₆D₆) spectrum of **2c**

(4-methoxyphenyl)methanamine hydrochloride (3d)

The isolation protocol was followed to yield **3d** as a white solid (17 mg, 44%).

^1H NMR spectroscopic data are consistent with literature values.¹¹



- ^1H NMR (500 MHz, D_2O): δ 7.40 (d, $J = 7.7$ Hz, 2H), 7.03 (t, $J = 7.7$ Hz, 2H), 4.11 (s, 2H), 3.82 (s, 3H).

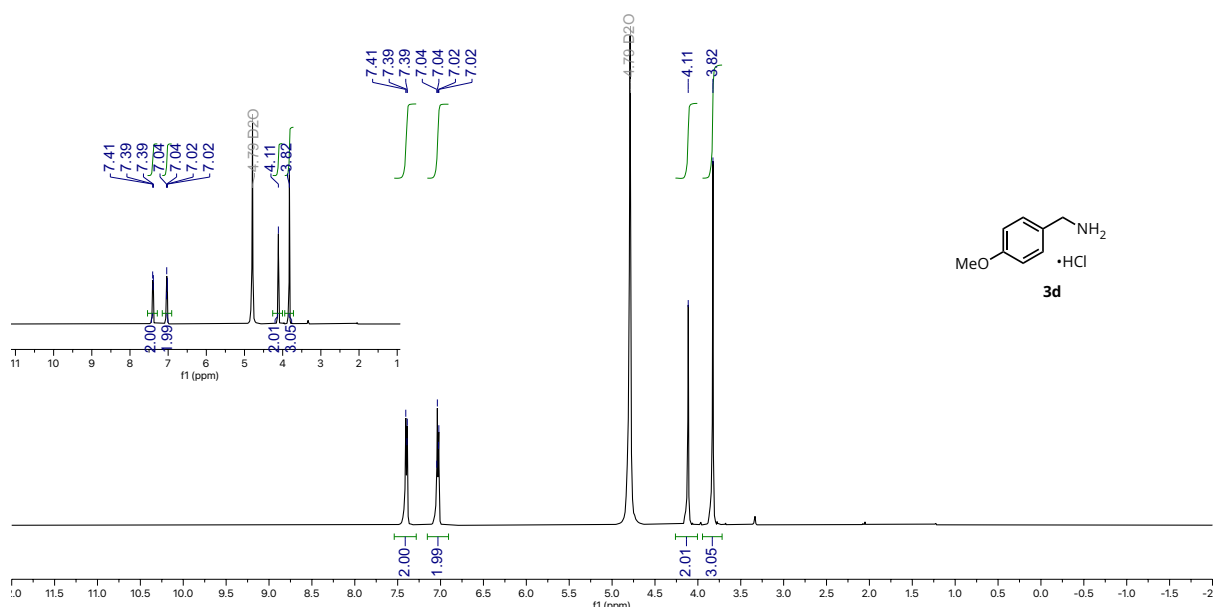
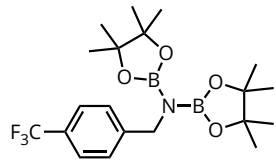


Figure S19. ^1H NMR (500 MHz, D_2O) spectrum of **3d**

*4,4,5,5-tetramethyl-N-(4,4,5,5-tetramethyl-1,3,2-dioxaborolan-2-yl)-N-(4-(trifluoromethyl)benzyl)-1,3,2-dioxaborolan-2-amine (**2e**)*

The general procedure was followed using 4-(trifluoromethyl)benzonitrile, pinacolborane and toluene (^1H NMR yield: 99%). ^1H , ^{13}C , ^{11}B and ^{19}F NMR spectroscopic data are consistent with literature values.¹⁶



- ^1H NMR (500 MHz, C_6D_6) δ 7.41 (s, 4H), 4.47 (s, 2H), 1.01 (s, 24H).
- ^{13}C NMR (125 MHz, C_6D_6): δ 147.7, 128.8, 126.3, 125.3, 125.3, 82.8, 47.5, 24.7.
- ^{11}B NMR (160 MHz, C_6D_6): δ 27.2.
- ^{19}F NMR (376 MHz, C_6D_6): δ -62.0.

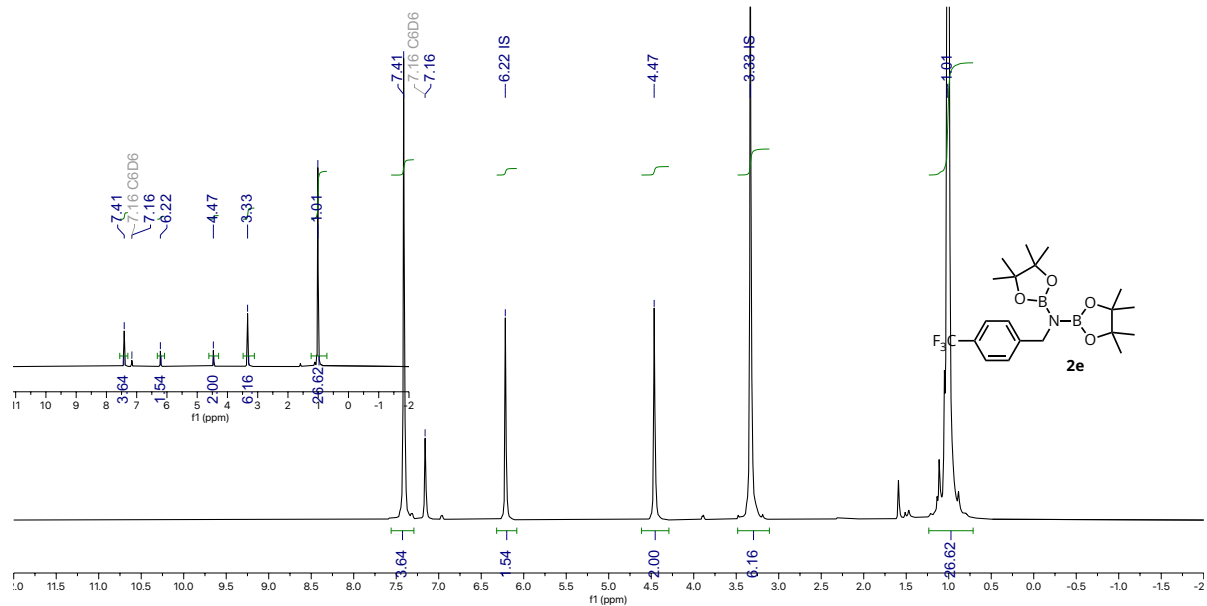


Figure S20. ^1H NMR (500 MHz, C_6D_6) spectrum of **2e**

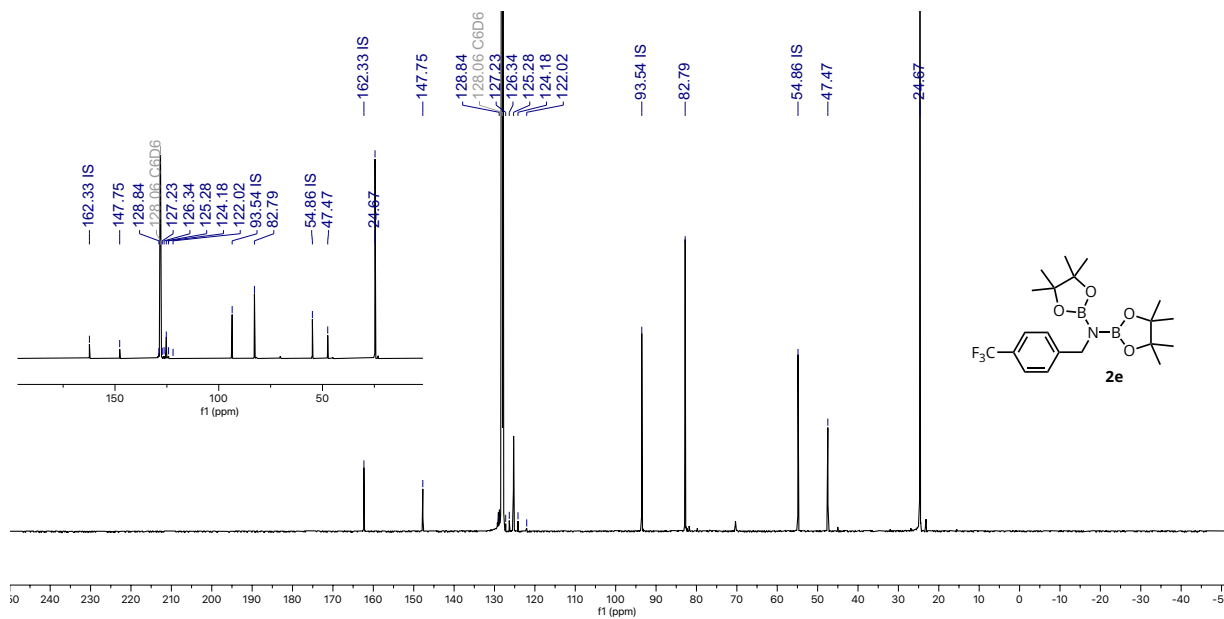


Figure S21. ^{13}C NMR (125 MHz, C_6D_6) spectrum of **2e**

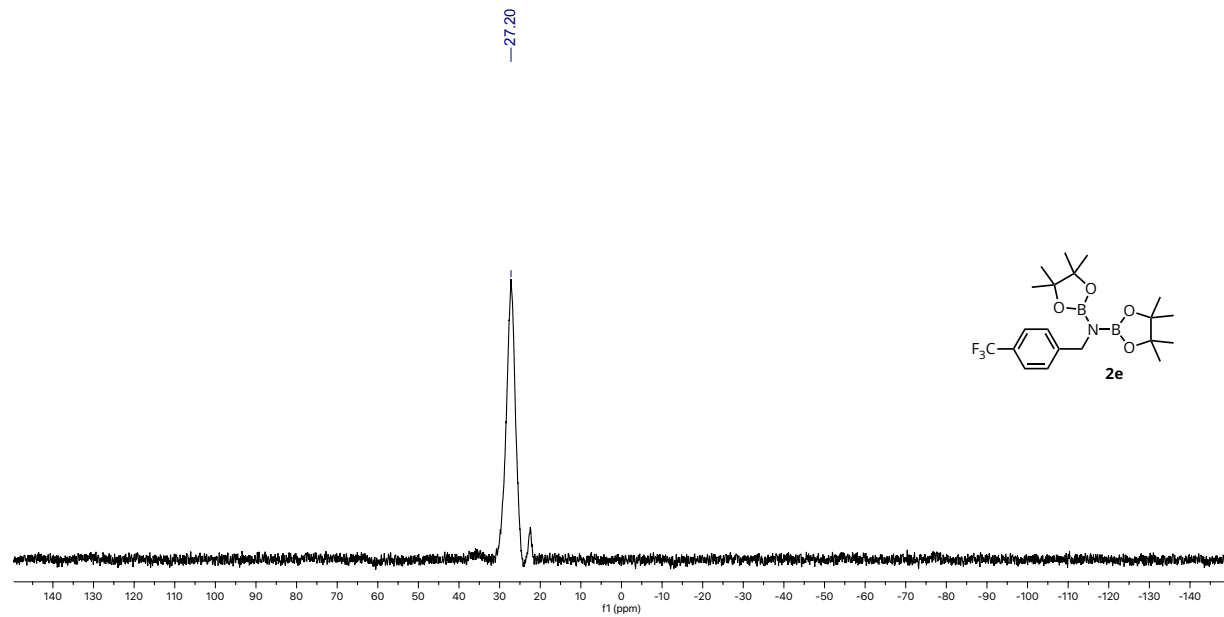


Figure S22. ^{11}B NMR (160 MHz, C_6D_6) spectrum of **2e**

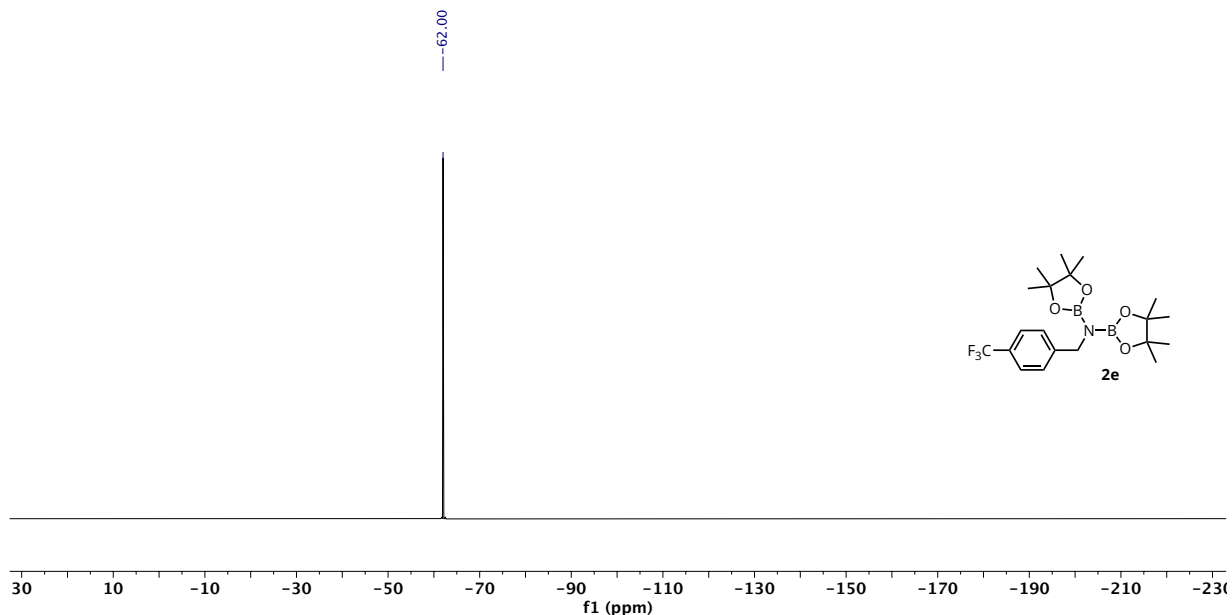
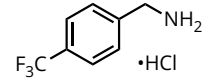


Figure S23. ¹⁹F NMR (376 MHz, C₆D₆) spectrum of **2e**

*(4-(trifluoromethyl)phenyl)methanamine hydrochloride (**3e**)*



The isolation protocol was followed to yield **3e** as a white solid (25 mg, 50%). ¹H NMR spectroscopic data are consistent with literature values.¹¹

- ¹H NMR (500 MHz, D₂O): δ 7.78 (d, *J* = 7.8 Hz, 2H), 7.60 (d, *J* = 7.9 Hz, 2H), 4.25 (s, 2H).

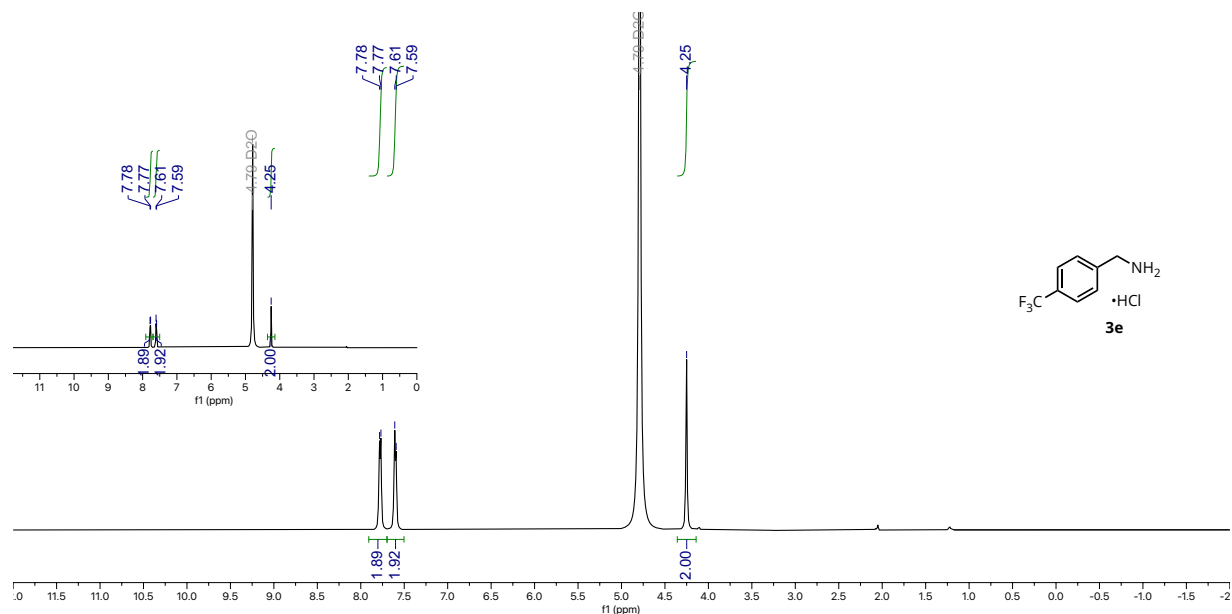
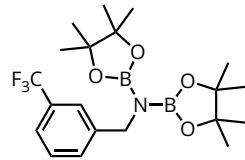


Figure S24. ¹H NMR (500 MHz, D₂O) spectrum of **3e**

4,4,5,5-tetramethyl-N-(4,4,5,5-tetramethyl-1,3,2-dioxaborolan-2-yl)-N-(3-(trifluoromethyl)benzyl)-1,3,2-dioxaborolan-2-amine (2f)



The general procedure was followed using 3-(Trifluoromethyl)benzonitrile, pinacolborane and toluene (^1H NMR yield: 81%).

- ^1H NMR (500 MHz, C_6D_6) δ 7.97 (s, 1H), 7.55 (d, $J = 7.8$ Hz, 1H), 7.31 (d, $J = 7.8$ Hz, 1H), 7.03 (dd, $J = 7.7, 7.5$ Hz, 1H), 4.45 (s, 2H), 1.01 (d, $J = 7.7$ Hz, 24H).
 - ^{13}C NMR (125 MHz, C_6D_6): δ 144.8, 131.7, 128.8, 125.3, 123.5, 82.8, 47.4, 24.7.
 - ^{19}F NMR (376 MHz, C_6D_6): δ 62.4.
 - ^{11}B NMR (160 MHz, C_6D_6): δ 27.1.

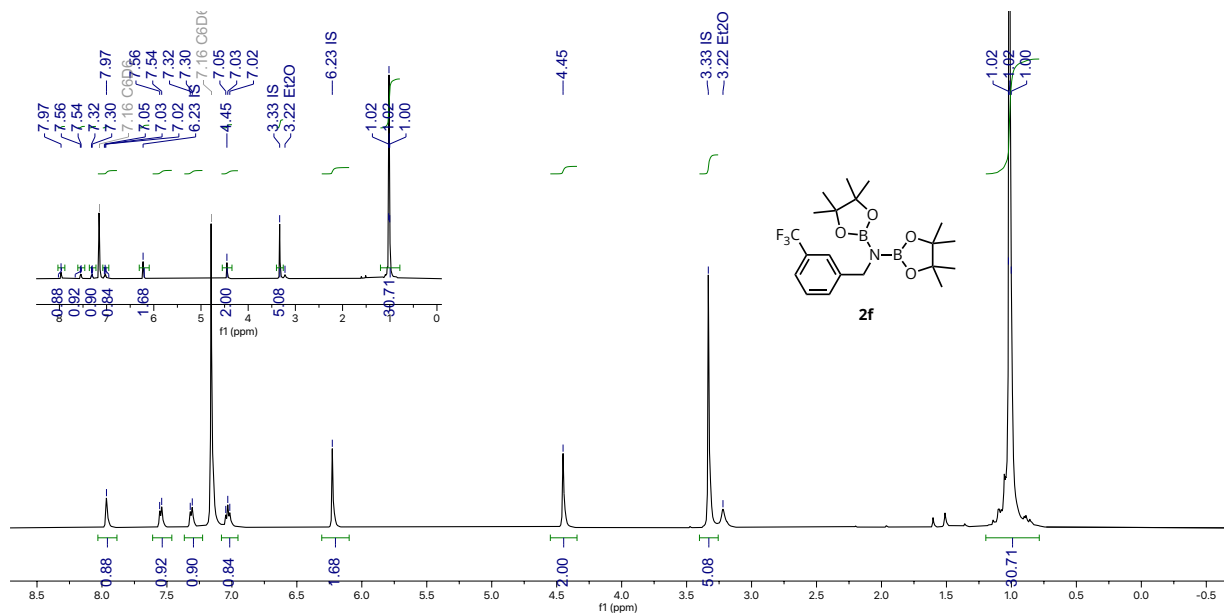


Figure S25. ^1H NMR (500 MHz, C_6D_6) spectrum of **2f**

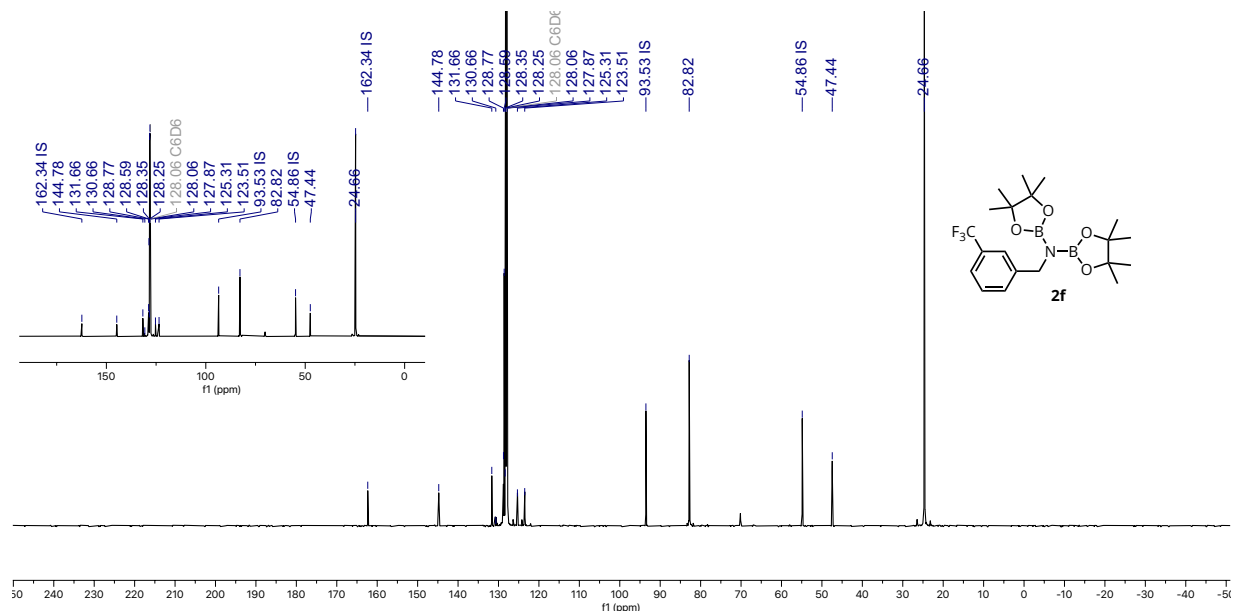


Figure S26. ^{13}C NMR (125 MHz, C_6D_6) spectrum of **2f**

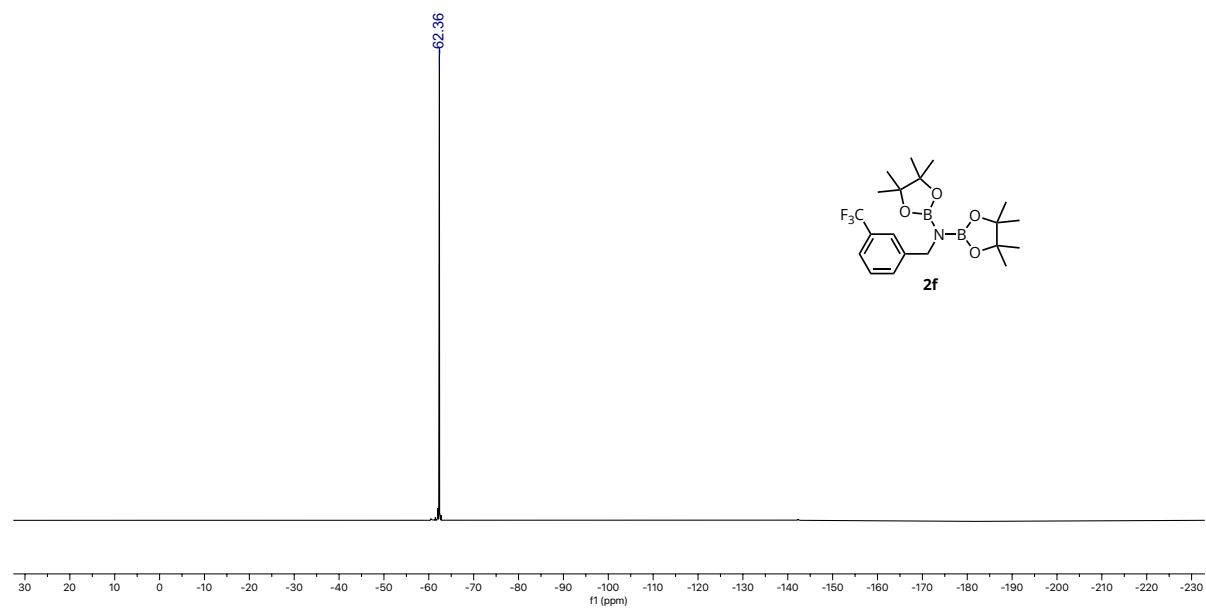


Figure S27. ^{19}F NMR (376 MHz, C_6D_6) spectrum of **2f**

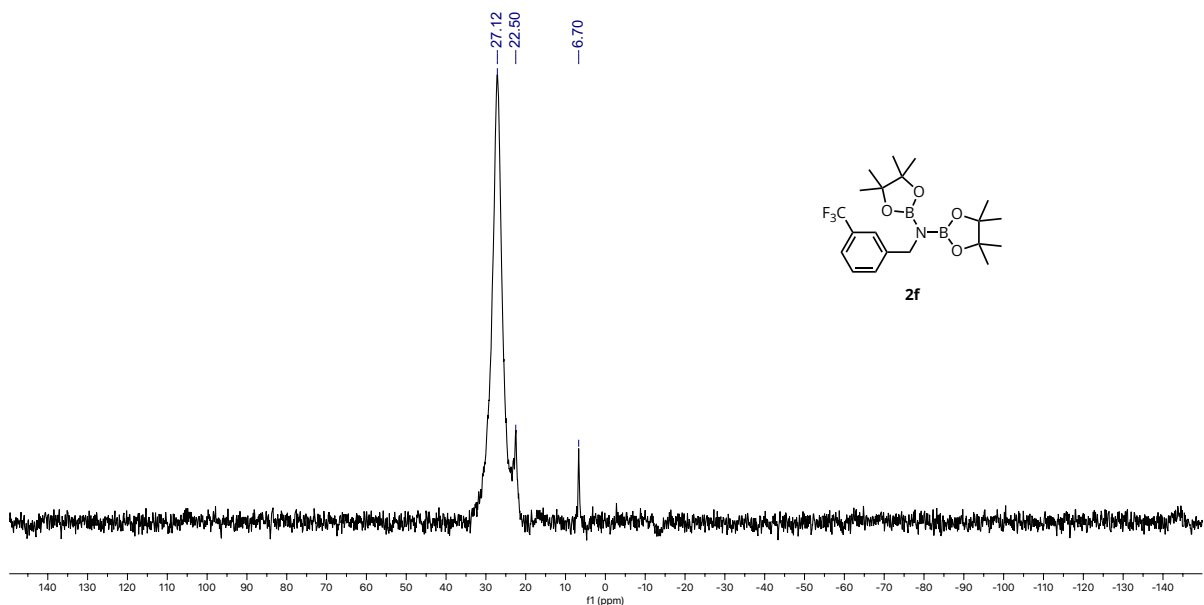
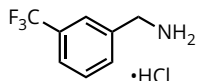


Figure S28. ^{11}B NMR (160 MHz, C_6D_6) spectrum of **2f**

*(3-(trifluoromethyl)phenyl)methanamine hydrochloride (**3f**)*



The isolation protocol was followed to yield **3f** as a white solid (36 mg, 72%).

- ^1H NMR (500 MHz, D_2O): δ 7.78 (s, 1H), 7.77 (d, $J = 7.7$ Hz, 1H), 7.68 (d, $J = 7.8$ Hz, 1H), 7.64 (dd, $J = 7.7, 7.8$, 1H), 4.25 (s, 1H).
- ^{13}C NMR (125 MHz, D_2O): δ 134.2, 133.3, 131.4, 130.7, 126.6, 125.7, 123.6, 43.4.
- ^{19}F NMR (376 MHz, D_2O): δ -62.7.
- LRMS (ESI): for $[\text{M}]^+ = [\text{C}_8\text{H}_9\text{F}_3\text{N}]^+$, calculated: $m/z = 176.07$; found: $m/z = 176.1$
- FT-IR (ATR, powder): 2925, 2140, 1608, 1461, 1441, 1327, 1209, 1191, 1171, 1118, 1076, 920, 904, 850, 803, 741, 702, 657 cm^{-1}

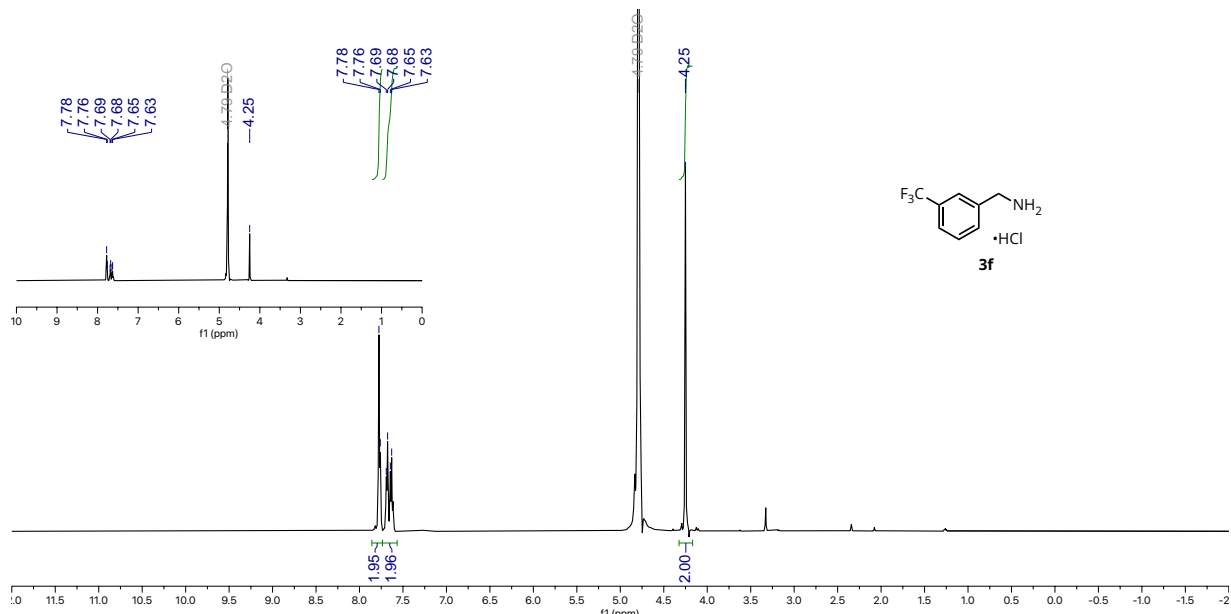


Figure S29. ^1H NMR (500 MHz, D_2O) spectrum of **3f**

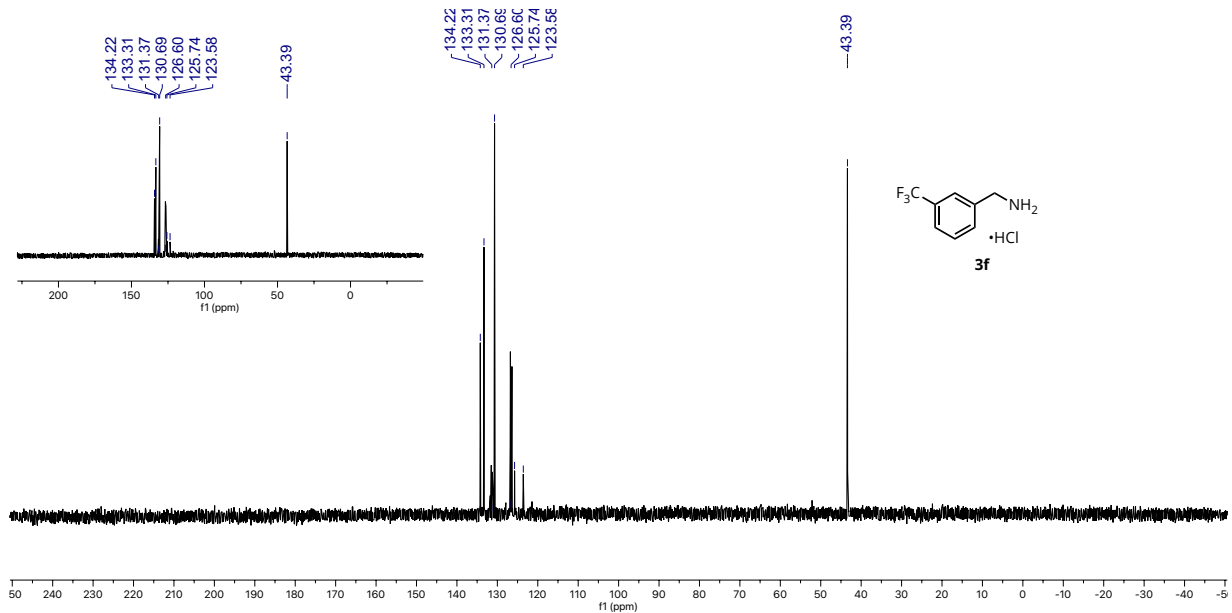


Figure S30. ^{13}C NMR (125 MHz, D_2O) spectrum of **3f**

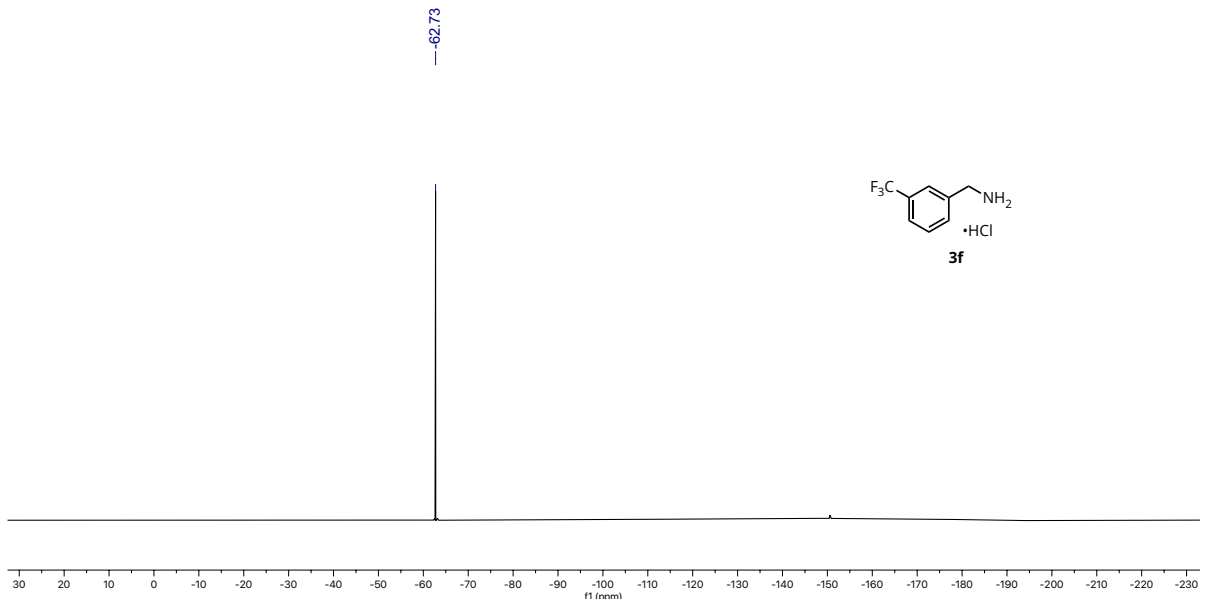


Figure S31. ^{19}F NMR (376 MHz, D_2O) spectrum of **3f**

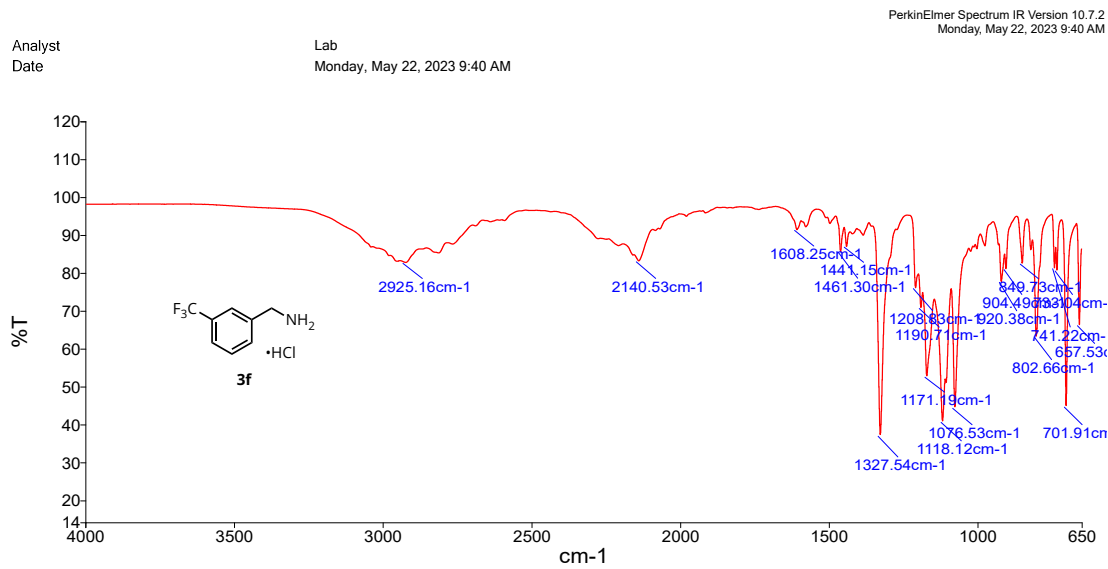
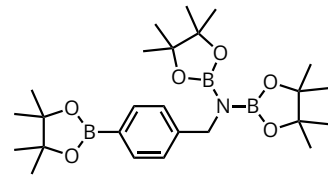


Figure S32. FTIR spectrum of **3f**

**4,4,5,5-tetramethyl-*N*-(4,4,5,5-tetramethyl-1,3,2-dioxaborolan-2-yl)-
N-(4-(4,4,5,5-tetramethyl-1,3,2-dioxaborolan-2-yl)benzyl)-1,3,2-
dioxaborolan-2-amine (**2g**)**



The general procedure was followed using 4-(4,4,5,5-tetramethyl-1,3,2-dioxaborolan-2-yl)benzonitrile, pinacolborane and toluene (^1H NMR yield: 99%)

- ^1H NMR (500 MHz, C_6D_6) δ 8.18 (d, $J = 7.6$ Hz, 2H), 7.62 (d, $J = 7.6$ Hz, 2H), 4.58 (s, 2H), 1.12 (d, $J = 5.5$ Hz, 12H), 1.01 (s, 36H).
- ^{13}C NMR (125 MHz, C_6D_6): δ 147.1, 135.4, 128.6, 127.4, 83.6, 82.6, 48.0, 25.0, 24.7.
- ^{11}B NMR (160 MHz, C_6D_6): δ 32.0, 27.4.

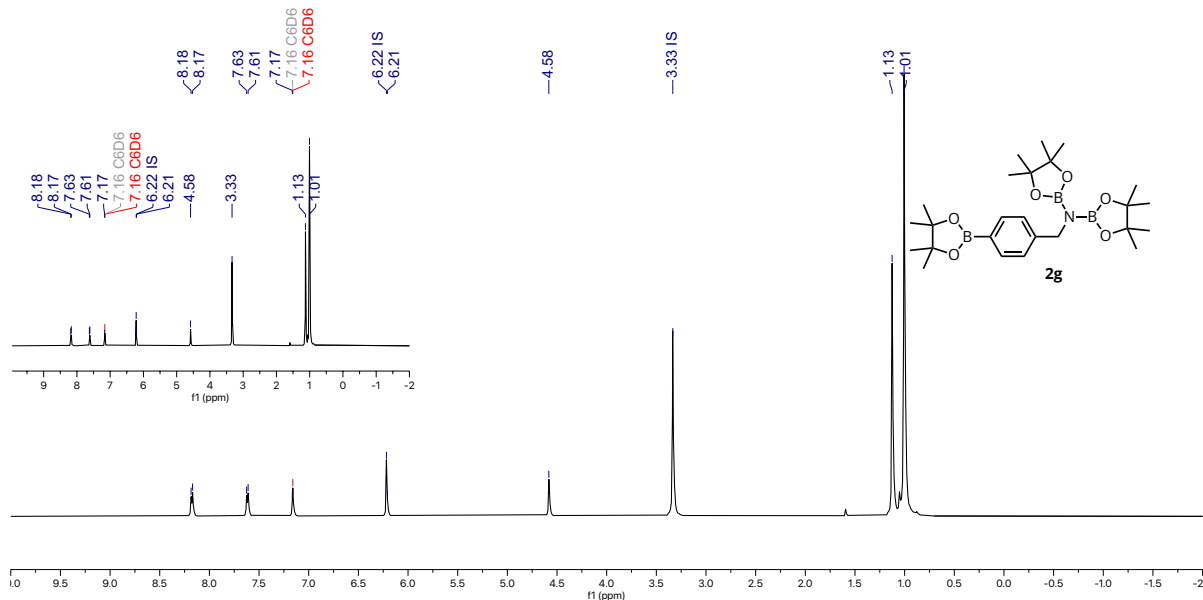
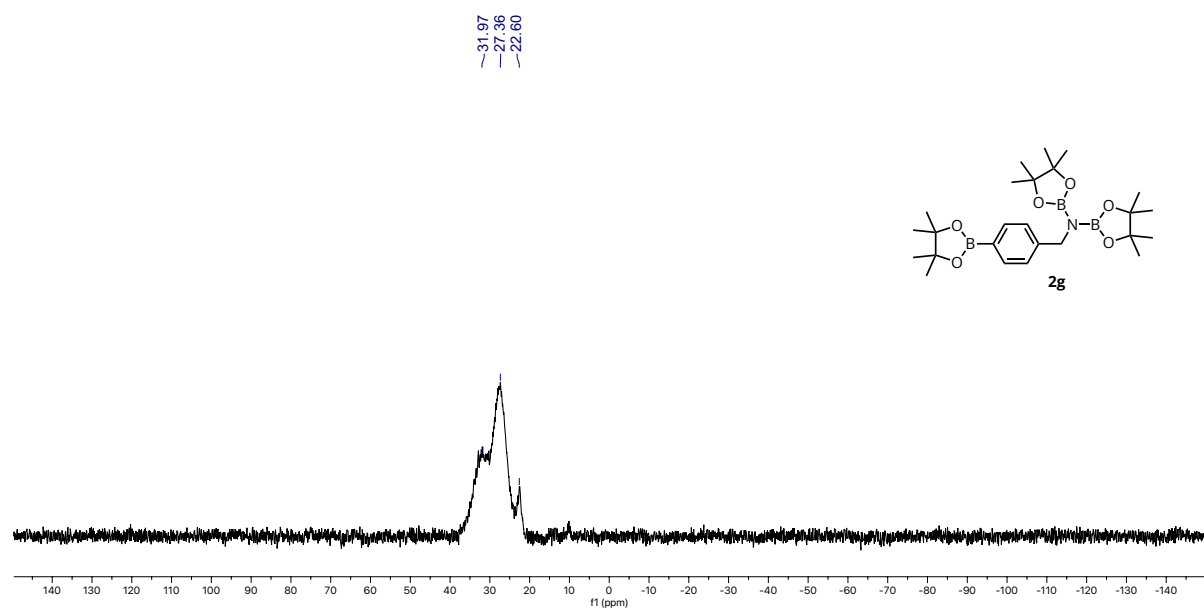
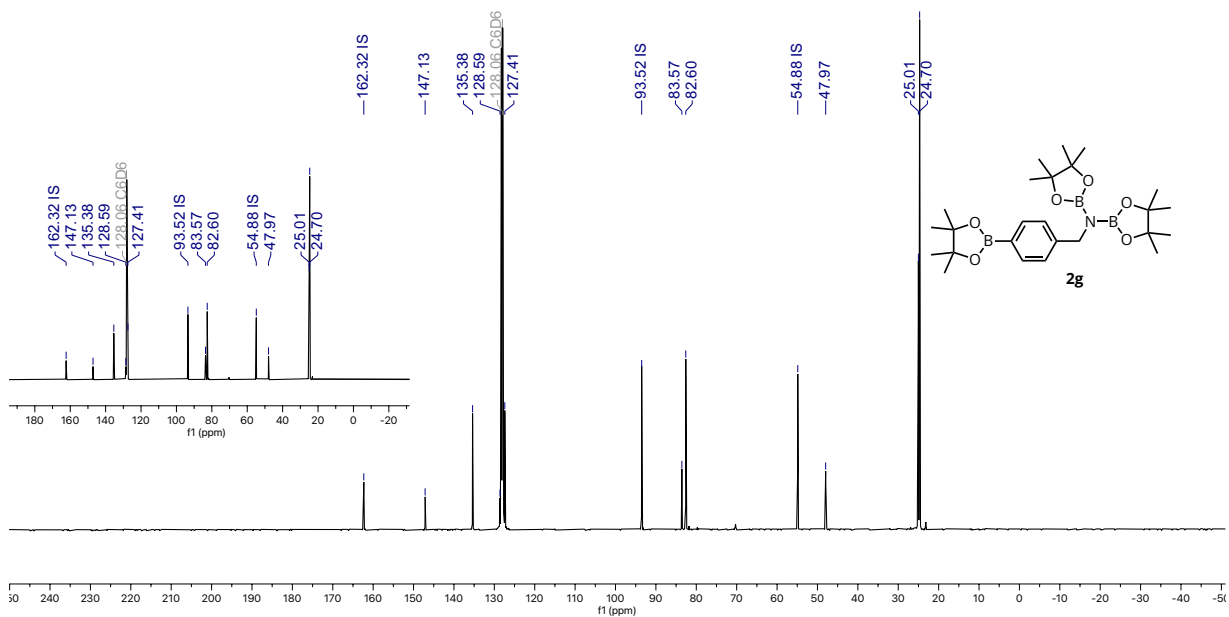
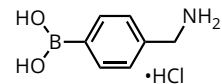


Figure S33. ^1H NMR (500 MHz, C_6D_6) spectrum of **2g**



(4-(4,4,5,5-tetramethyl-1,3,2-dioxaborolan-2-yl)phenyl)methanamine hydrochloride (3g)



The isolation protocol was followed to yield **3g** as a white solid (22 mg, 37%).

- ^1H NMR (500 MHz, D_2O): δ 7.77 (d, $J = 8.0$ Hz, 2H), 7.45 (d, $J = 8.0$ Hz, 2H), 4.17 (s, 2H)
- ^{13}C NMR (125 MHz, D_2O): δ 135.8, 135.1, 128.9, 43.8
- ^{11}B NMR (160 MHz, D_2O): δ 29.5.
- LRMS (ESI): for $[\text{M}]^+ = [\text{C}_7\text{H}_{11}\text{BNO}_2]^+$, calculated: $m/z = 152.09$; not found for $[\text{M}]^+ = [\text{C}_7\text{H}_{10}\text{BN}_2\text{O}]^+$ (arising from B–N coordination and condensation under ionization conditions) calculated: $m/z = 149.09$; found: $m/z = 149.1$
- FTIR (ATR, powder): 2925, 2141, 1608, 1461, 1441, 1327, 1209, 1190, 1171, 1118, 1076, 919, 904, 849, 803, 741, 702, 657 cm^{-1}

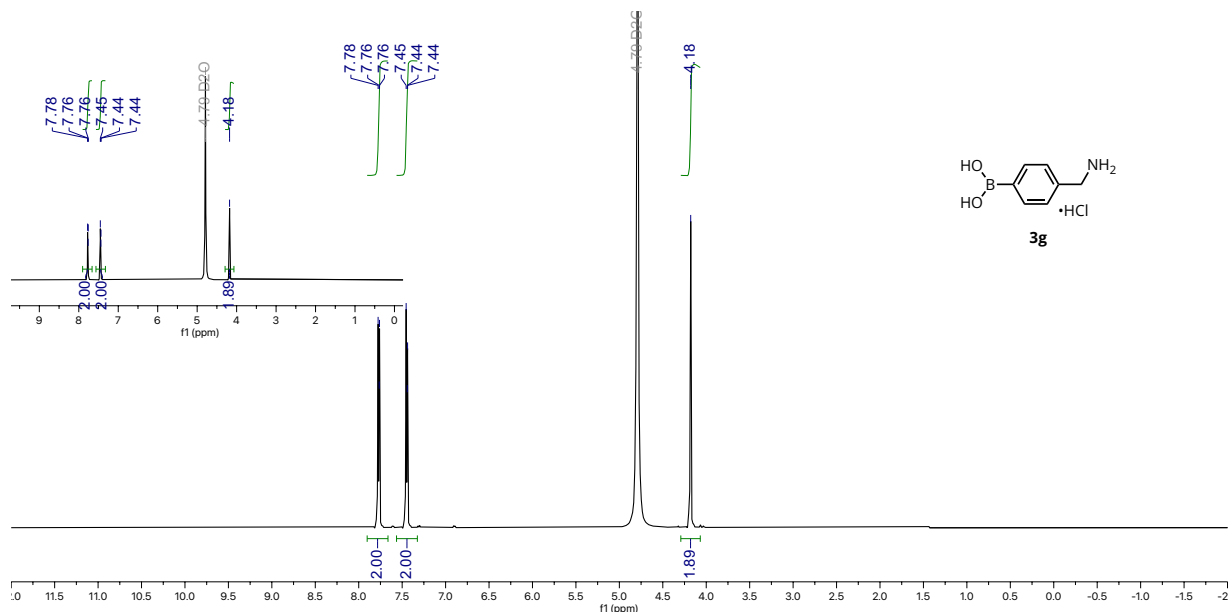


Figure S36. ^1H NMR (500 MHz, D_2O) spectrum of **3g**

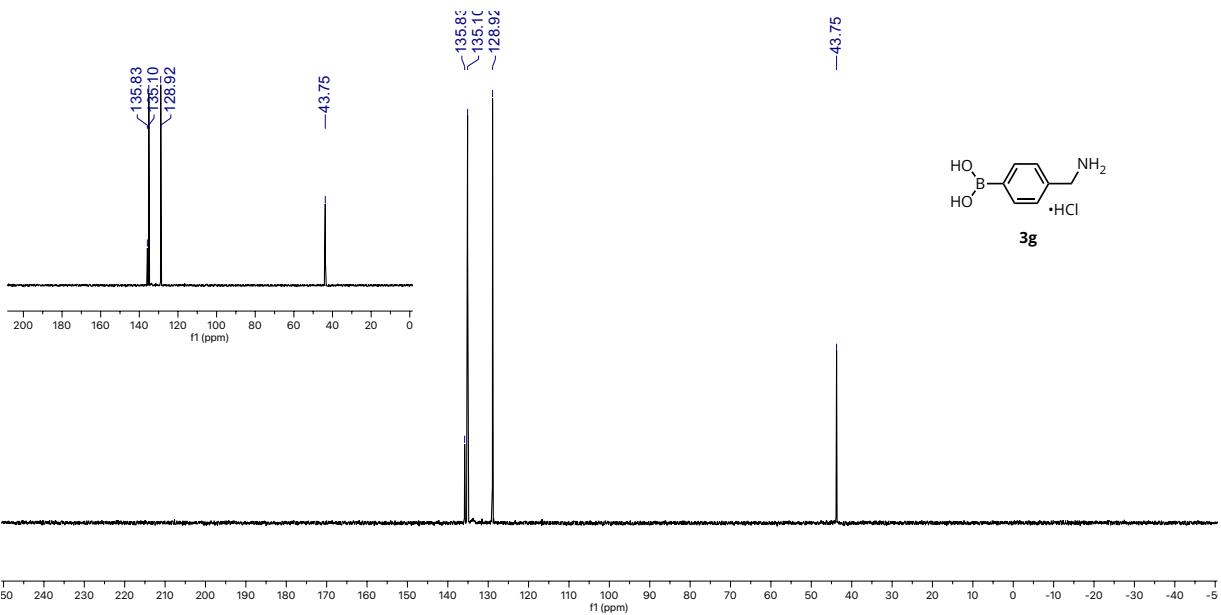


Figure S37. ^{13}C NMR (125 MHz, D_2O) spectrum of **3g**

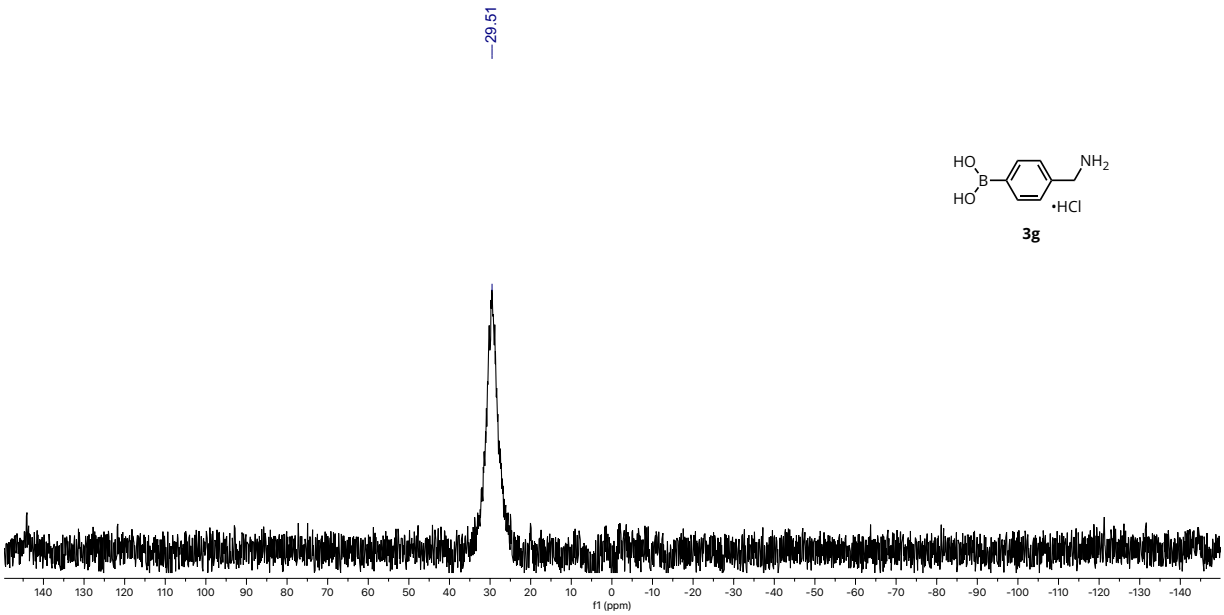


Figure S38. ^{11}B NMR (160 MHz, D_2O) spectrum of **3g**

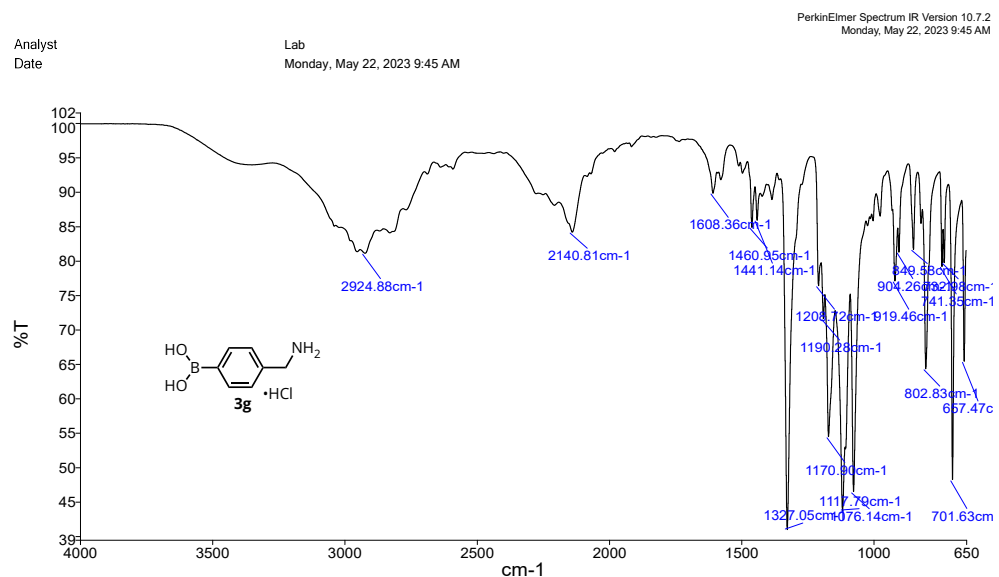
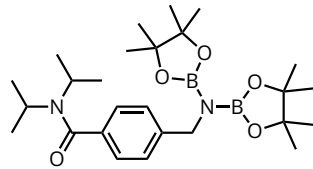


Figure S39. FTIR spectrum of **3g**

*4-((bis(4,4,5,5-tetramethyl-1,3,2-dioxaborolan-2-yl)amino)methyl)-
N,N-diisopropylbenzamide (**2h**)*



The general procedure was followed using 4-cyano-N,N-diisopropylbenzamide, pinacolborane and toluene (^1H NMR yield: 90%).

- ^1H NMR (500 MHz, C_6D_6) δ 7.47 (d, $J = 7.8$ Hz, 2H), 7.27 (d, $J = 7.8$ Hz, 2H), 4.49 (s, 2H), 1.01 (d, $J = 2.4$ Hz, 36H).
- ^{11}B NMR (160 MHz, C_6D_6): δ 28.6.

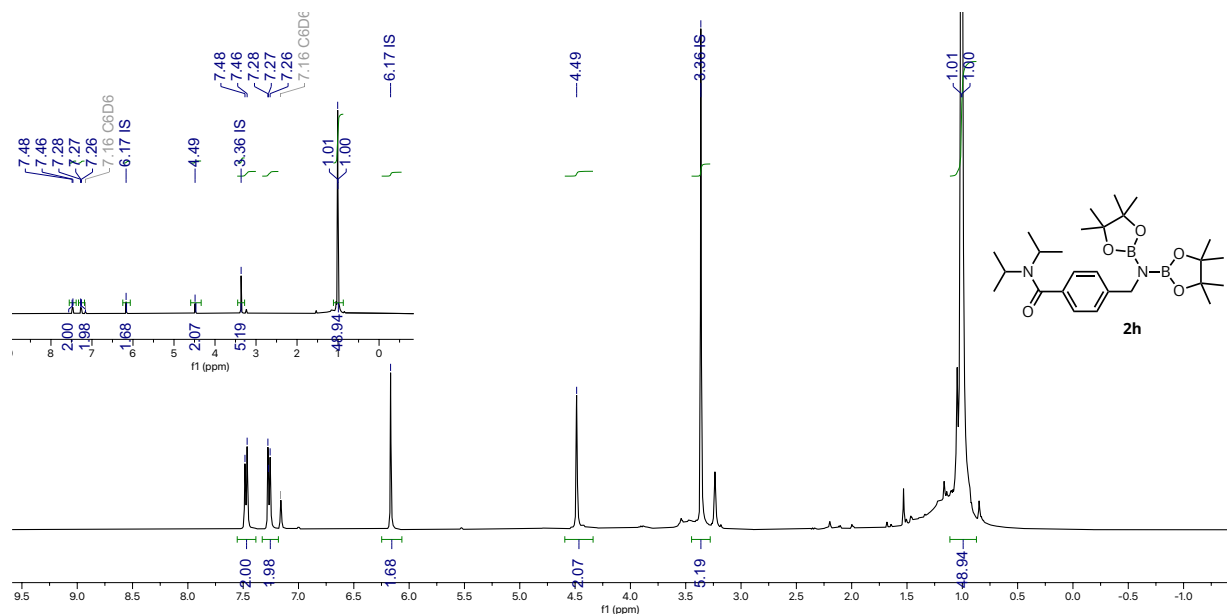


Figure S40. ^1H NMR (500 MHz, C_6D_6) spectrum of **2h**

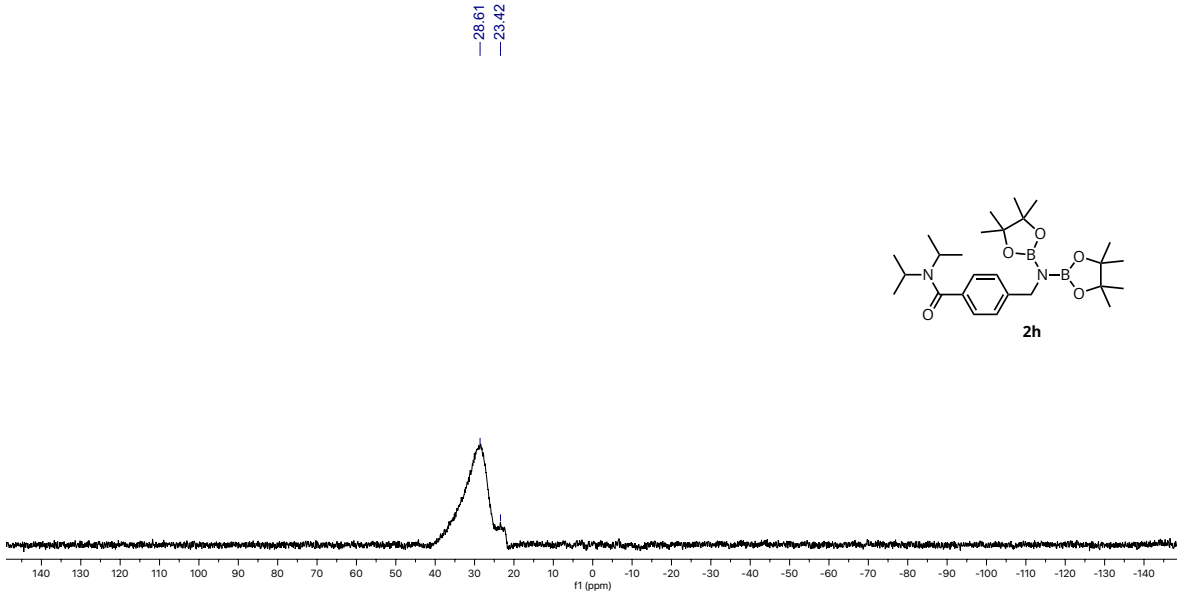
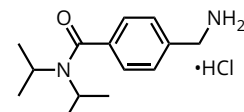


Figure S41. ^{11}B NMR (160 MHz, C_6D_6) spectrum of **2h**

*4-(aminomethyl)-N,N-diisopropylbenzamide hydrochloride (**3h**)*

The isolation protocol was followed to yield **3h** as white solid (36 mg, 64%).



- ^1H NMR (500 MHz, D_2O) δ 7.54 (d, $J = 8.2$ Hz, 2H), 7.41 (d, $J = 8.2$ Hz, 2H), 4.23 (s, 2H), 3.76 (sep, $J = 6.7$ Hz, 1H), 3.75 (sep, $J = 6.7$ Hz, 1H), 1.48 (d, $J = 6.8$ Hz, 6H), 1.15 (d, $J = 6.6$ Hz, 6H).
- ^{13}C NMR (125 MHz, D_2O) δ 172.5, 138.1, 133.5, 129.2, 125.8, 52.2, 46.0, 42.6, 19.6, 19.4.
- LRMS (ESI): for $[\text{M}]^+ = [\text{C}_{14}\text{H}_{23}\text{N}_2\text{O}]^+$, calculated: m/z = 235.18; found: m/z = 235.5
- FTIR (ATR, powder): 3364, 2975, 2206, 1621, 1509, 1444, 1372, 1341, 1154, 1216, 1097, 919, 877, 850, 835 cm^{-1}

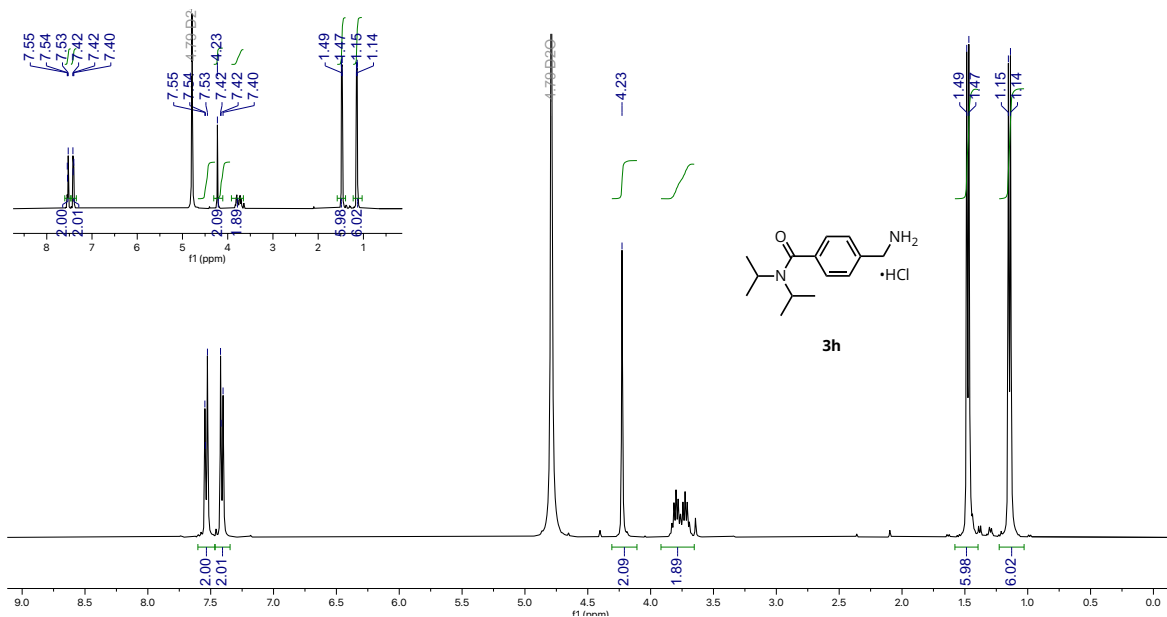


Figure S42. ^1H NMR (500 MHz, D_2O) spectrum of **3h**

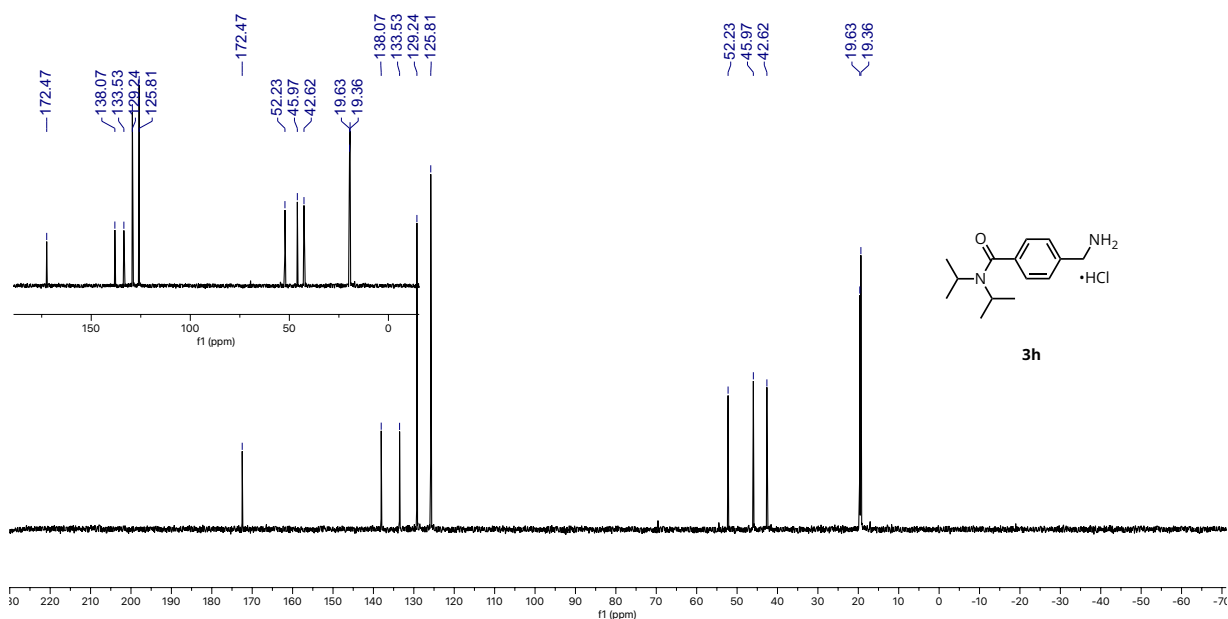


Figure S43. ^{13}C NMR (125 MHz, D_2O) spectrum of **3h**

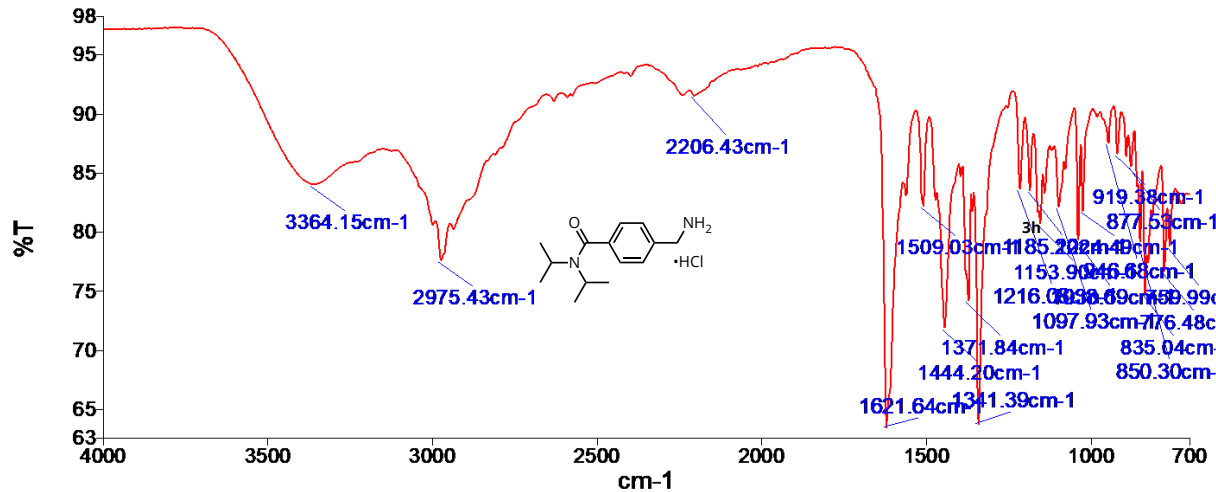
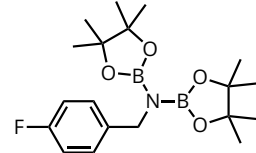


Figure S44. FTIR spectrum of **3g**

N-(4-fluorobenzyl)-4,4,5,5-tetramethyl-*N*-(4,4,5,5-tetramethyl-1,3,2-dioxaborolan-2-yl)-1,3,2-dioxaborolan-2-amine (**2k**)



The general procedure was followed using 4-fluorobenzonitrile, pinacolborane and C₆D₆ (¹H NMR yield: 99%). ¹H and ¹⁹F NMR spectroscopic data are consistent with literature values.¹¹

- ¹H NMR (500 MHz, C₆D₆) δ 7.38 (t, J = 8.6 Hz, 2H), 6.87 (t, J = 8.6 Hz, 2H), 4.41 (s, 2H), 1.01 (d, J = 5.8 Hz, 24H)
- ¹⁹F NMR (376 MHz, C₆D₆): δ -117.1.

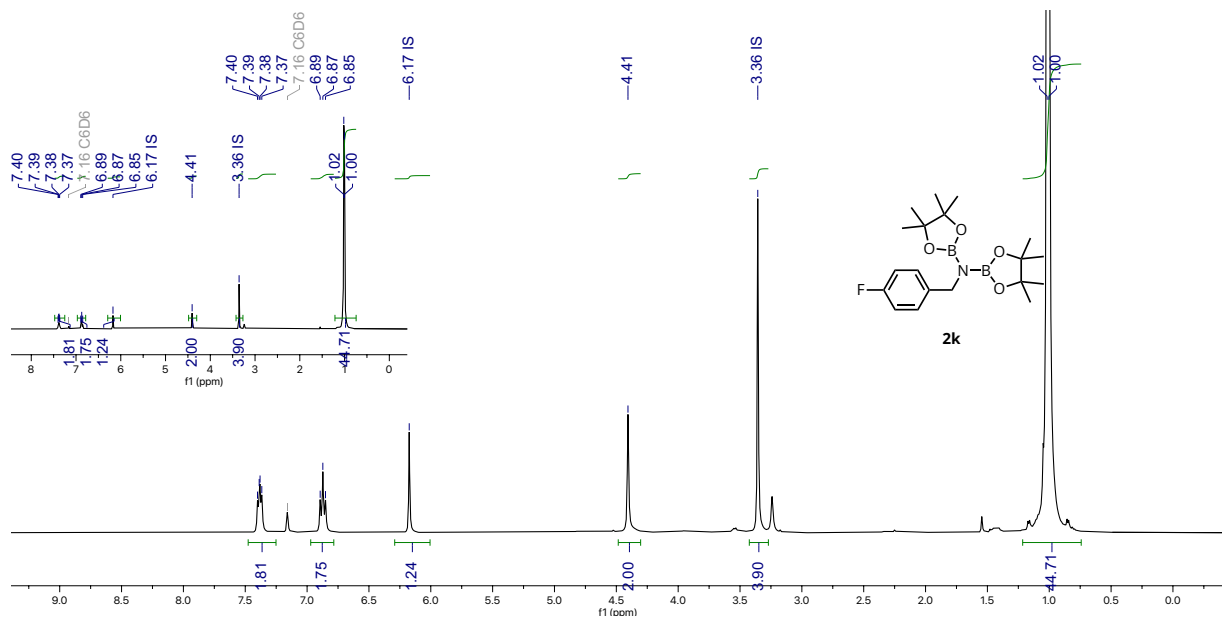


Figure S45. ^1H NMR (500 MHz, C_6D_6) spectrum of **2k**

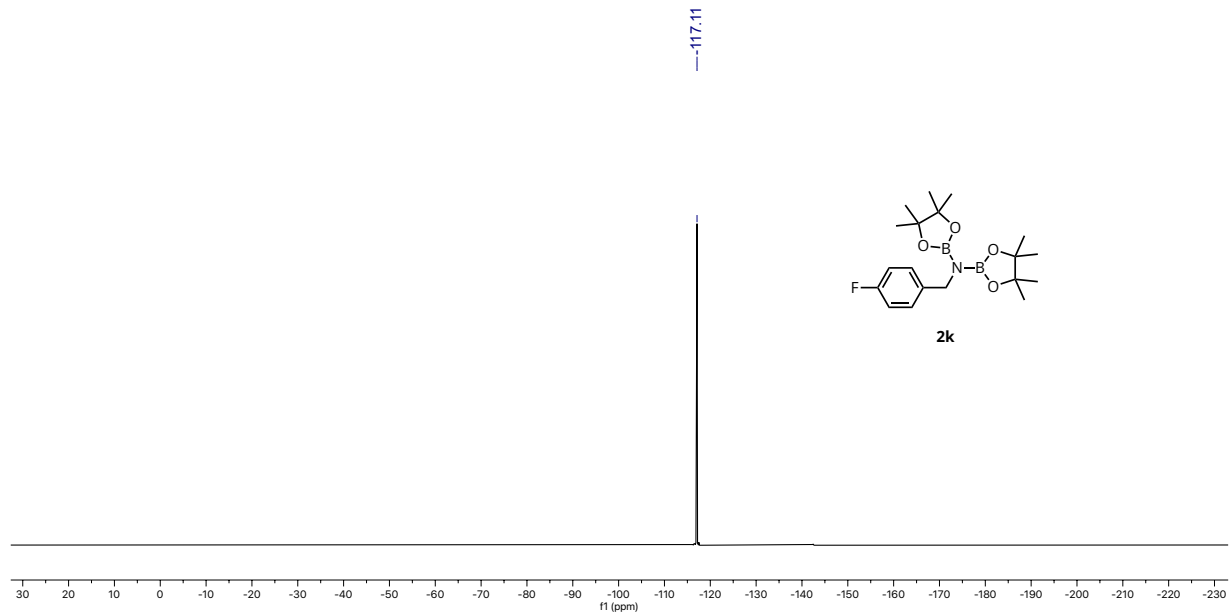
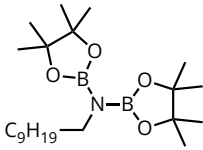


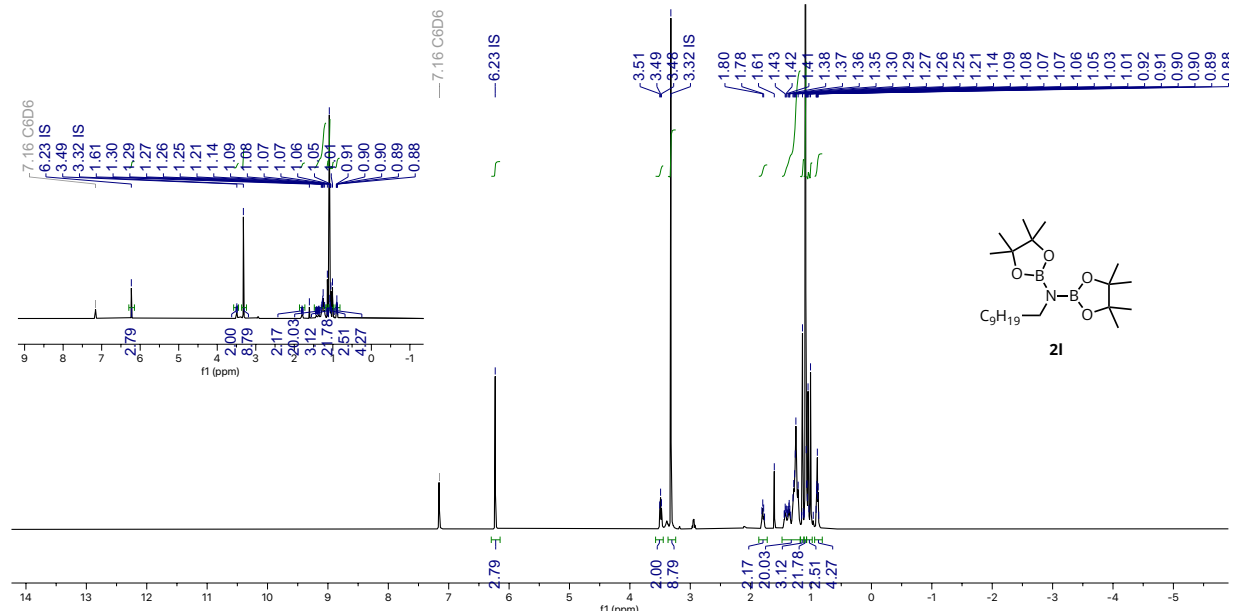
Figure S46. ^{19}F NMR (376 MHz, C_6D_6) spectrum of **2k**

N-decyl-4,4,5,5-tetramethyl-*N*-(4,4,5,5-tetramethyl-1,3,2-dioxaborolan-2-yl)-1,3,2-dioxaborolan-2-amine (**2I**)



The general procedure was followed using decanenitrile, pinacolborane and toluene (¹H NMR yield: 97%)

- ¹H NMR (500 MHz, C₆D₆) δ 3.49 (t, *J* = 7.2 Hz, 2H), 1.79 (tt, *J* = 7.2, 7.2 Hz, 2H), 1.48 – 1.17 (m, 11H), 1.14 (s, 2H), 1.09 (s, 24H), 1.05 (s, 1H), 1.01 (s, 1H), 0.94 – 0.81 (m, 3H)
- ¹³C NMR (125 MHz, C₆D₆): δ 82.2, 44.4, 34.0, 32.3, 30.2, 30.1, 30.1, 29.8, 27.3, 24.8, 23.1, 14.4.
- ¹¹B NMR (160 MHz, C₆D₆): δ 27.2



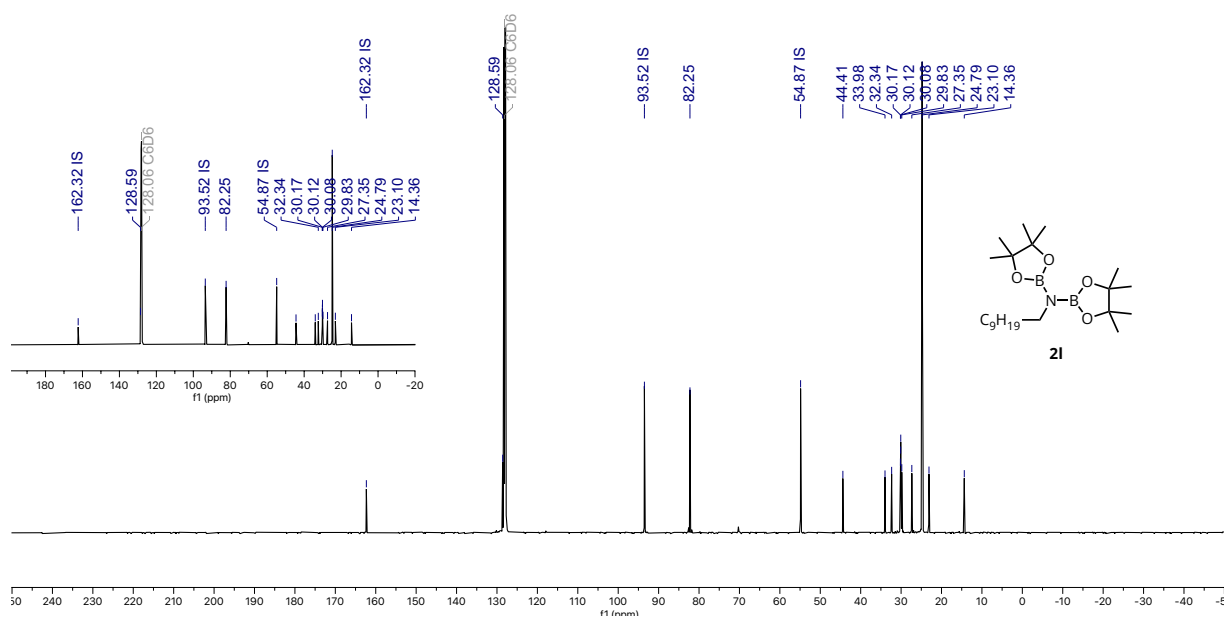


Figure S48. ^{13}C NMR (125 MHz, C_6D_6) spectrum of **2I**

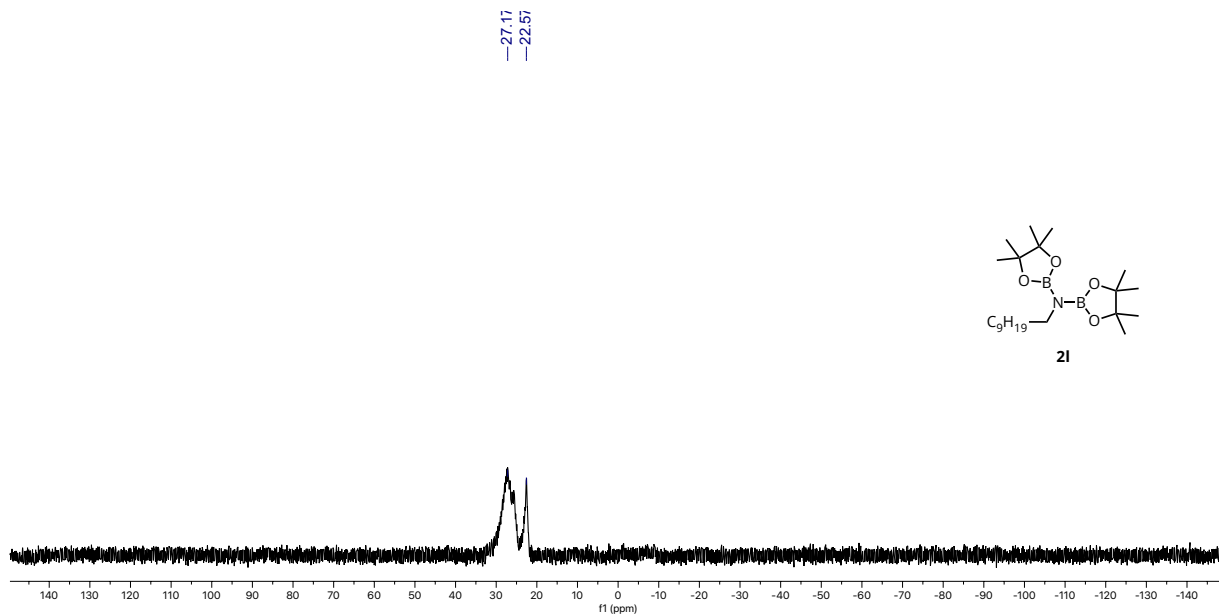
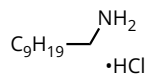


Figure S49. ^{11}B NMR (160 MHz, C_6D_6) spectrum of **2I**

decan-1-amine hydrochloride (3I)



The isolation protocol was followed to yield **3I** as white solid (19 mg, 49%). ^1H NMR spectroscopic data are consistent with literature value.¹⁷

- ^1H NMR (500 MHz, D_2O) δ 2.97 (t, $J = 7.8$ Hz, 2H), 2.10 (s, 1H), 1.64 (t, $J = 7.5$ Hz, 2H), 1.39 – 1.24 (m, 14H) 0.84 (d, $J = 7.3$ Hz, 3H).

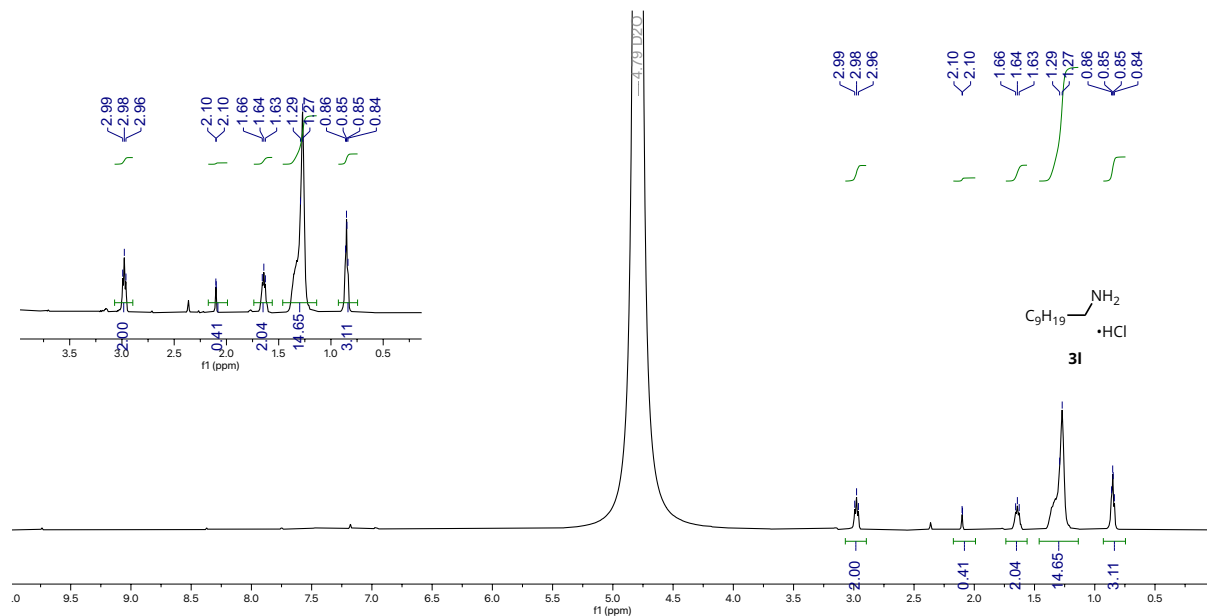
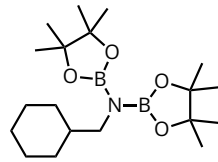


Figure S50. ^1H NMR (500 MHz, D_2O) spectrum of **3I**

N-(cyclohexylmethyl)-4,4,5,5-tetramethyl-N-(4,4,5,5-tetramethyl-1,3,2-dioxaborolan-2-yl)-1,3,2-dioxaborolan-2-amine (2m)



The general procedure was followed using cyclohexanecarbonitrile, pinacolborane and toluene (^1H NMR yield: 78%). ^1H NMR spectroscopic data are consistent with literature values.¹⁴

- ^1H NMR (500 MHz, C_6D_6) δ 3.32 (d, $J = 7.4$ Hz, 2H), 2.00 – 1.85 (m, 2H), 1.85 – 1.67 (m, 3H), 1.61 (s, 1H), 1.51 (s, 1H), 1.39 – 0.77 (m, 28H).

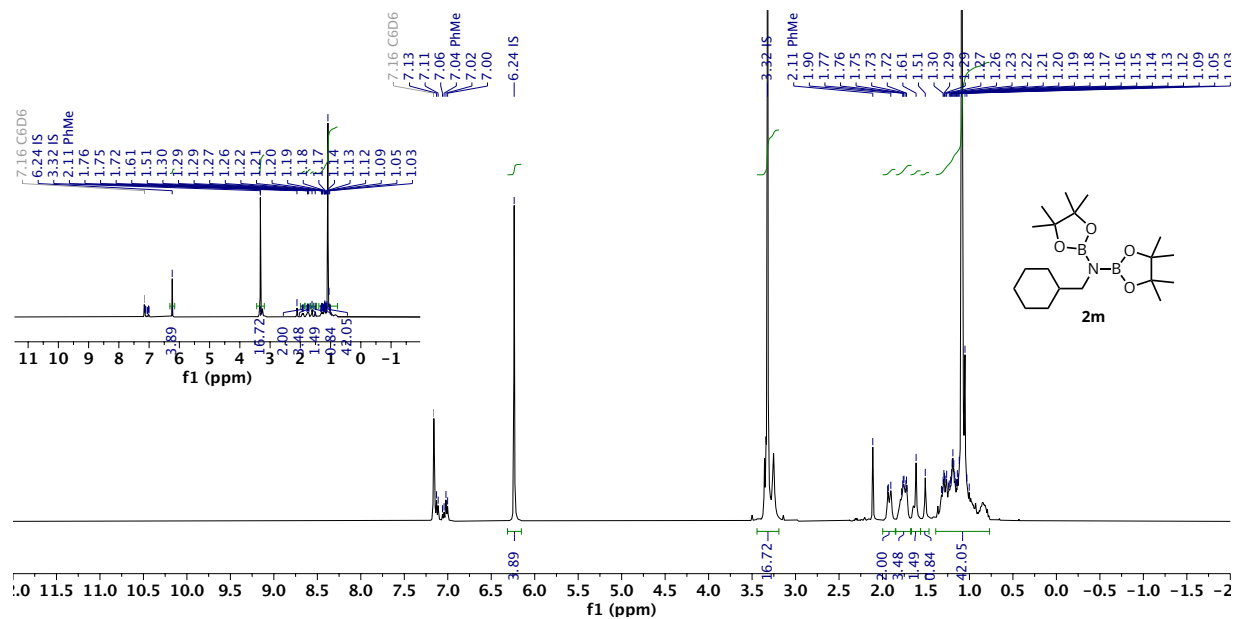
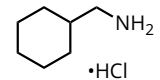


Figure S51. ^1H NMR (500 MHz, C_6D_6) spectrum of **2m**

cyclohexylmethanamine hydrochloride (3m)



The isolation protocol was followed to yield **3m** as white solid (13 mg, 44%). ¹H NMR spectroscopic data are consistent with literature values.¹³

¹H NMR (500 MHz, D₂O) δ 2.83 (d, *J* = 7.0 Hz, 2H), 1.77 – 1.67 (m, 4H), 1.67 – 1.57 (m, 2H), 1.34 – 1.09 (m, 3H), 1.06 – 0.90 (m, 2H).

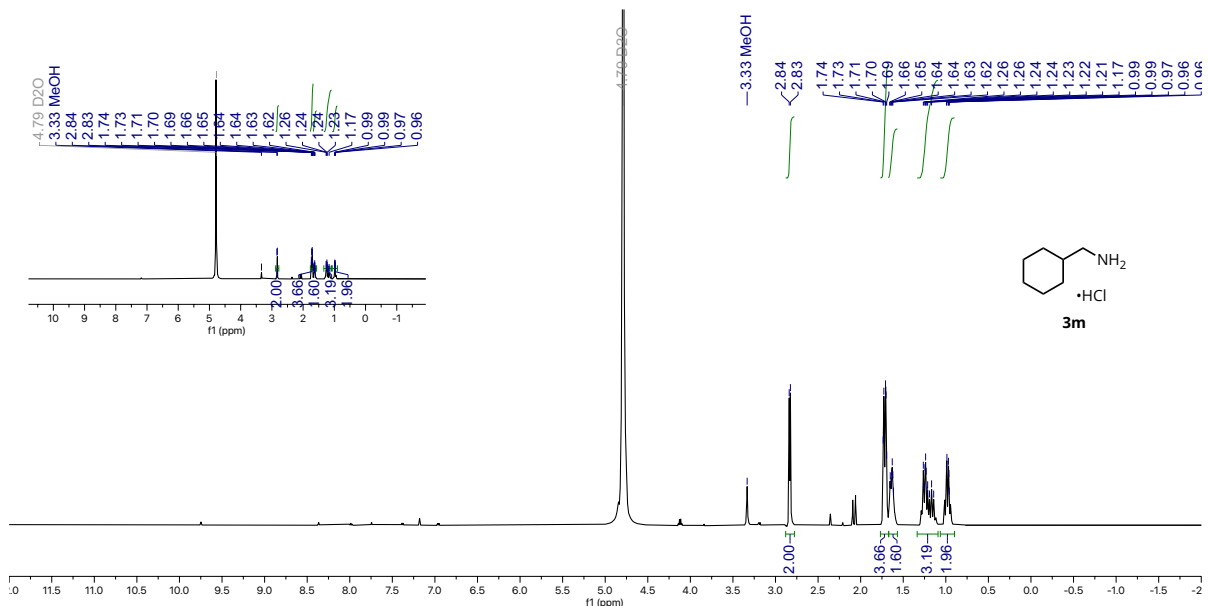
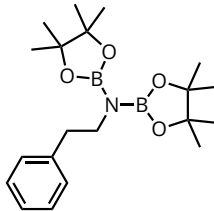


Figure S52. ^1H NMR (500 MHz, D_2O) spectrum of **3m**

4,4,5,5-tetramethyl-N-phenethyl-N-(4,4,5,5-tetramethyl-1,3,2-dioxaborolan-2-yl)-1,3,2-dioxaborolan-2-amine (2n)



The general procedure was followed using 2-phenylacetonitrile, pinacolborane and toluene (^1H NMR yield: 96%). ^1H , ^{13}C and ^{11}B spectroscopic data are consistent with literature values.¹²

- ^1H NMR (500 MHz, C_6D_6) δ 7.30 (d, $J = 7.6$ Hz, 2H), 7.22 – 6.97 (m, 3H), 3.69 (t, $J = 6.9$ Hz, 2H), 3.02 (t, $J = 6.9$ Hz, 2H), 1.03 (s, 24H).
 - ^{13}C NMR (126 MHz, C_6D_6): δ 140.8, 129.8, 128.5, 126.1, 82.3, 46.1, 40.3, 24.8.
 - ^{11}B NMR (160 MHz, C_6D_6): δ 27.2.

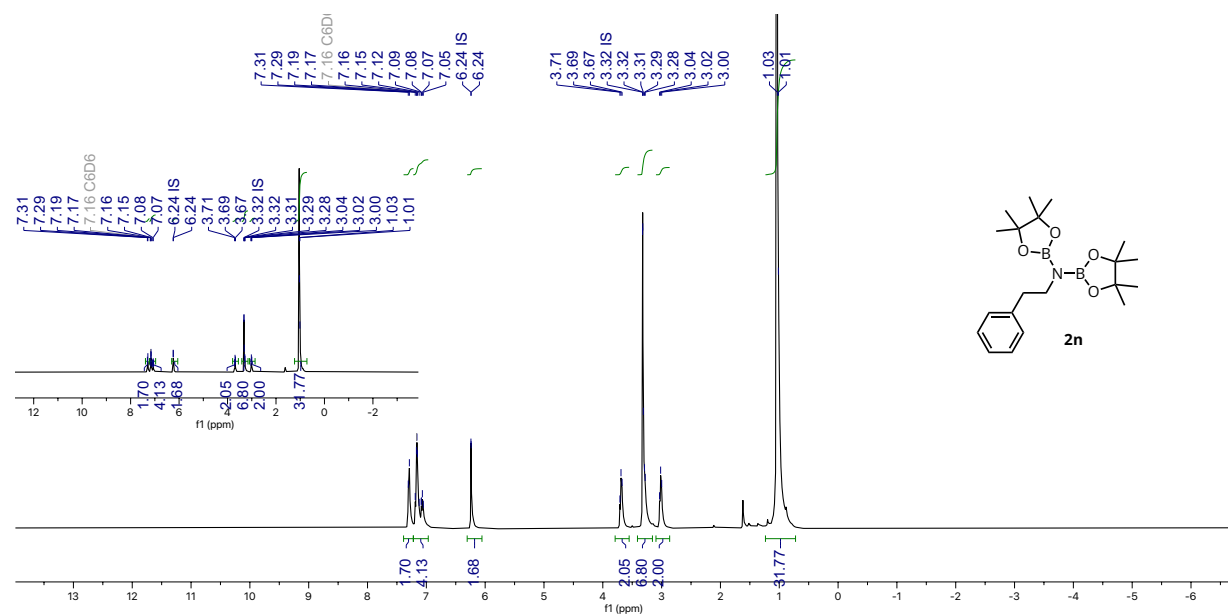


Figure S53. ^1H NMR (500 MHz, C_6D_6) spectrum of **2n**

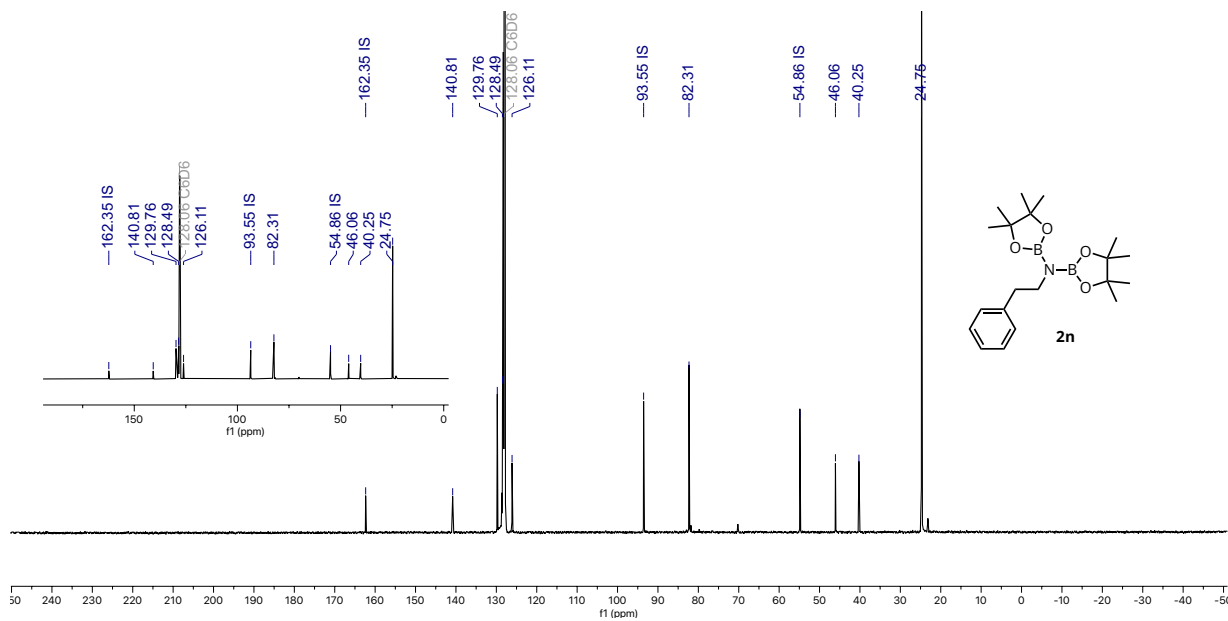


Figure S54. ^{13}C NMR (125 MHz, C_6D_6) spectrum of **2n**

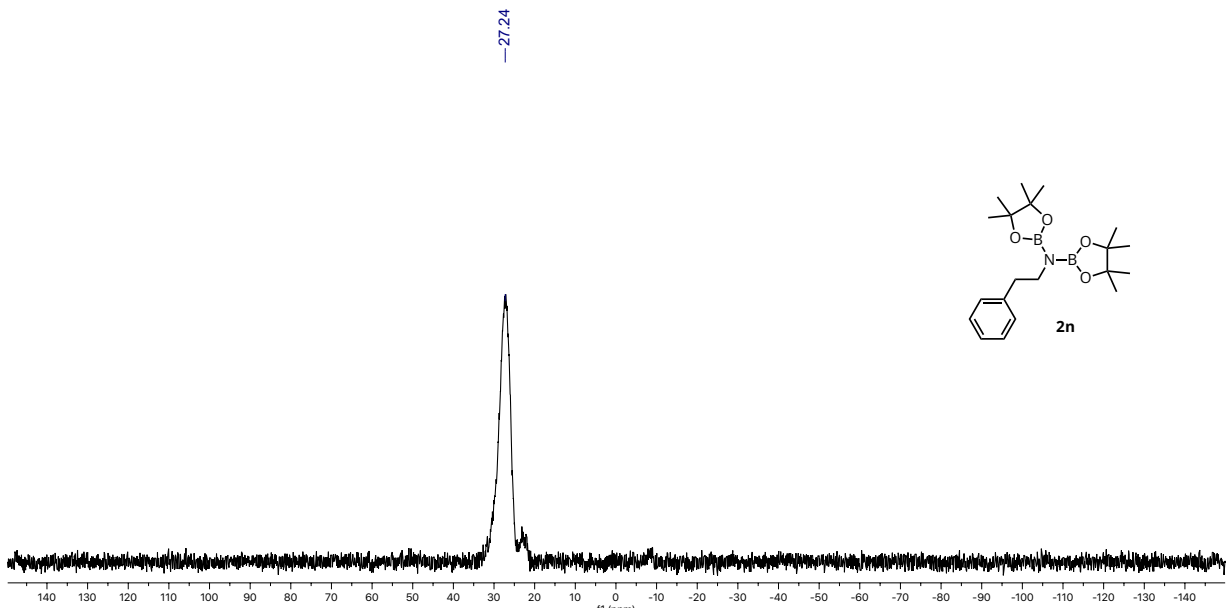
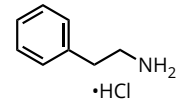


Figure S55. ^{11}B NMR (160 MHz, C_6D_6) spectrum of **2n**

2-phenylethan-1-amine hydrochloride (3n)

The isolation protocol was followed to yield **3n** as a white solid (23 mg, 74%). ¹H NMR spectroscopic data are consistent with literature values.¹⁸



- ¹H NMR (500 MHz, D₂O) δ 7.59 – 7.09 (m, 5H), 3.30 (t, J = 7.3 Hz, 2H), 3.02 (t, J = 7.3 Hz, 2H).

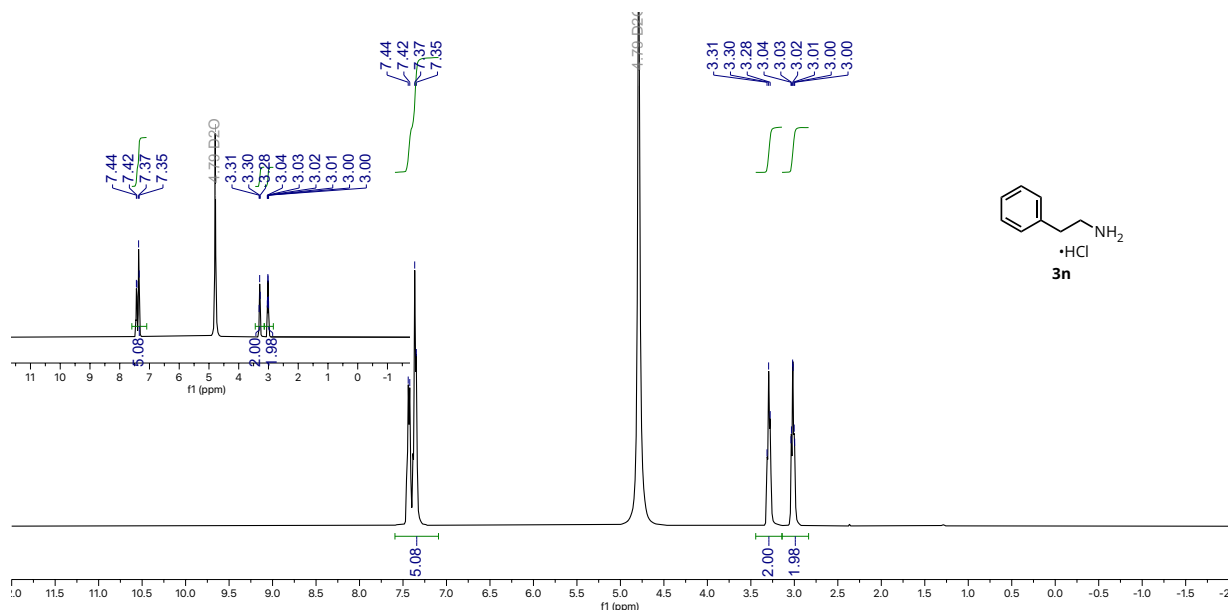
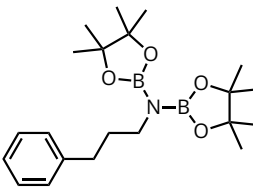


Figure S56. ¹H NMR (500 MHz, D₂O) spectrum of **3n**

4,4,5,5-tetramethyl-N-(3-phenylpropyl)-N-(4,4,5,5-tetramethyl-1,3,2-dioxaborolan-2-yl)-1,3,2-dioxaborolan-2-amine (2o**)**

The general procedure was followed using 3-phenylpropanenitrile, pinacolborane and toluene (^1H NMR yield: 99%).



- ^1H NMR (500 MHz, C_6D_6) δ 7.24 – 7.09 (m, 5H), 3.50 (t, J = 7.8 Hz, 2H), 2.68 (t, J = 7.8 Hz, 2H), 2.14 – 1.97 (m, 2H), 1.07 (s, 24H).
- ^{11}B NMR (160 MHz, C_6D_6): δ 27.4.

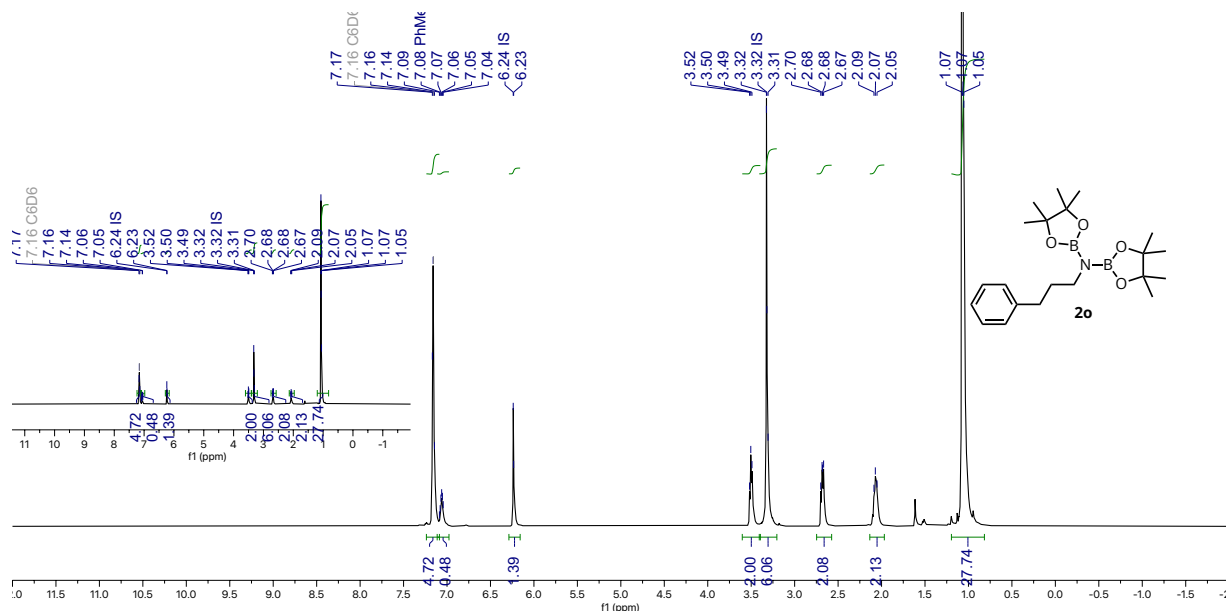


Figure S57. ^1H NMR (500 MHz, C_6D_6) spectrum of **2o**

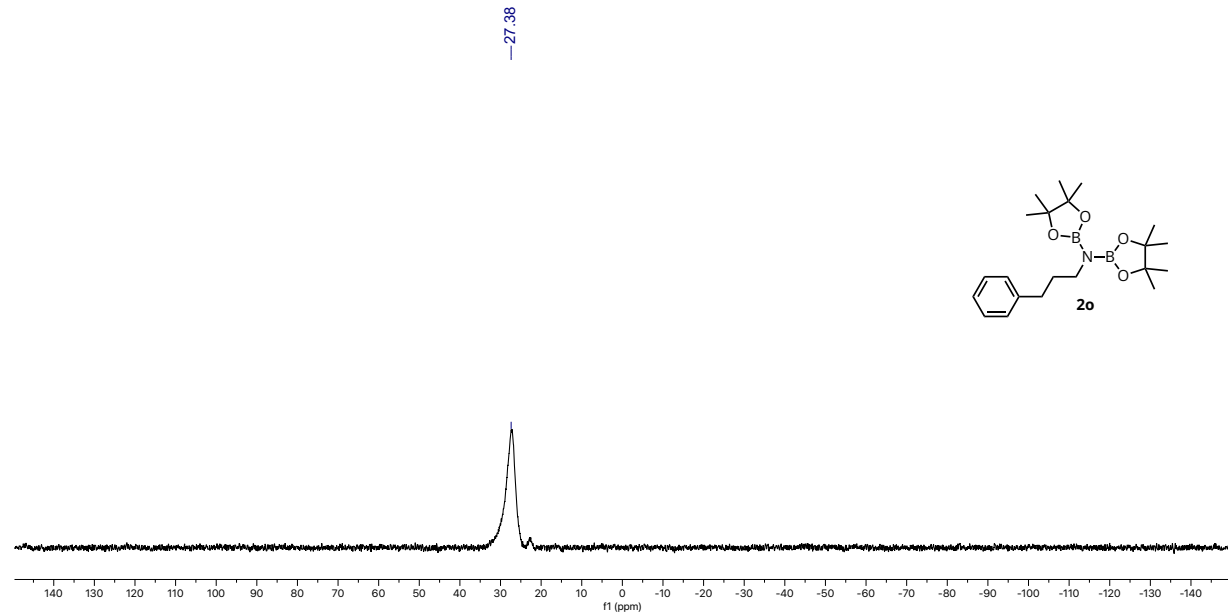
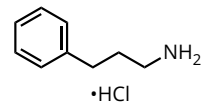


Figure S58. ¹¹B NMR (160 MHz, C₆D₆) spectrum of **2o**

3-phenylpropan-1-amine hydrochloride (**3o**)

The isolation protocol was followed to yield **3o** as a white solid (Isolated yield: 44%). ¹H NMR spectroscopic data are consistent with literature values.¹³



- ¹H NMR (500 MHz, D₂O) δ 7.51 – 7.15 (m, 5H), 3.13 – 2.89 (m, 2H), 2.84 – 2.61 (m, 2H), 2.15 – 1.83 (m, 2H).

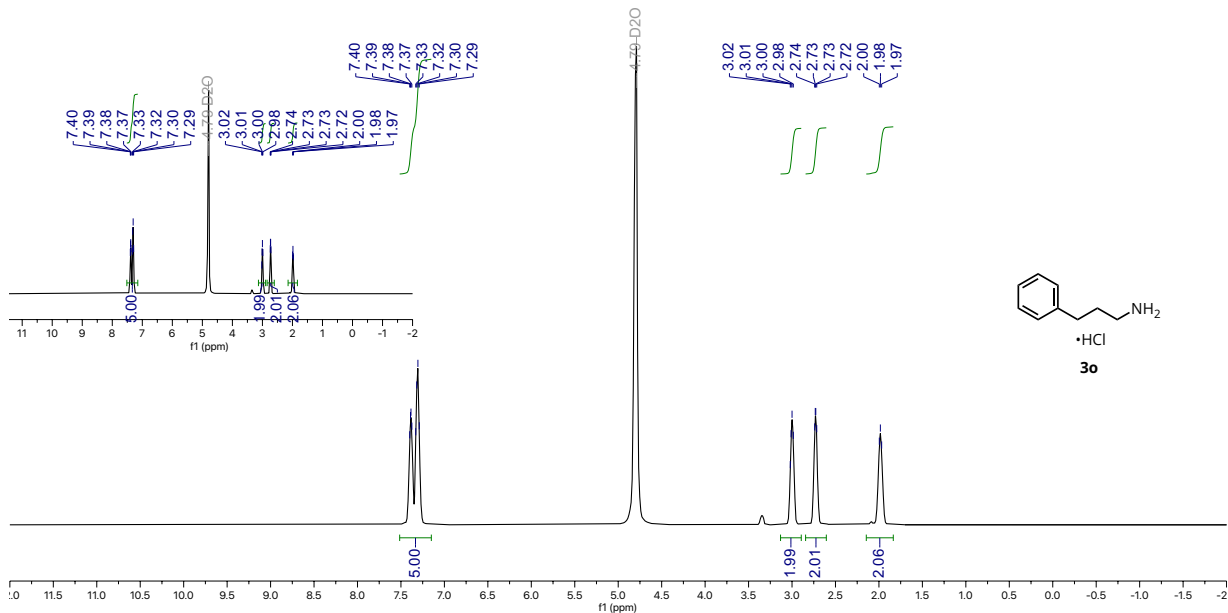
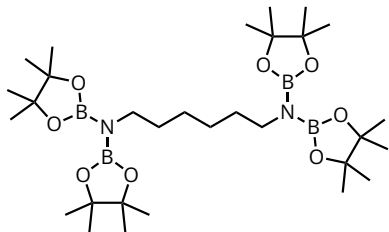


Figure S59. ¹H NMR (500 MHz, D₂O) spectrum of **3o**

N¹,N¹,N⁶,N⁶-tetrakis(4,4,5,5-tetramethyl-1,3,2-dioxaborolan-2-yl)hexane-1,6-diamine (2p)

The general procedure was followed using decanenitrile, pinacolborane and toluene (¹H NMR yield: 99%)



- ¹H NMR (500 MHz, C₆D₆) δ 3.44 (t, *J* = 7.1 Hz, 4H), 1.88 – 1.65 (m, 4H), 1.54 – 1.40 (m, 4H), 1.08 (s, 48H).
- ¹³C NMR (125 MHz, C₆D₆): δ 82.2, 44.4, 34.3, 27.5, 24.8.
- ¹¹B NMR (160 MHz, C₆D₆): δ 27.9

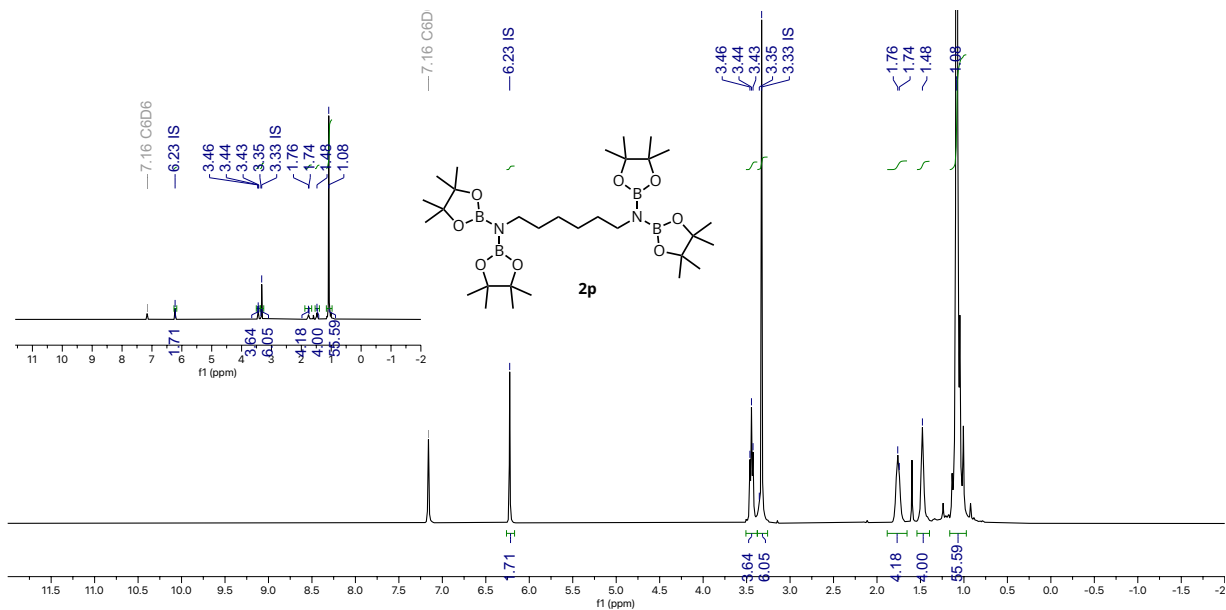


Figure S60. ¹H NMR (500 MHz, C₆D₆) spectrum of **2p**

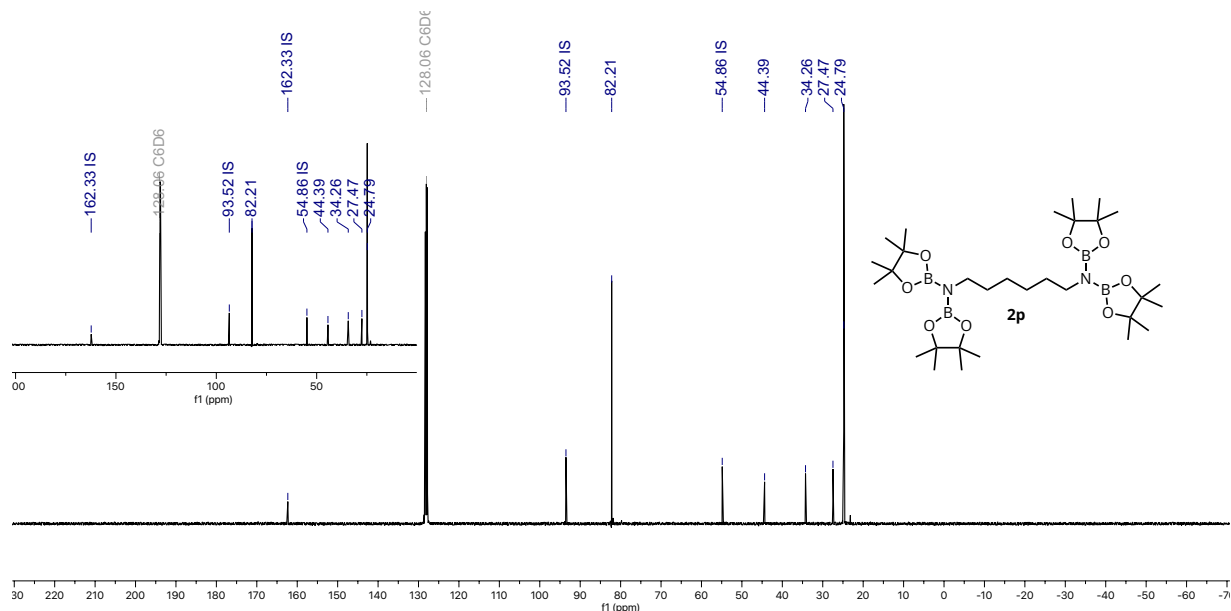


Figure S61. ^{13}C NMR (125 MHz, C_6D_6) spectrum of **2p**

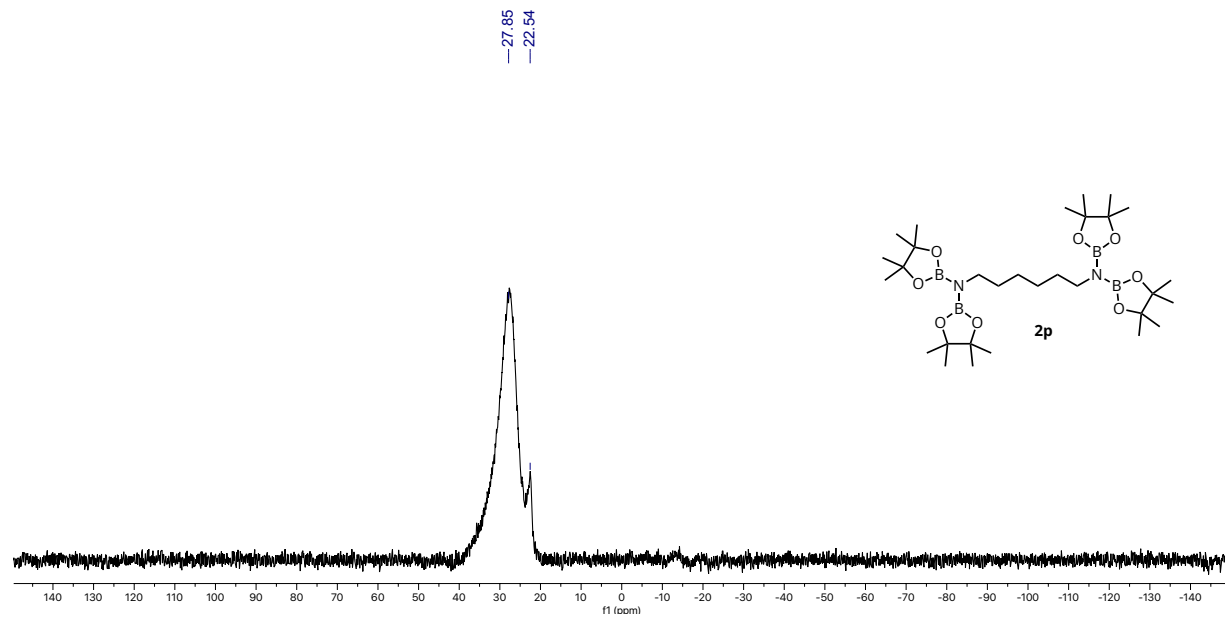
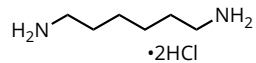


Figure S62. ^{11}B NMR (160 MHz, C_6D_6) spectrum of **2p**

hexane-1,6-diamine di(hydrochloride) (3p)



The isolation protocol was followed to yield **3p** as white solid (23 mg, 66 %).

- ^1H NMR (500 MHz, D_2O) δ 2.97 (br s, 4H), 1.65 (br s, 4H), 1.39 (br s, 4H).
- ^{13}C NMR (125 MHz, D_2O) δ 40.5, 28.5, 26.1.
- LRMS (ESI): for $[\text{M}]^+ = [\text{C}_6\text{H}_{17}\text{N}_2]^+$, calculated: $m/z = 117.1$; found: $m/z = 117.2$
- FTIR (ATR, powder): 2926.3, 2162.1, 1564.2, 1463.0, 1323.6, 1162.2, 1105.4, 924.3, 997.0, 851.5, 799.3, 704.4, 657.2 cm^{-1}

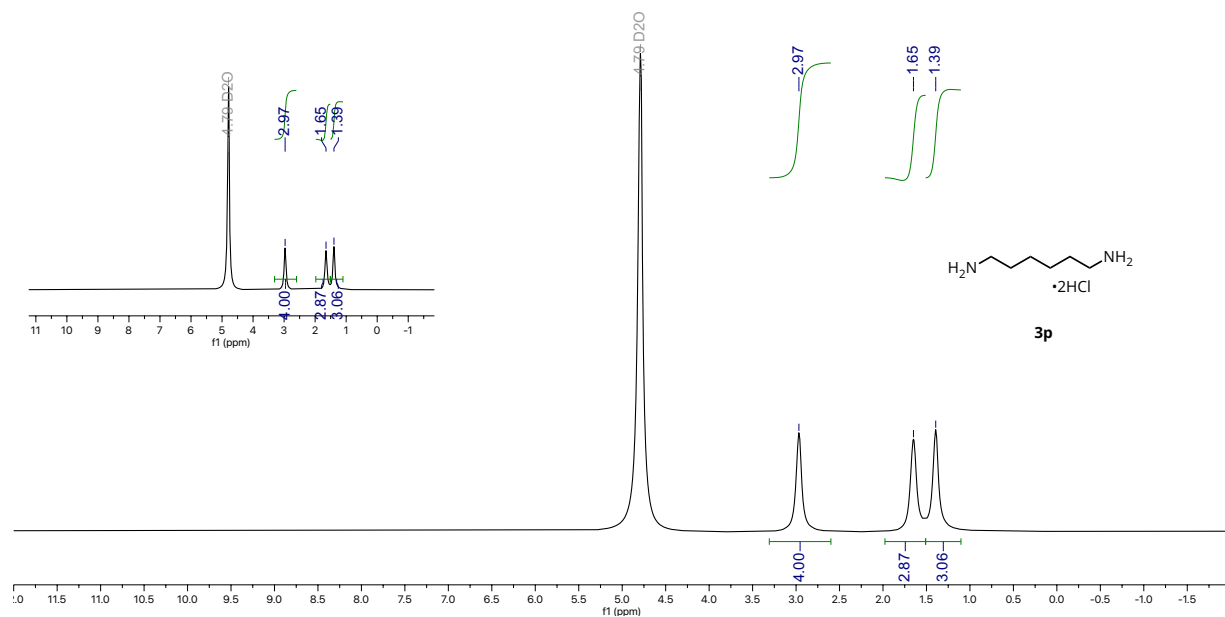


Figure S63. ^1H NMR (500 MHz, D_2O) spectrum of **3p**

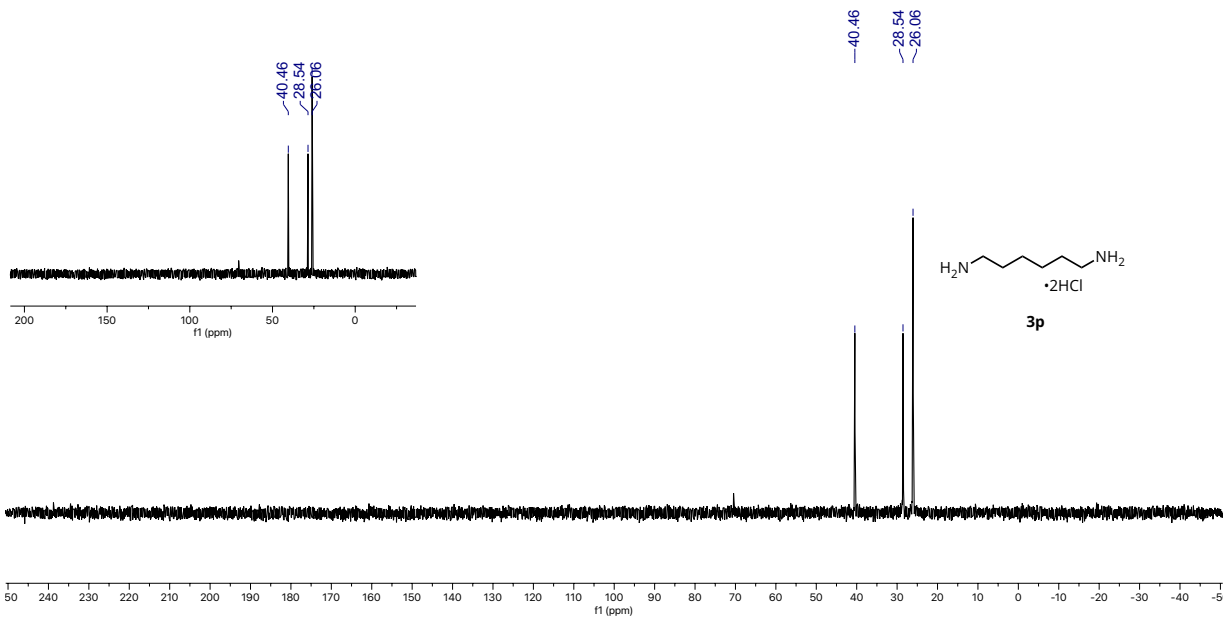


Figure S64. ^{13}C NMR (125 MHz, D_2O) spectrum of **3p**

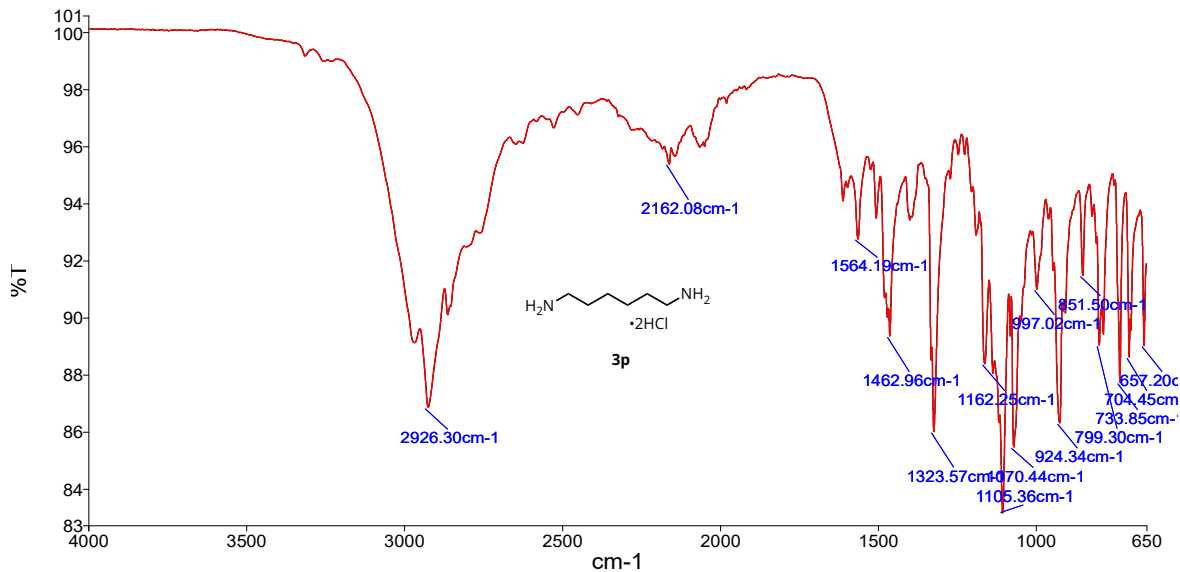


Figure S65. FTIR spectrum of **3p**

4,4,5,5-tetramethyl-N-(4,4,5,5-tetramethyl-1,3,2-dioxaborolan-2-yl)-N-(4-(1-((4,4,5,5-tetramethyl-1,3,2-dioxaborolan-2-yl)oxy)ethyl)benzyl)-1,3,2-dioxaborolan-2-amine (2q**)**

The general procedure was followed using 4-acetylbenzonitrile, pinacolborane and toluene (^1H NMR yield: 98%). ^1H , ^{11}B and ^{13}C NMR spectroscopic data are consistent with literature values.¹⁹

- ^1H NMR (500 MHz, C_6D_6) δ 7.52 (d, J = 8.2 Hz, 2H), 7.39 (d, J = 8.2 Hz, 2H), 5.41 (q, J = 6.4 Hz, 1H), 4.54 (s, 2H), 1.46 (d, J = 6.4 Hz, 3H), 1.02 (d, J = 6.3 Hz, 36H)
- ^{13}C NMR (125 MHz, C_6D_6): δ 143.4, 142.6, 129.3, 128.6, 125.5, 82.5, 82.4, 72.9, 47.6, 25.7, 24.7
- ^{11}B NMR (160 MHz, C_6D_6): δ 27.2, 23.1

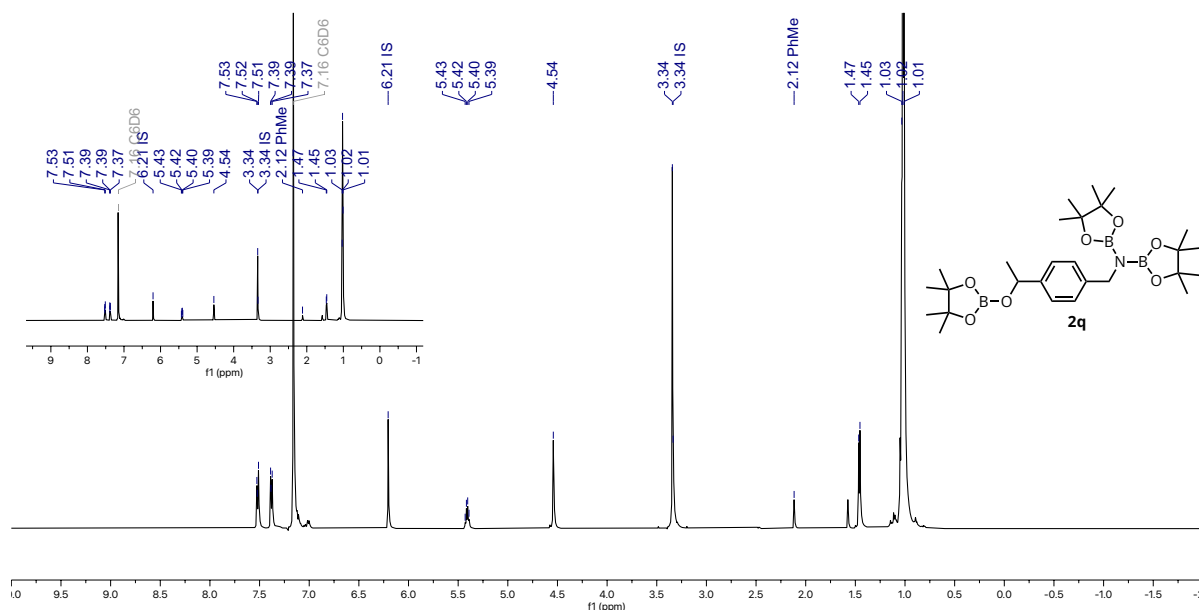
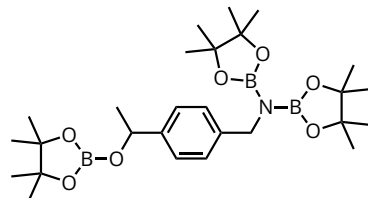


Figure S66. ^1H NMR (500 MHz, C_6D_6) spectrum of **2q**

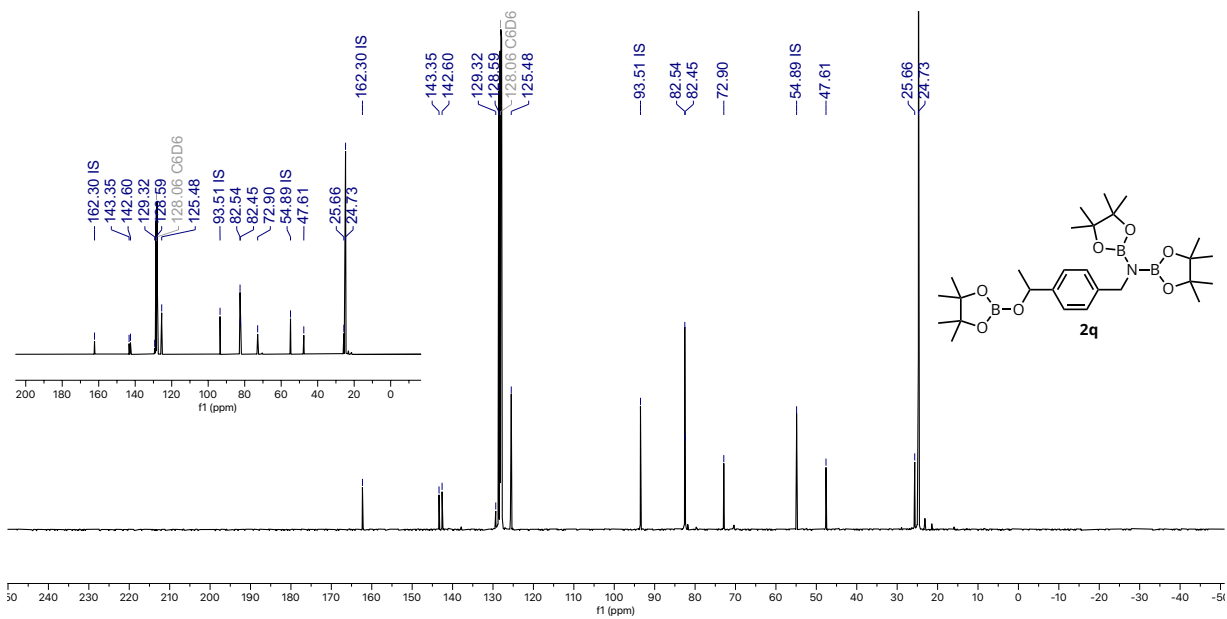


Figure S67. ^{13}C NMR (125 MHz, C_6D_6) spectrum of $\textbf{2q}$

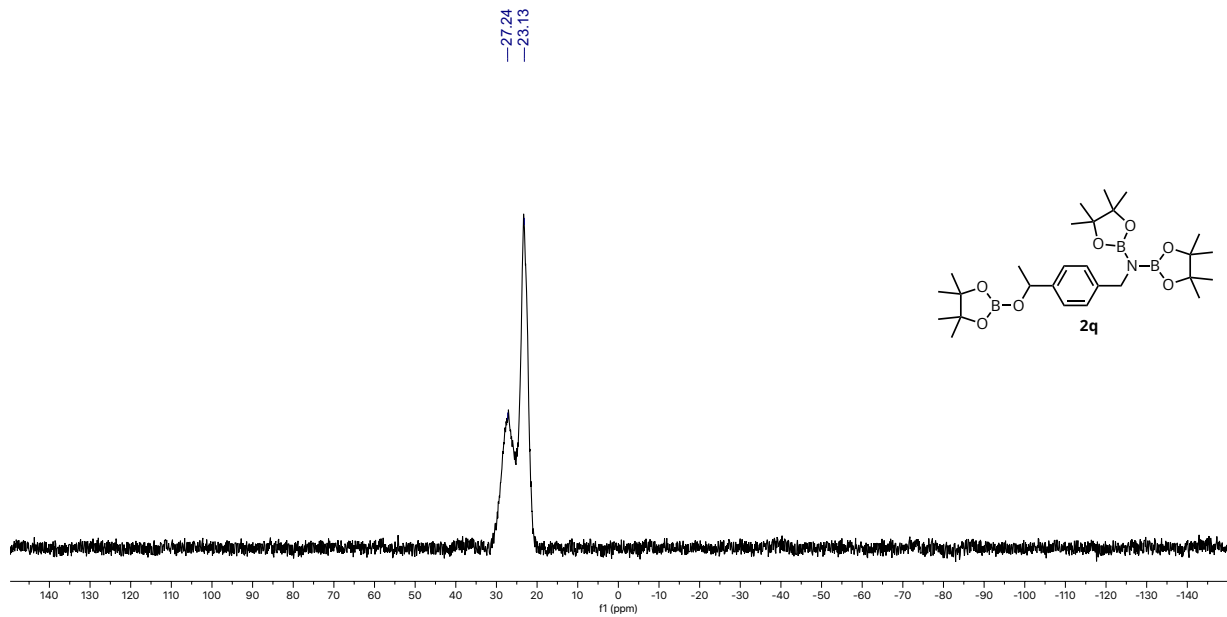
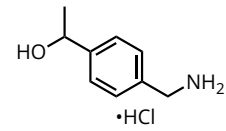


Figure S68. ^{11}B NMR (160 MHz, C_6D_6) spectrum of $\textbf{2q}$

1-(4-(aminomethyl)phenyl)ethan-1-ol hydrochloride (3q)

The isolation protocol was followed to yield **3q** as white solid (25 mg, 67%). ¹H NMR spectroscopic data are consistent with literature values.²⁰



- ¹H NMR (500 MHz, D₂O) δ 7.44 (s, 4H), 4.92 (q, *J* = 6.5 Hz, 1H), 4.16 (s, 2H), 1.45 (d, *J* = 6.5 Hz, 3H).

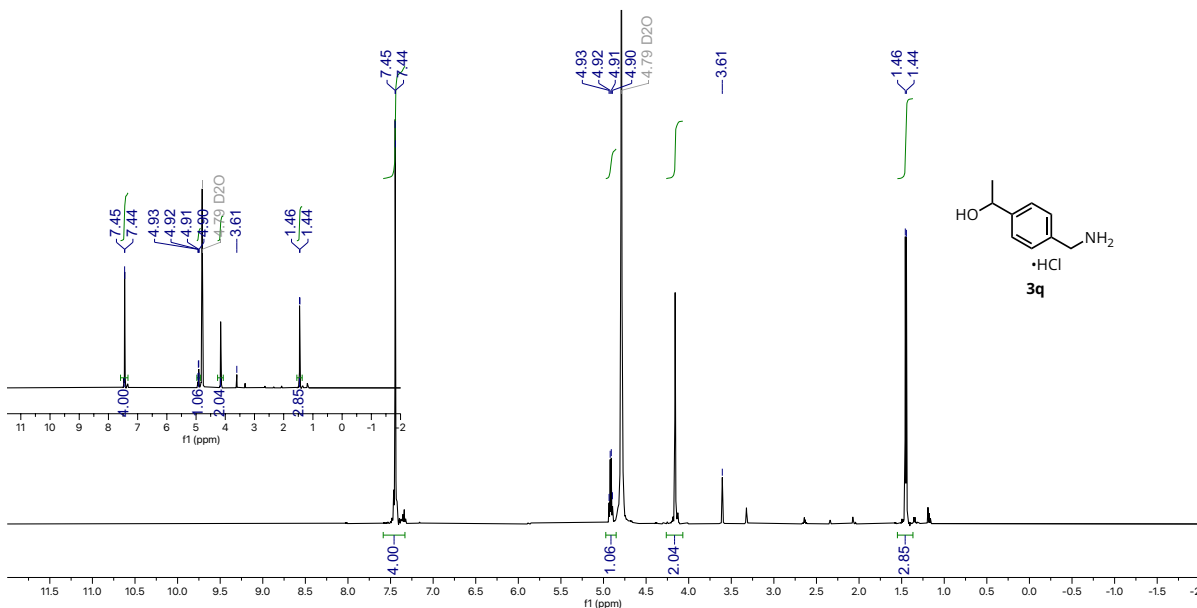


Figure S69. ¹H NMR (500 MHz, D₂O) spectrum of **3q**

4,4,5,5-tetramethyl-N-(4,4,5,5-tetramethyl-1,3,2-dioxaborolan-2-yl)-N-((4,4,5,5-tetramethyl-1,3,2-dioxaborolan-2-yl)oxy)methylbenzyl)-1,3,2-dioxaborolan-2-amine (2r)

The general procedure was followed using methyl 4-cyanobenzoate, pinacolborane and toluene (^1H NMR yield: 38%).

¹H NMR spectroscopic data for **2r** in a mixture with partially hydroborated products are consistent with literature values.¹²

- ^1H NMR (500 MHz, C_6D_6) δ 7.53 (d, $J = 7.6$ Hz, 2H), 7.35 (d, $J = 7.6$ Hz, 2H), 4.97 (s, 2H), 4.55 (s, 2H), 1.26 – 0.74 (s, 36H)

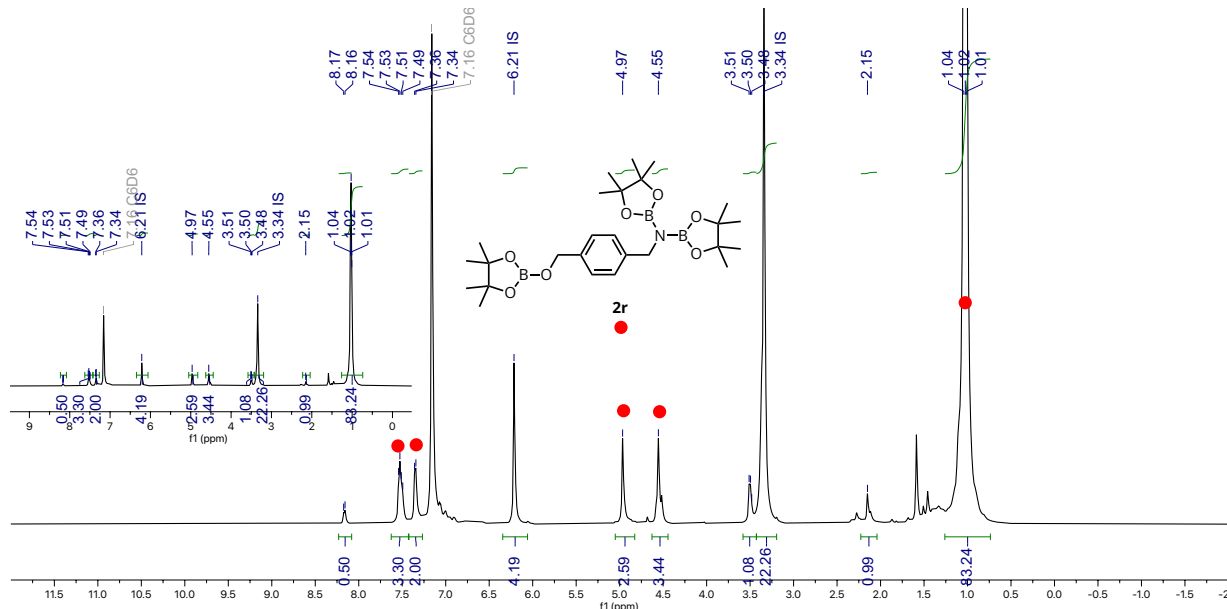
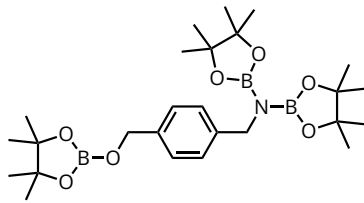
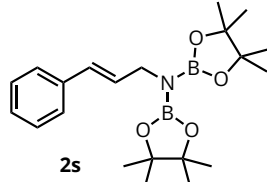


Figure S70. ^1H NMR (500 MHz, C_6D_6) spectrum of **2r**

Bis-N,N-(4,4,5,5-tetramethyl-1,3,2-dioxaborolan-2-yl)-cinnamylamine (2s)

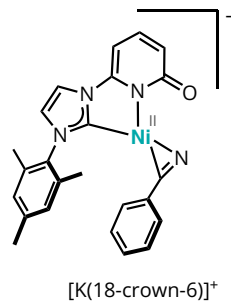
The general procedure was followed using cinnamonnitrile, pinacolborane (6.0 equiv), and toluene. Poor reactivity was observed at ambient temperature, so the reaction temperature was increased to 50 °C for 22 hours. Although the cinnamonnitrile starting material was consumed, a complex mixture of multiple resulting products was observed by ^1H NMR spectroscopy. These products were tentatively assigned as a mixture of **2s**, **2o**, and intermediate reduction species. However, decomposition of crude material upon workup precluded application of further analytical methods to obtain a more quantitative assessment of reactivity.



4. Mechanistic Experiments

4.1 Synthesis and Characterization of Nitrile Adducts 5a–c

In a glovebox, a 3.7 mL vial was charged with $[K(18\text{-crown}\text{-}6)][(^hIMesPyO)Ni(\text{cod})]$ (31.2 mg, 0.04 mmol, 1.0 equiv.), benzonitrile or 4-fluorobenzonitrile (0.04 mmol, 1.0 equiv.) and C_6D_6 (0.03 M). The pumpkin-orange-colored solution was transferred to a J-Young tube and concentrated in vacuo. The crude reaction mixture was characterized by 1H NMR.



[$K(18\text{-crown}\text{-}6)$][(hIMesPyO) $Ni(\eta^2\text{-}NCPh)$] (5a)

Benzonitrile (NCPh , 4.0 equiv) was used following the standard procedure. Single crystals suitable for X-ray diffraction analysis were obtained after recrystallization from C_6D_6 at room temperature (see Section 5).

- ^1H NMR (400 MHz, C_6D_6): 7.35 (dd, $J = 8.5, 7.0$ Hz, 1H), 7.25 – 7.18 (m, 1H), 7.11 (s, 2H), 6.91 – 6.78 (m, 6H), 6.13 (d, $J = 1.8$ Hz, 1H), 5.93 (d, $J = 7.1$ Hz, 1H), 3.31 (s, 24H), 2.24 (s, 3H), 2.15 (s, 6H)

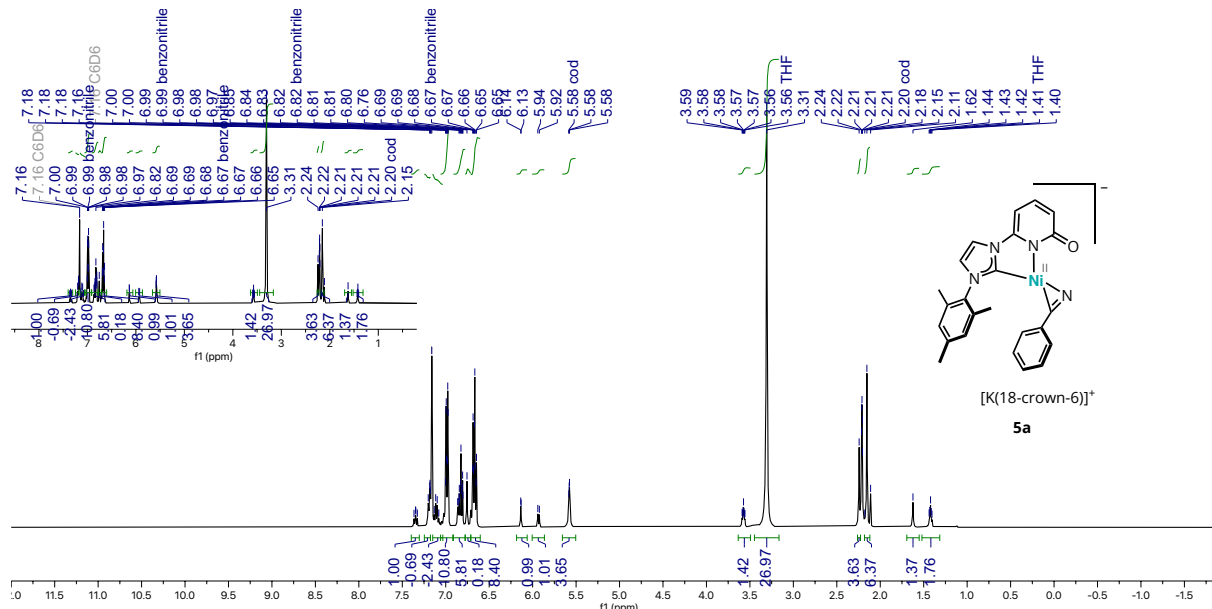


Figure S71. ^1H NMR (500 MHz, C_6D_6) spectrum of **5a**

$[K(18\text{-crown}\text{-}6)][^nIMesPyO]Ni(\eta^2\text{-NC(4-FPh)}](\mathbf{5b})$

4-Fluorobenzonitrile (NC(4-FPh) , 4.0 equiv) was used following the standard procedure. Single crystals suitable for X-ray diffraction analysis were obtained after recrystallization from toluene at -30°C (see Section 5).

- ^1H NMR (400 MHz, C_6D_6): 7.34 (t, $J = 8.5$ Hz, 2H), 7.14 – 7.06 (m, 1H), 6.88 – 6.76 (m, 2H), 6.71 (s, 4H), 6.76 – 6.67 (m, 3H), 6.09 (s, 1H), 5.90 (d, $J = 7.0$ Hz, 1H), 3.28 (s, 24H), 2.18 (s, 3H), 2.12 (s, 6H).
- ^{19}F NMR (376 MHz, C_6D_6): δ -116.7

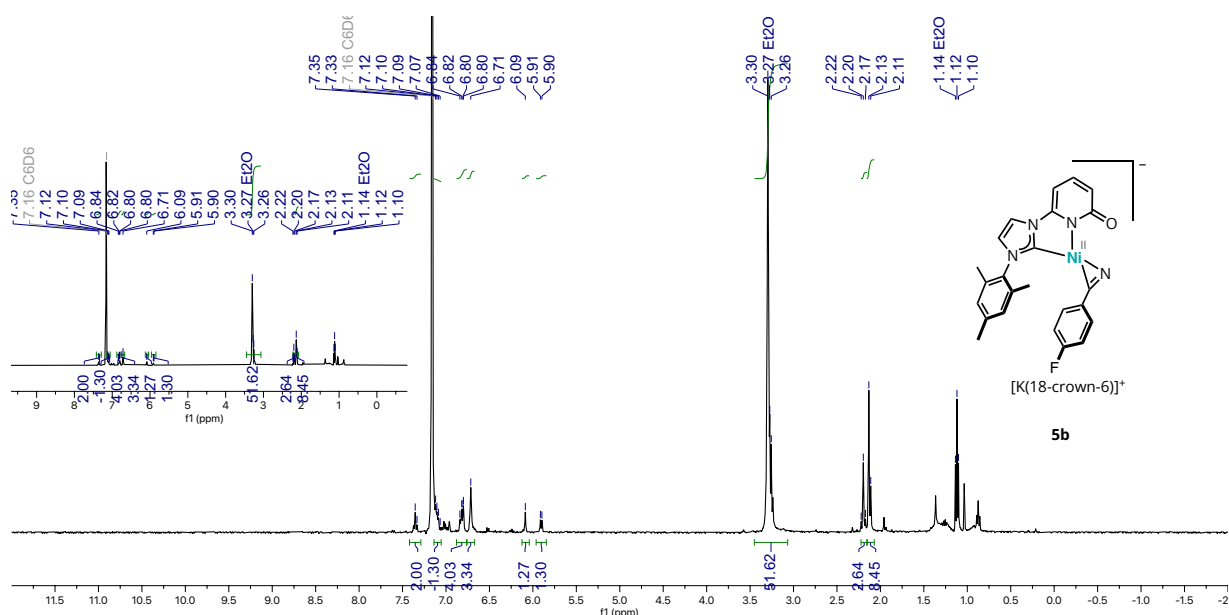
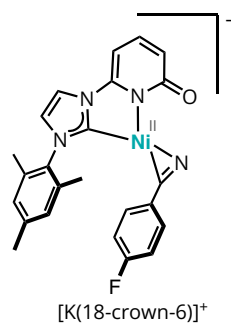


Figure S72. ^1H NMR (500 MHz, C_6D_6) spectrum of **5b**

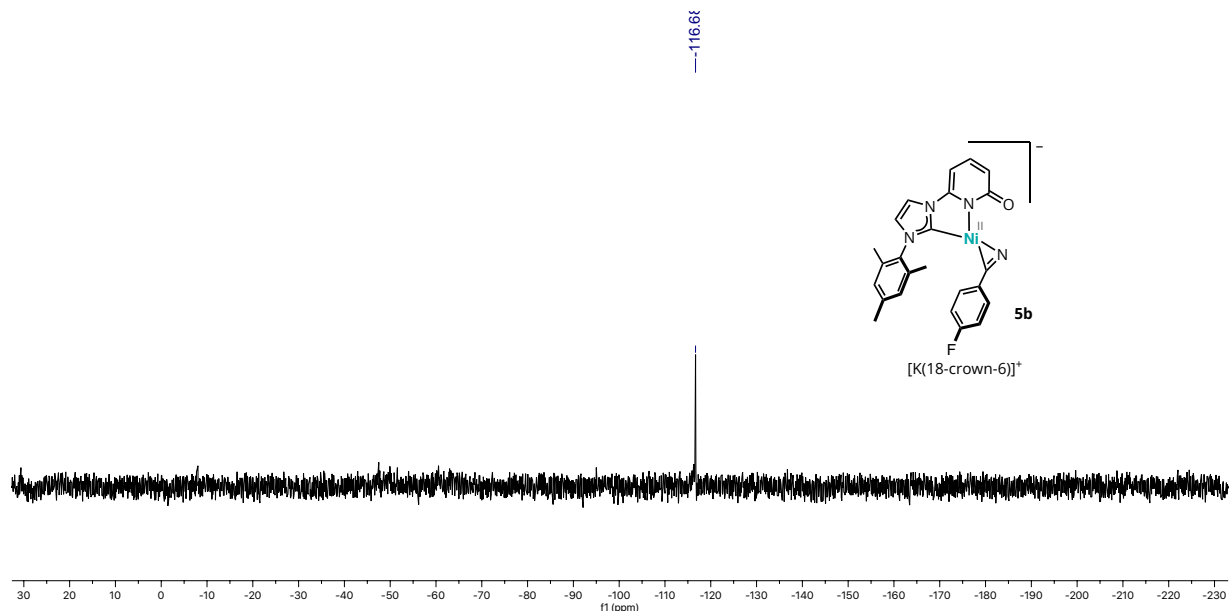


Figure S73. ^{19}F NMR (376 MHz, C_6D_6) spectrum of **5b**

$[K(18\text{-crown}\text{-}6)][(^h\text{IMesPyO})Ni(\eta^2\text{-NCCy})]$ (**5c**)

Cyclohexanecarbonitrile (NCCy, 4.0 equiv) was used following the standard procedure. Single crystals suitable for X-ray diffraction analysis were obtained after recrystallization from C₆D₆ at room temperature (see Section 5).

- ¹H NMR (400 MHz, C₆D₆): 7.34 (t, *J* = 7.8 Hz, 2H), 6.89 (s, 2H), 6.77 – 6.65 (m, 1H), 6.16 (s, 1H), 5.98 (d, *J* = 7.3 Hz, 2H), 3.34 (s, 24 H), 1.86 – 1.61 (m, 6H), 1.61 – 1.47 (m, 1H), 1.47 – 1.33 (m, 5H), 1.33 – 1.17 (m, 4H), 1.17 – 0.87 (m, 4H).

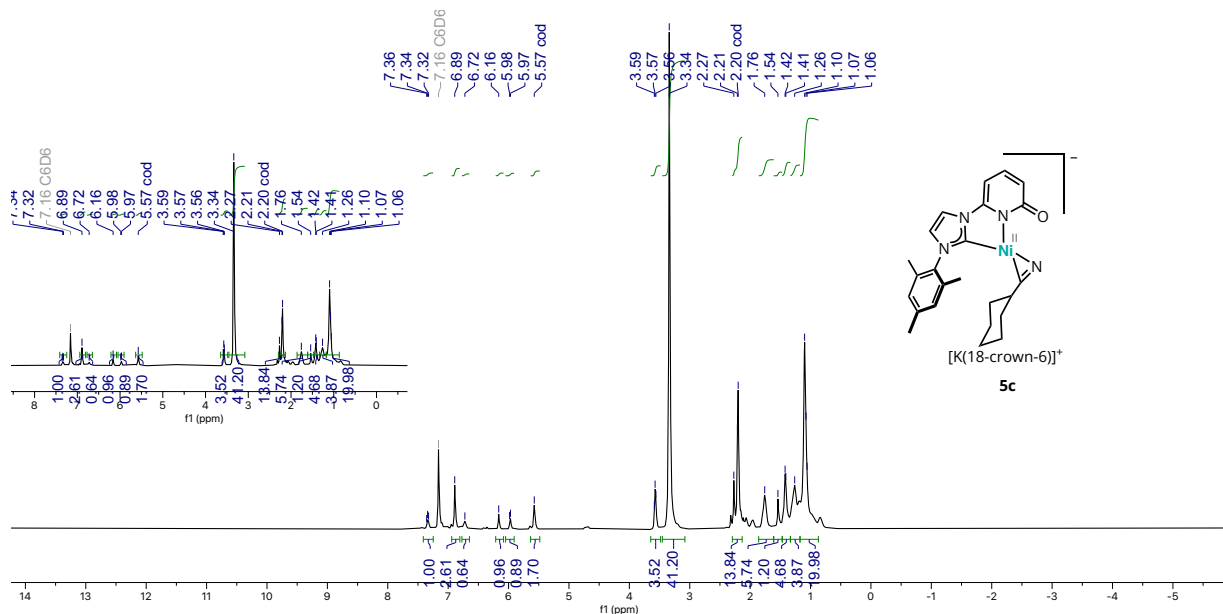
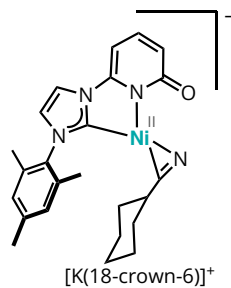


Figure S74. ¹H NMR (500 MHz, C₆D₆) spectrum of **5c**

4.2 Experiments with Nickel Complex 5c and HBpin

In a N₂-filled glovebox, a 1-dram vial was charged with [K(18-crown-6)][(^hIMesPyO)Ni(cod)] (20 mg, 0.03 mmol, 1.0 equiv.), HBpin (5.9 μ L, 1.5 equiv.) and **1m** (3.2 μ L, 1.0 equiv.). C₆D₆ (0.75 mL) was added, and the reagents were mixed until fully dissolved. The reaction solution was transferred to a J-Young tube, which was sealed and removed from the glovebox. The reaction was monitored over 24 hours by obtaining ¹H NMR spectra at the indicated intervals. The major product formed was identified as **5c** in addition to a small amount of **2m**.

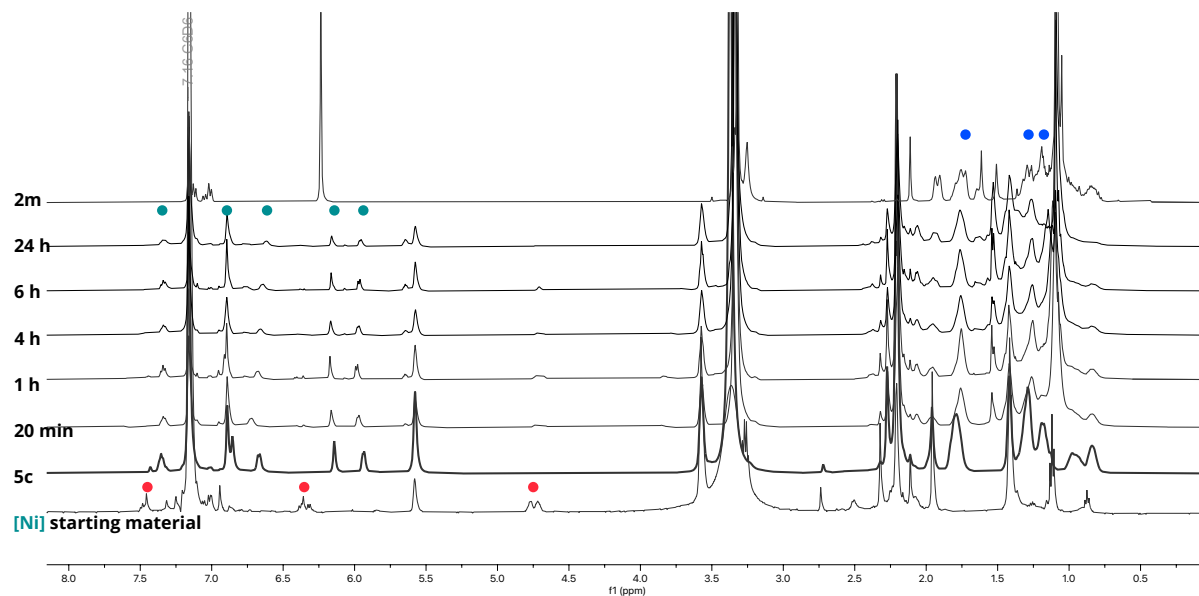
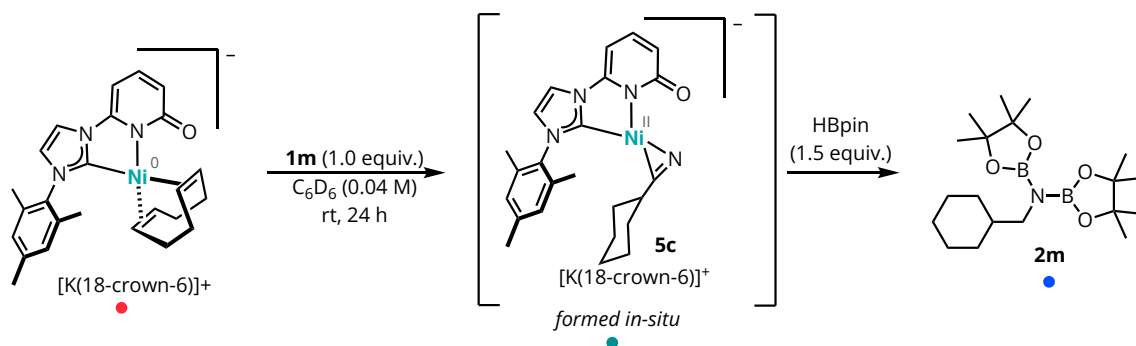


Figure S75. ¹H NMR (500 MHz, C₆D₆) spectra obtained to monitor reaction progress upon treating complex **5c** with additional HBpin (1.5 equiv).

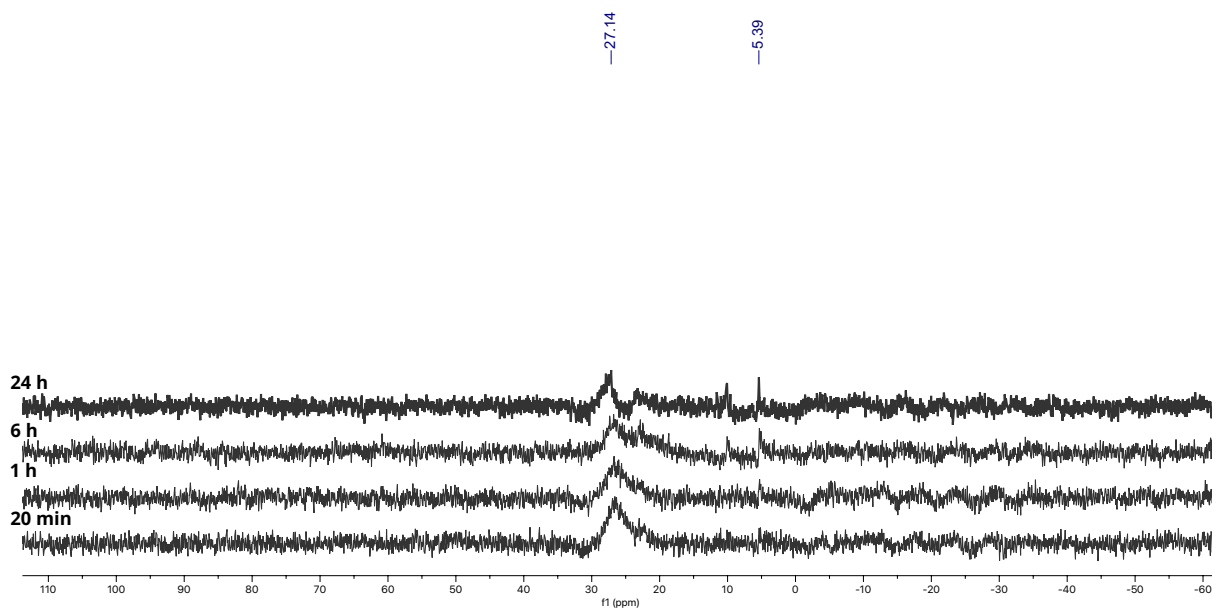
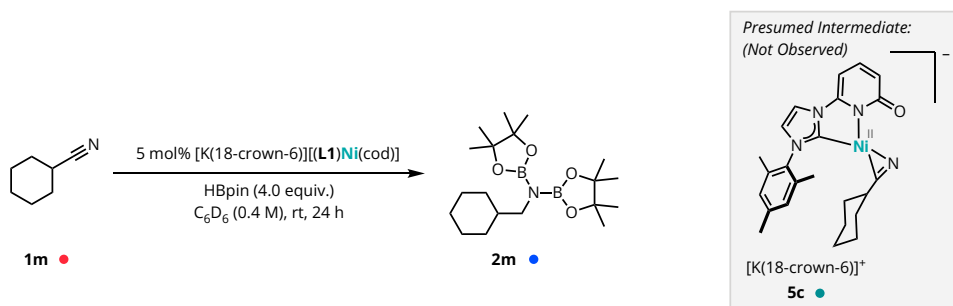


Figure S76. ^{11}B NMR (160 MHz, C_6D_6) spectra obtained to monitor reaction progress upon treating complex **5c** with additional HBpin (1.5 equiv).

In a N_2 -filled glovebox, a 1-dram vial was charged with $[\text{K}(18\text{-crown-6})][({}^{\text{n}}\text{IMesPyO})\text{Ni}(\text{cod})]$ (7.5 mg, 0.01 mmol, 0.05 equiv.), **1m** (21.8 mg, 0.20 mmol, 1.0 equiv.) and C_6D_6 (0.5 mL, 0.4 M). The reagents were mixed until fully dissolved, and the reaction solution was transferred to a J-Young tube. HBpin (116.1 μL , 0.8 mmol, 4.0 equiv.) was then added. The J-Young tube was sealed, inverted several times to mix, and removed from the glovebox. The reaction was monitored over 24 hours by obtaining ^1H NMR spectra at the indicated intervals. The major product formed were identified as **2m**, but nickel complex **5c** was not observed as the resting state.



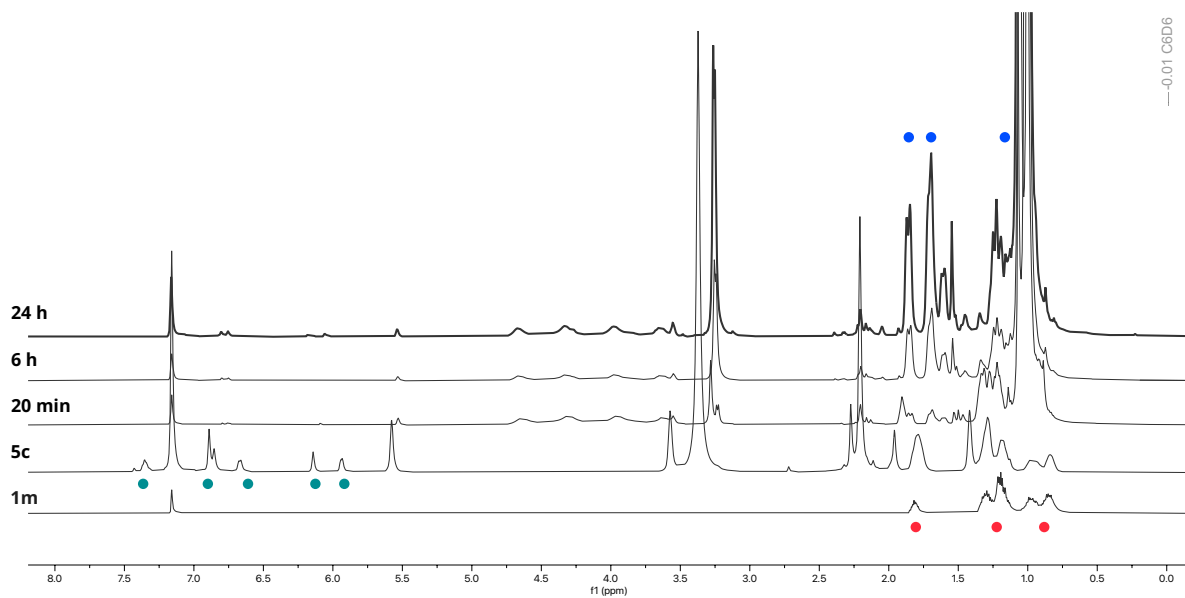


Figure S77. ^1H NMR (500 MHz, C_6D_6) spectra obtained to monitor reaction progress upon combining nitrile **1m** and HBpin (4.0 equiv) in the presence of nickel precatalyst [K(18-crown-6)] $[({\bf L1})\text{Ni}(\text{cod})]$ (5 mol%).

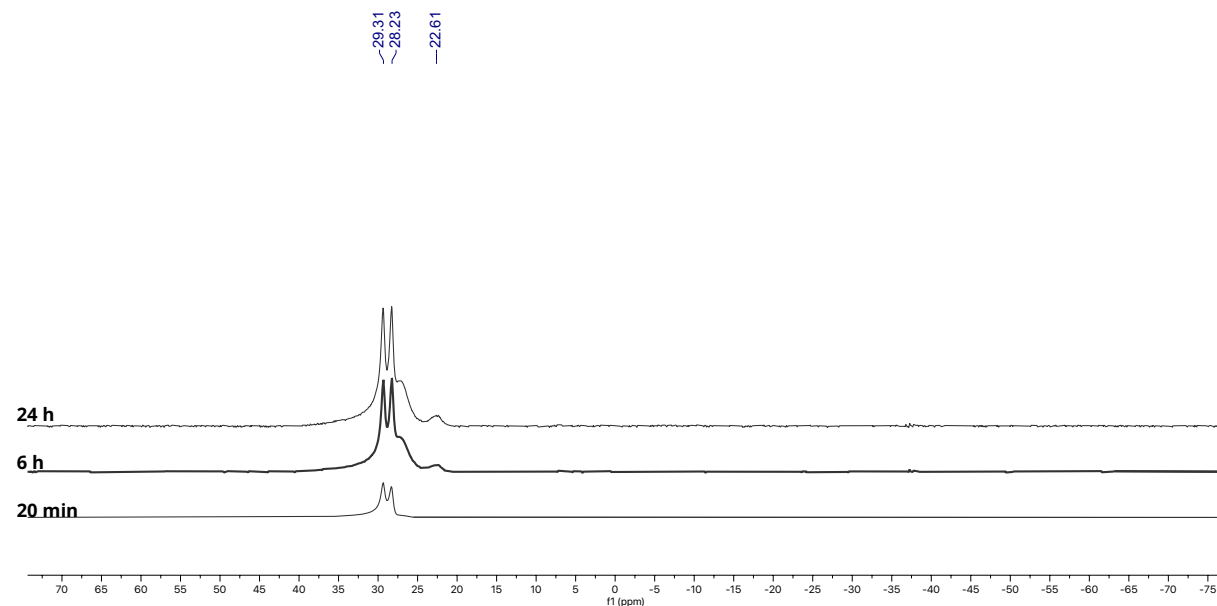
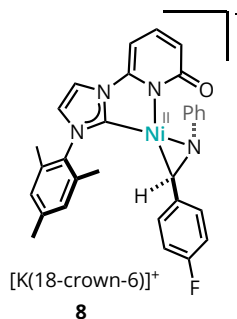


Figure S78. ^{11}B NMR (160 MHz, C_6D_6) of the reaction progress

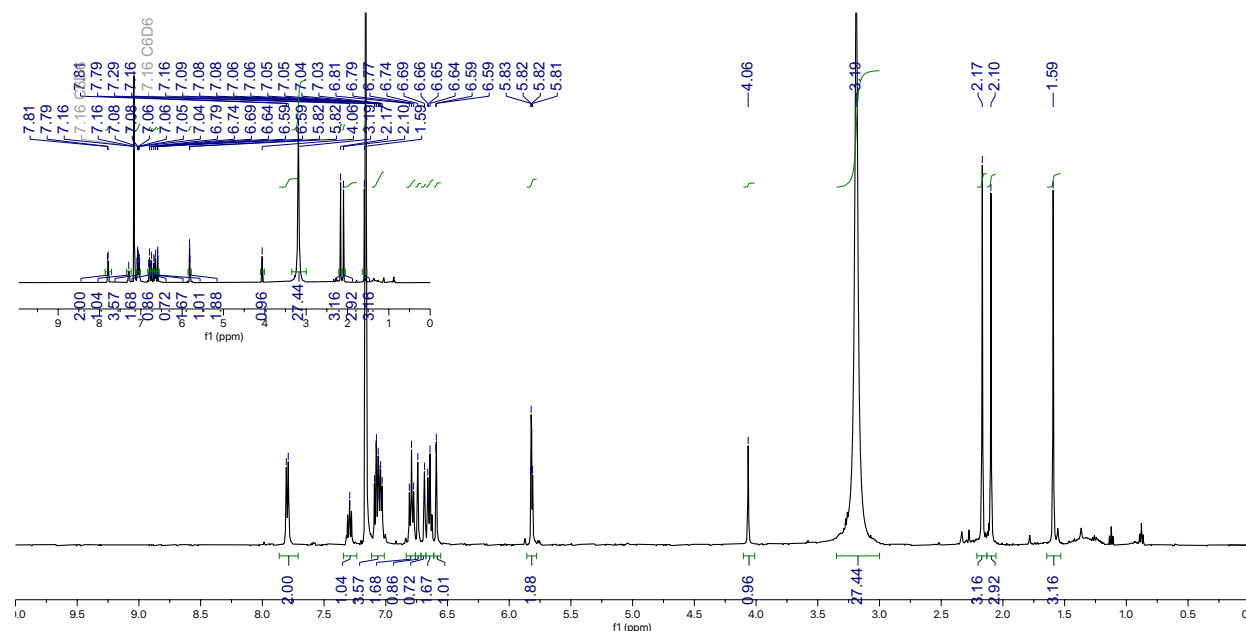
4.3 Synthesis and Characterization of Imine Adduct 8

In a N₂-filled glovebox, a 1-dram vial was charged with [K(18-crown-6)][(^hIMesPyO)Ni(cod)] (20.0 mg, 0.03 mmol, 1.0 equiv.), imine **7** (5.3 mg, 0.03 mmol, 1.0 equiv.), benzene (0.5 mL, 0.05 M) and a PTFE-coated magnetic stir bar. The resulting pomegranate-colored solution was stirred for one hour and then concentrated in vacuo to give a magenta-colored solid.



The crude residue was suspended in pentane and passed through a short pad of Celite. The pentane filtrate was discarded. The material remaining on top of the Celite pad was eluted then with benzene. The benzene filtrate was collected and concentrated in vacuo to give **8** as a magenta solid (21.7 mg, 67% yield). Single crystals suitable for X-ray diffraction were obtained by recrystallization from benzene at room temperature (see Section 5).

- ¹H NMR (500 MHz, C₆D₆) δ 7.80 (d, *J* = 7.9 Hz, 2H), 7.29 (dd, *J* = 7.9, 6.8 Hz, 1H), 7.12 – 7.01 (m, 4H), 6.79 (t, *J* = 8.8 Hz, 2H), 6.74 (s, 1H), 6.69 (s, 1H), 6.67 – 6.61 (m, 2H), 6.59 (d, *J* = 2.1 Hz, 1H), 5.86 – 5.78 (m, 2H), 4.06 (s, 1H), 3.19 (s, 24H), 2.17 (s, 3H), 2.10 (s, 3H), 1.59 (s, 3H).
- ¹³C NMR (125 MHz, C₆D₆): δ 193.0, 172.0, 162.3, 160.2, 158.3, 152.0, 148.0, 137.7, 137.6, 136.7, 136.3, 135.8, 129.6, 129.2, 128.9, 128.5, 125.7, 125.7, 122.8, 122.2, 114.4, 114.1, 113.9, 113.7, 88.7, 70.0, 54.4, 21.0, 18.6, 17.4.
- ¹⁹F NMR (376 MHz, C₆D₆): δ -124.6



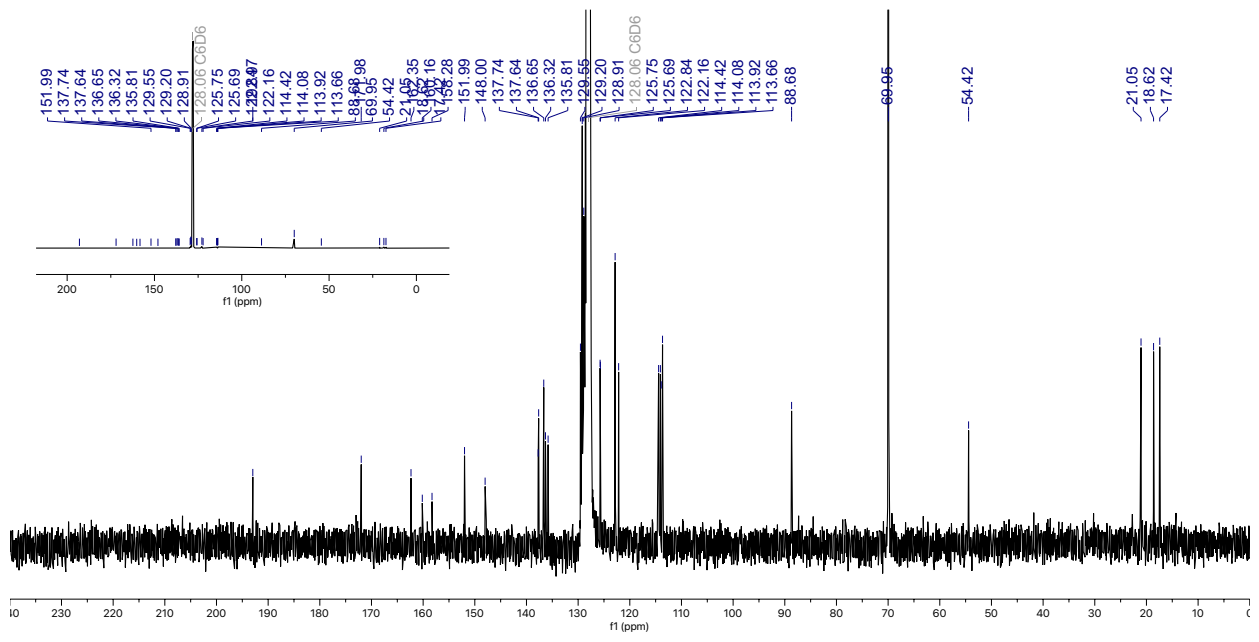


Figure S80. ^{13}C NMR (125 MHz, C_6D_6) spectrum of **8**

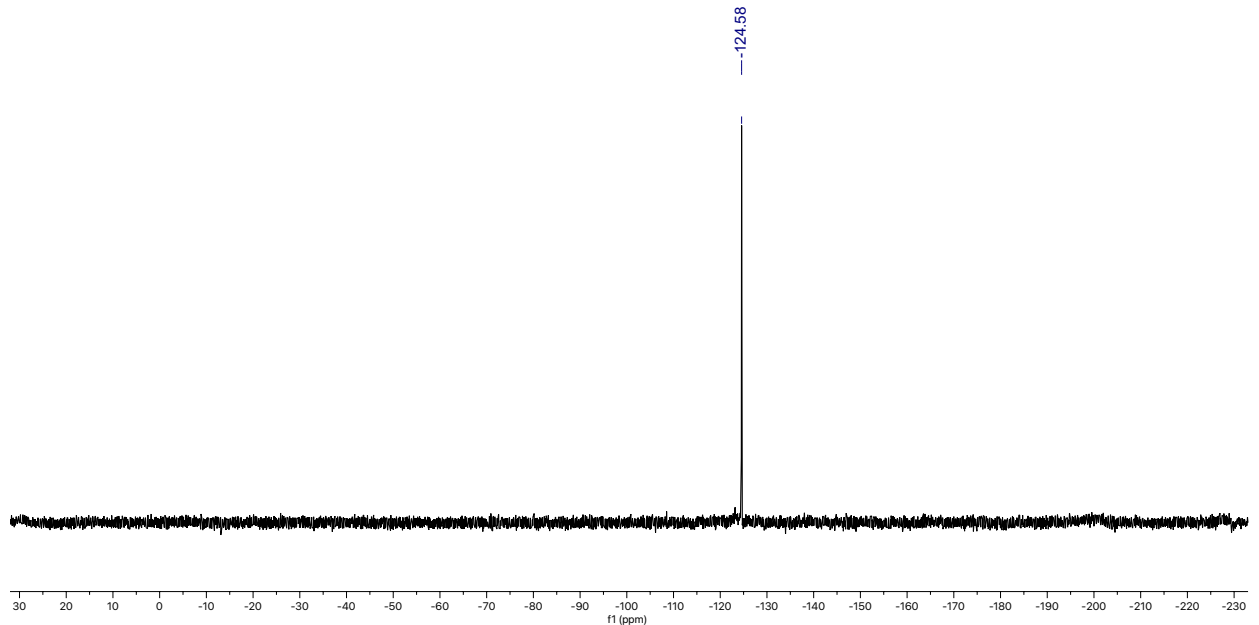


Figure S81. ^{19}F NMR (376 MHz, C_6D_6) spectrum of **8**

4.4 Experiments with Nickel Complex 8 and HBpin

In a N₂-filled glovebox, a 1-dram vial was charged with **8** (24.4 mg, 0.03 mmol, 1.0 equiv.) and C₆D₆ (0.8 mL, 0.04 M). The reagents were mixed until fully dissolved and then transferred to a J-Young tube. HBpin (4.3 μ L, 0.03 mmol, 1.0 equiv.) was then added. The J-Young tube was sealed, inverted several times to mix, and removed from the glovebox. The reaction was monitored over 48 hours by obtaining ¹H and ¹⁹F NMR spectra at the indicated intervals. A small amount of **9** was formed, but nickel complex **8** remained the predominant species.

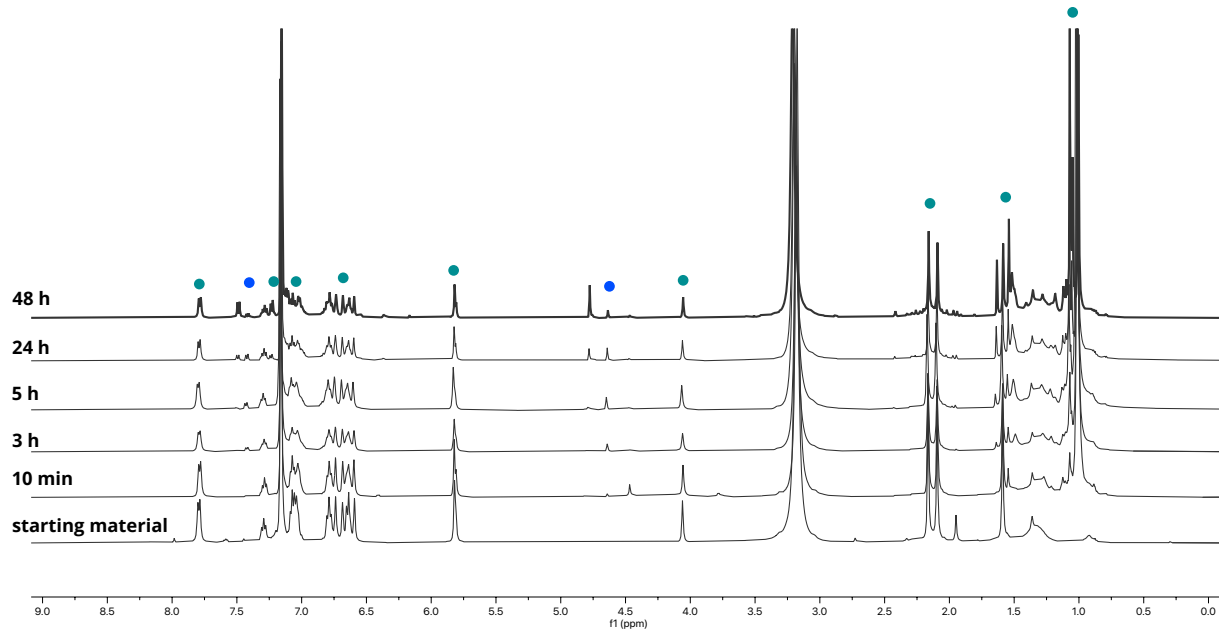
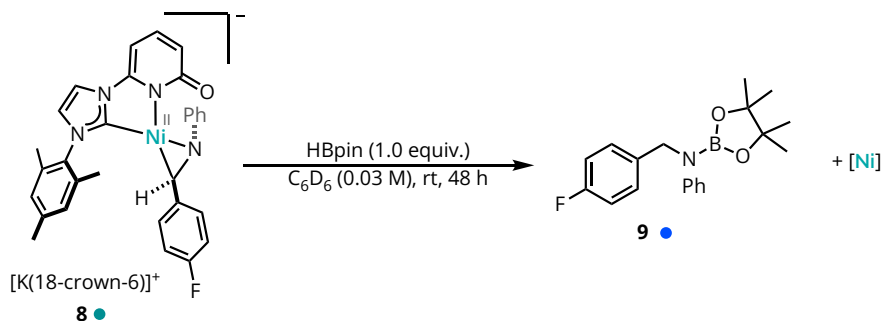


Figure S82. ¹H NMR (500 MHz, C₆D₆) spectra obtained to monitor reaction progress upon treating complex **8** with additional HBpin (1.0 equiv).

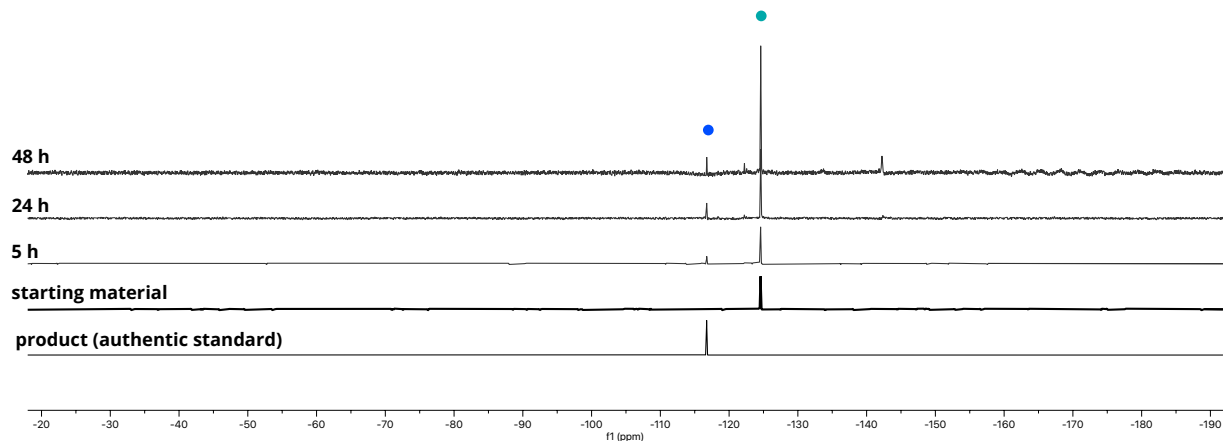


Figure S83. ^{19}F NMR (376 MHz, C_6D_6) spectra obtained to monitor reaction progress upon treating complex **8** with additional HBpin (1.0 equiv).

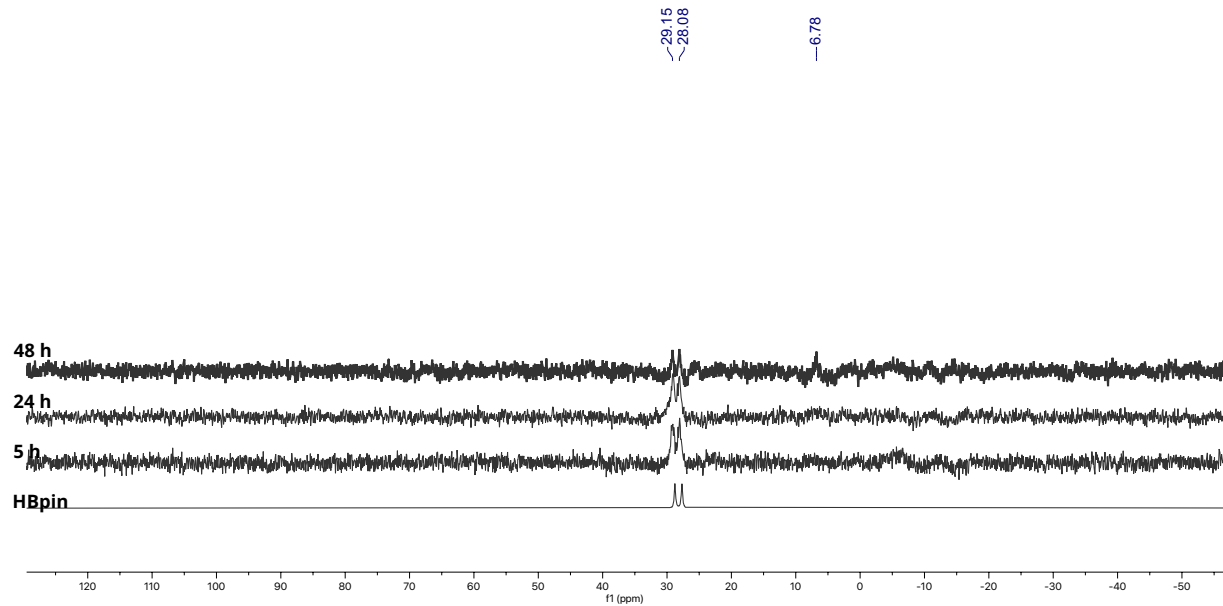


Figure S84. ^{11}B NMR (160 MHz, C_6D_6) spectra obtained to monitor reaction progress upon treating complex **8** with additional HBpin (1.0 equiv).

In a N_2 -filled glovebox, a 1-dram vial was charged with of $[\text{K}(18\text{-crown-6})][(\text{hIMesPyO})\text{Ni}(\text{cod})]$ (7.5 mg, 0.01 mmol, 5.0 mol%) and a PTFE-coated magnetic stir bar. Imine substrate **7** (0.2 mmol, 1.0 equiv) was added, followed by HBPin (0.8 mmol, 4.0 equiv) and (optionally) 1,3,5-trimethoxybenzene (17 mg, 0.10 mmol) as an internal standard. C_6D_6 (0.50 mL, 0.4 M) was added. The reagents were mixed until fully dissolved and then transferred to a J-Young tube. The J-Young tube was sealed and removed from the glovebox. The reaction was monitored over 48 hours by obtaining ^1H , ^{11}B , and ^{19}F NMR spectra at the indicated intervals. Complex **8** was observed as a catalyst resting state until imine **7** was fully consumed.

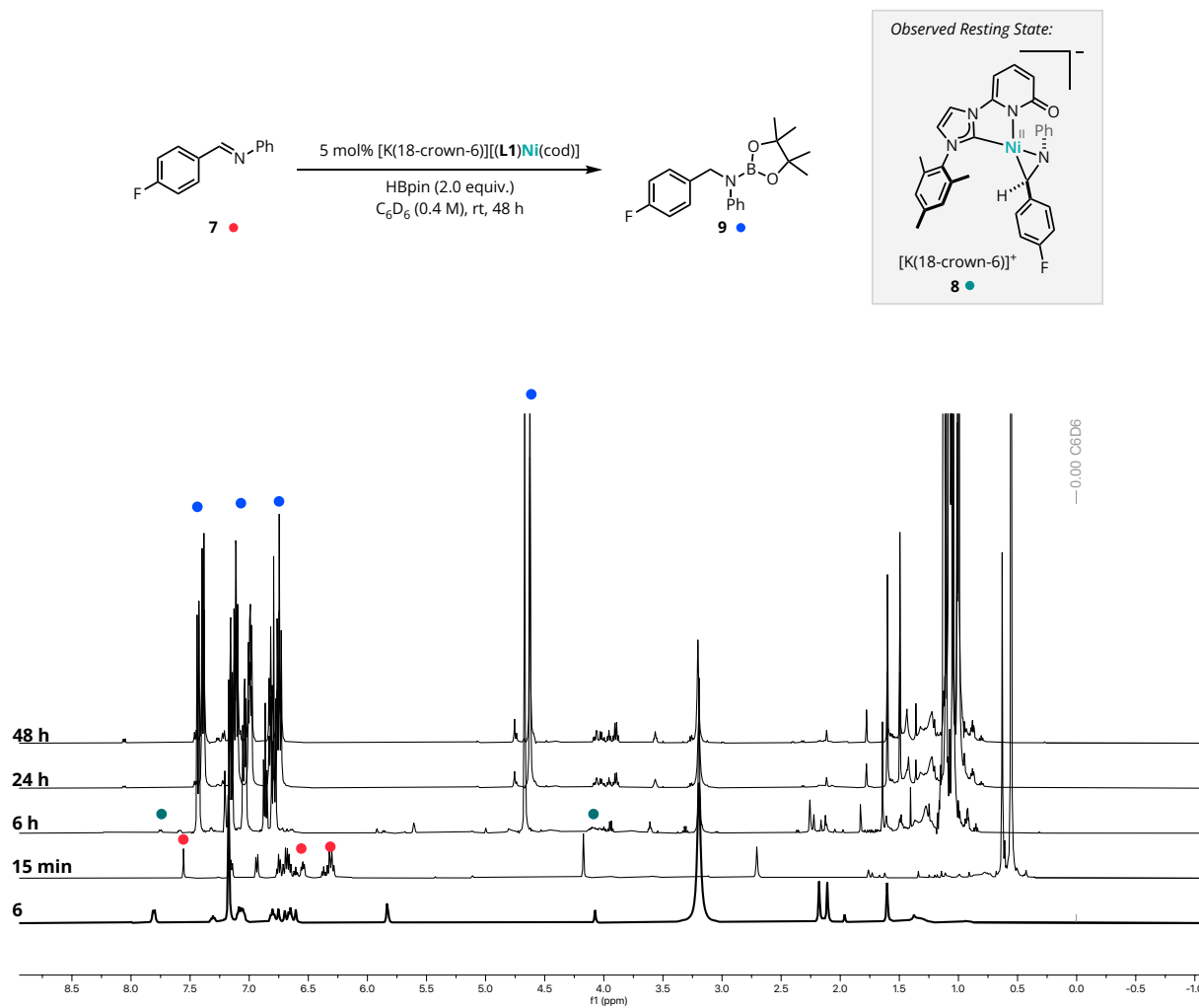


Figure S85. ^1H NMR (500 MHz, C_6D_6) spectra obtained to monitor reaction progress upon combining imine **7** and HBPin (2.0 equiv) in the presence of nickel precatalyst $[\text{K}(18\text{-crown-6})][(\text{L1})\text{Ni}(\text{cod})]$ (5 mol%).

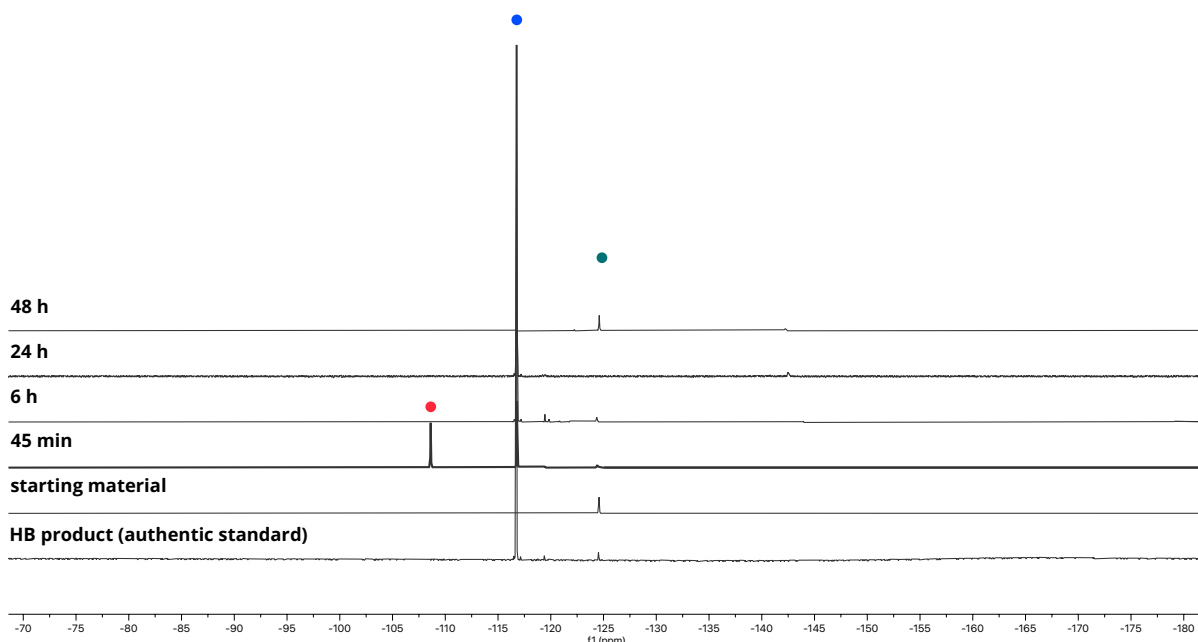


Figure S86. ^{19}F NMR (376 MHz, C_6D_6) spectra obtained to monitor reaction progress upon combining imine **7** and HBpin (2.0 equiv) in the presence of nickel precatalyst [K(18-crown-6)] $[(\text{L1})\text{Ni}(\text{cod})]$ (5 mol%).

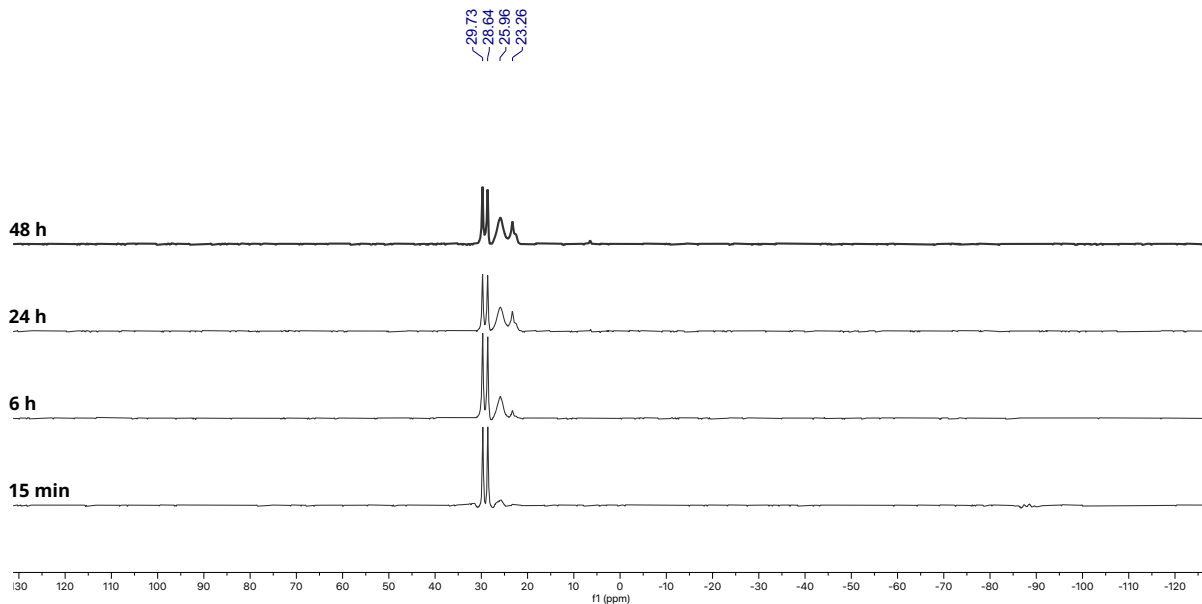


Figure S87. ^{11}B NMR (160 MHz, C_6D_6) spectra obtained to monitor reaction progress upon combining imine **7** and HBpin (2.0 equiv) in the presence of nickel precatalyst [K(18-crown-6)] $[(\text{L1})\text{Ni}(\text{cod})]$ (5 mol%).

4.5 Evaluating Homogeneity

In a glovebox, a 2-dram vial was charged with of $[K(18\text{-crown}\text{-}6)][(L1)\text{Ni}(\text{cod})]$ (7.5 mg, 0.01 mmol, 5.0 mol%) and a PTFE-coated magnetic stir bar. Nitrile **1f** (0.2 mmol, 1.0 equiv) and 1,3,5-trimethoxybenzene (0.1 mmol, 0.5 equiv) were added, followed by HBPin (0.8 mmol, 4.0 equiv) and C_6D_6 (0.50 mL, 0.4 M). The sample transferred into a J-Young NMR tube and removed from the glovebox. Reaction progress was monitored by collecting 1H NMR spectra at the indicated intervals for 20–30 minutes (approximately 25% conversion). At that point, the sample was returned to the glovebox, where the reaction solution was passed through a short plug of glass microfiber and Celite, and transferred into a new J-Young NMR tube. Reaction progress was monitored for an additional five hours by collecting 1H NMR spectra at the indicated intervals. No induction period was observed, and filtering the reaction medium after ~25% conversion did NOT diminish subsequent reaction efficiency compared to the standard condition. Taken together, these findings suggest that the active catalyst is homogeneous and that nickel nanoparticles are likely not responsible for the observed reactivity.²¹

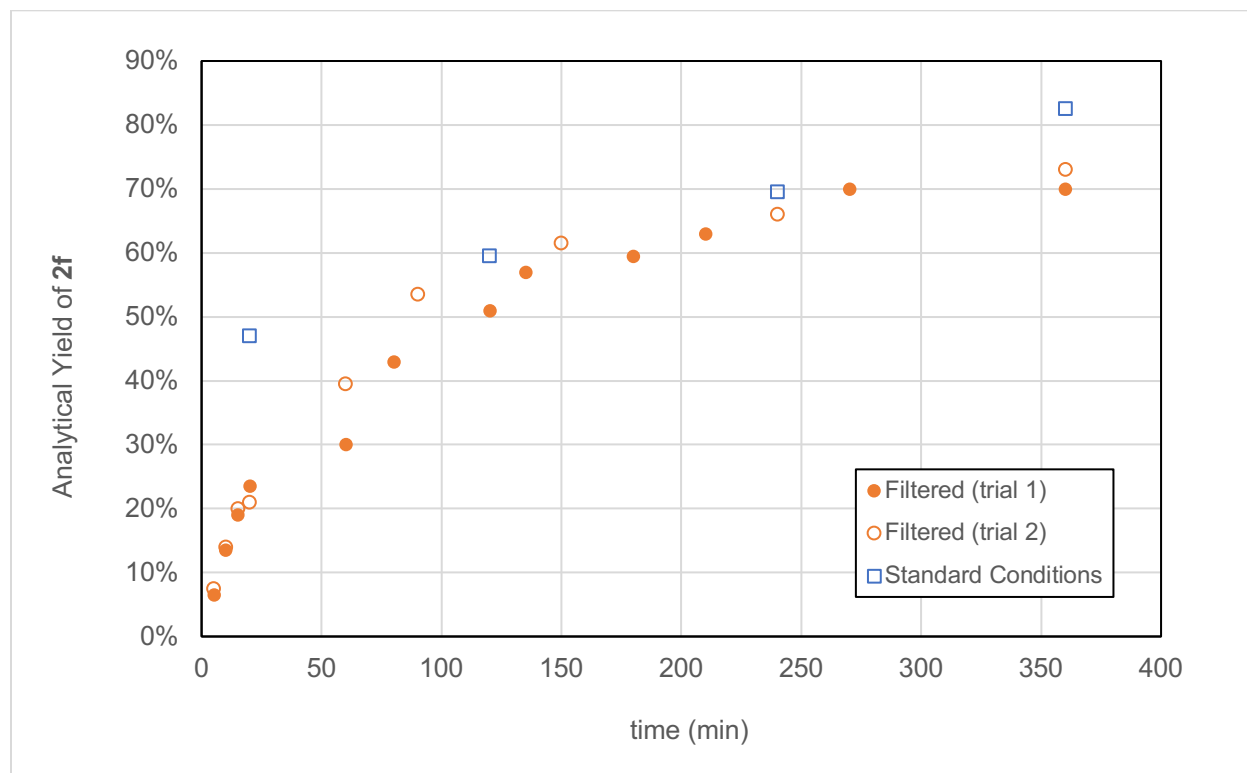


Figure S88. Time-course comparing reaction progress under standard conditions (blue) vs. filtration at ~25% conversion (orange). NMR Yield calculated from the relative 1H NMR integration of diagnostic product peaks compared to 1,3,5-trimethoxybenzene added as an internal standard.

4.6 Excluding Hidden Borane Catalysis

To evaluate the possibility of “hidden borane generation”, we adopted the experimental protocol developed by Thomas and co-workers, wherein *N,N,N’,N’*-tetramethylethylenediamine (TMEDA) is added to a reaction under otherwise standard conditions.²² If BH_3 is formed under the reaction conditions, it should be sequestered through in situ formation of $(\text{BH}_3)_2\bullet\text{TMEDA}$, enabling its quantification by ^{11}B NMR. Furthermore, if BH_3 is responsible for the observed rate enhancement, formation of the $(\text{BH}_3)_2\bullet\text{TMEDA}$ should inhibit the overall reaction, resulting in substantially decreased reaction yields.

In a glovebox, a 1-dram vial was charged with $[\text{K}(18\text{-crown-6})][(\text{L1})\text{Ni}(\text{cod})]$ (7.5 mg, 0.01 mmol, 5.0 mol%) and a PTFE-coated magnetic stir bar. 1,3,5-Trimethoxybenzene (0.1 mmol, 0.5 equiv), HBpin (0.8 mmol, 4.0 equiv), and nitrile **2n** (0.2 mmol, 1.0 equiv) were subsequently added, followed by TMEDA (0.02 mmol, 0.1 equiv) in C_6D_6 (0.50 mL, 0.4 M). The sample was transferred into a J-Young NMR tube and removed from the glovebox. Reaction progress was tracked by collecting ^1H NMR spectra over a 6-hour period. NMR yields were calculated from the relative ^1H NMR integration of diagnostic product peaks compared to 1,3,5-trimethoxybenzene added as an internal standard. In contrast the cases of “hidden borane generation”, no inhibition was observed in the presence of TMEDA when compared against standard conditions in side-by-side reactions (Figure 89). Additionally, $(\text{BH}_3)_2\bullet\text{TMEDA}$ formation was not detected (Figures 90–91).

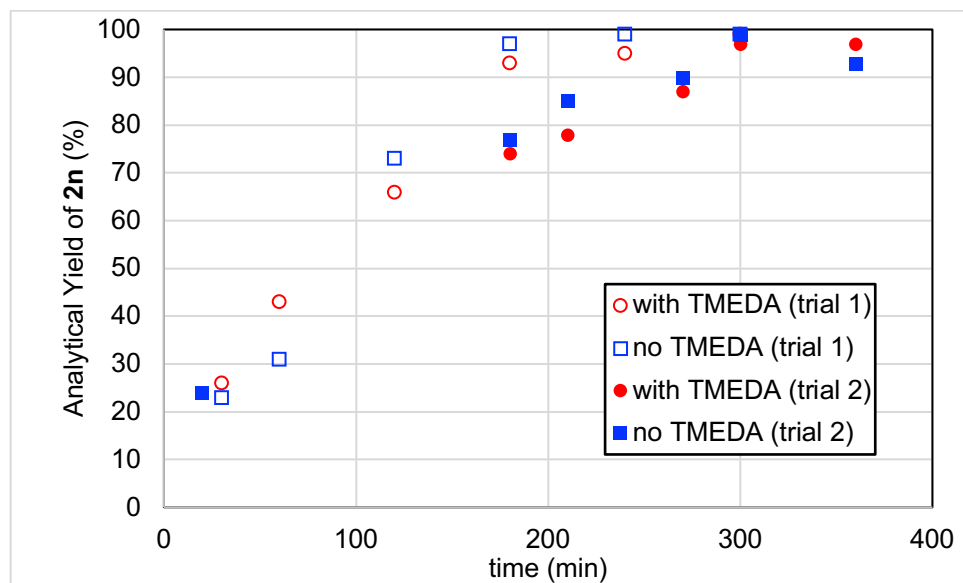


Figure S89. Time-course comparing reaction progress under standard conditions (square) vs. with TMEDA (circle). NMR Yield calculated from the relative ^1H NMR integration of diagnostic product peaks compared to 1,3,5-trimethoxybenzene added as an internal standard.

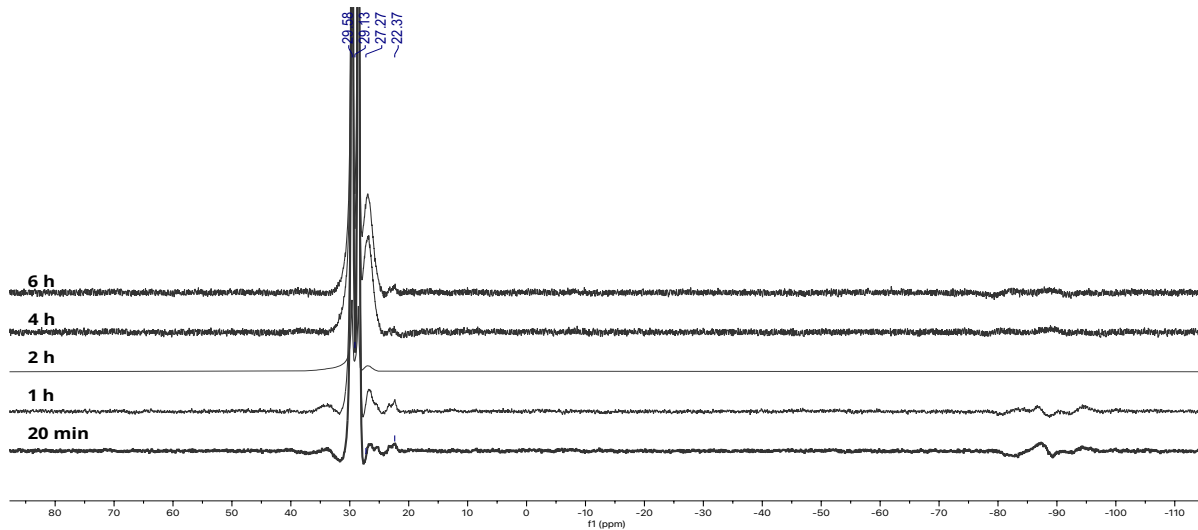


Figure S90. ^{11}B NMR (160 MHz, C_6D_6) spectra obtained to monitor reaction progress upon combining nitrile **1n** and HBpin (4.0 equiv) in the presence of nickel precatalyst [K(18-crown-6)] $[({\bf L}1)\text{Ni}(\text{cod})]$ (5 mol%) in the presence of TMEDA.

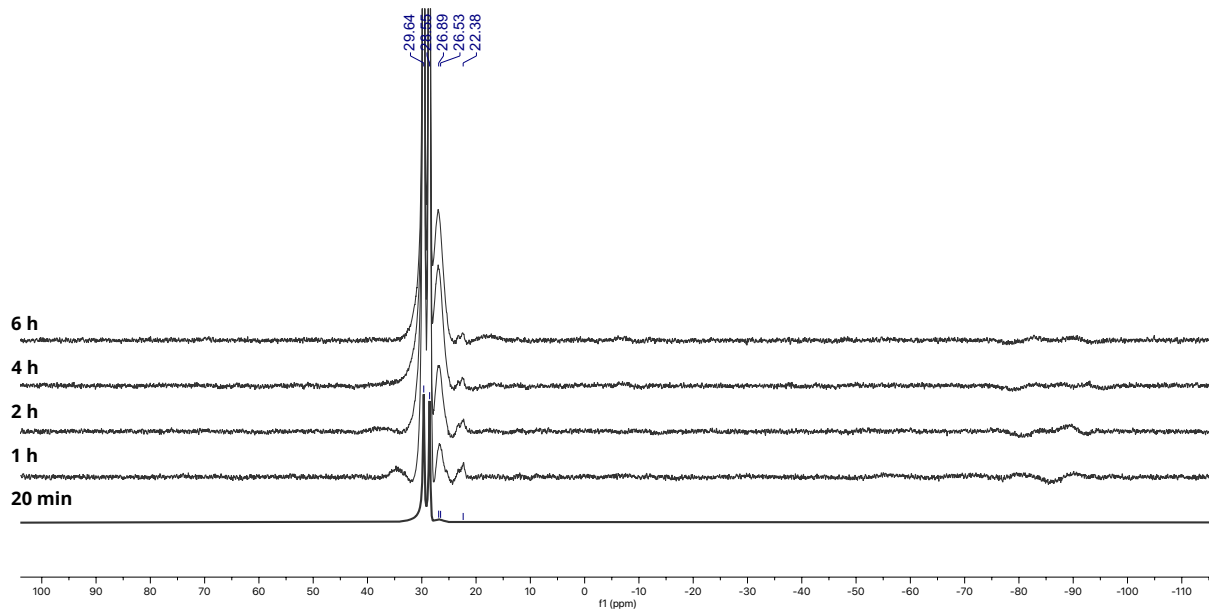


Figure S91. ^{11}B NMR (160 MHz, C_6D_6) spectra obtained to monitor reaction progress upon combining nitrile **1n** and HBpin (4.0 equiv) in the presence of nickel precatalyst [K(18-crown-6)] $[({\bf L}1)\text{Ni}(\text{cod})]$ (5 mol%) in the absence of TMEDA.

5. SC-XRD Data

5.1 General Procedure for SC-XRD Data Collection

A crystal was placed onto a thin glass optical fiber or a nylon loop and mounted on a Rigaku XtaLAB Synergy-S Dualflex diffractometer equipped with a HyPix-6000HE HPC area detector for data collection at 100.0 K. A preliminary set of cell constants and an orientation matrix were calculated from a small sampling of reflections. A short pre-experiment was run, from which an optimal data collection strategy was determined. The full data collection was carried out using a PhotonJet (Cu) X-ray source. Series of frames were collected in 0.50° steps in w at different $2q$, k , and f settings. After the intensity data were corrected for absorption, the final cell constants were calculated from the xyz centroids of strong reflections from the actual data collection after integration. See Table S2 for additional crystal and refinement information. Structures were solved using SHELXT²³ and refined using SHELXL.²⁴ The space group was determined based on systematic absences and intensity statistics. Most or all non-hydrogen atoms were assigned from the solution. Full-matrix least squares / difference Fourier cycles were performed which located any remaining non-hydrogen atoms. All non-hydrogen atoms were refined with anisotropic displacement parameters. For **6** and **8** the hydrogen atom on metal-coordinating atom C18 was found from the difference Fourier map and refined freely. All other hydrogen atoms were placed in ideal positions and refined as riding atoms with relative isotropic displacement parameters. For complex **5a**, the crown ether and benzene solvent molecule C43-C48 are modeled as disordered over two positions each (0.82:0.18 and 0.58:0.42, respectively).

Table S2. Crystallographic data and refinement details

	[K(18-crown-6)] [(^h IMesPyO)Ni(PhCN)] (5a) • 2C ₆ D ₆	[K(18-crown-6)] [(^h IMesPyO)Ni(1k) (5b) • CD ₃ CN]	[K(18-crown-6)] [(^h IMesPyO)Ni(CyCN)] (5c) • C ₆ D ₆	[(^h IMesPyO)Ni (CyHCN(Bpin) ₂)] (6) • ½C ₆ D ₆	[K(18-crown-6)] [(^h IMesPyO)Ni(7) (8)]
CCDC	2267003	2267001	2267004	2267002	2267000
Empirical formula	C ₄₈ H ₄₅ D ₁₂ KN ₄ NiO ₇	C ₃₈ H ₄₄ D ₃ FKN ₅ NiO ₇	C ₄₂ H ₅₁ D ₆ KN ₄ NiO ₇	C ₃₉ H ₅₂ B ₂ D ₃ N ₄ NiO ₅	C ₄₂ H ₅₀ FKN ₄ NiO ₇
Formula weight	911.86	805.63	833.76	743.22	839.67
Crystal system	monoclinic	monoclinic	monoclinic	monoclinic	Monoclinic
Space group	P2 ₁ /n	P2 ₁ /n	P2 ₁ /c	C2/c	P2 ₁ /n
Unit cell dimensions (Å)					
<i>a</i>	15.32140(10)	11.20850(11)	15.01330(10)	23.69320(10)	12.3104(3)
<i>b</i>	11.93520(10)	30.7037(3)	10.92400(10)	15.81900(10)	21.2220(6)
<i>c</i>	25.59080(10)	11.62735(12)	25.6552(2)	21.87530(10)	15.5022(4)
Volume (Å ³)	4665.11(5)	3953.48(7)	4155.62(6)	7936.33(8)	4047.22(18)
<i>Z</i>	4	4	4	8	4
Calculated density (Mg/m ³)	1.298	1.354	1.333	1.244	1.378
Absorption coefficient (mm ⁻¹)	1.829	2.135	2.001	1.068	2.104
<i>F</i> (000)	1904	1688	1760	3160	1768
Crystal color, morphology	red, block	orange, needle	red, plate	orange, block	red-orange, plate
Crystal size (mm ³)	0.13 × 0.076 × 0.06	0.267 × 0.031 × 0.026	0.139 × 0.101 × 0.053	0.168 × 0.136 × 0.06	0.076 × 0.043 × 0.021
θ range (°)	3.253 to 80.270	4.109 to 80.220	3.489 to 80.678	3.394 to 80.698	3.532 to 77.827
Index ranges	-19 ≤ <i>h</i> ≤ 19 -13 ≤ <i>k</i> ≤ 15 -32 ≤ <i>l</i> ≤ 32	-14 ≤ <i>h</i> ≤ 14 -33 ≤ <i>k</i> ≤ 38 -14 ≤ <i>l</i> ≤ 13	-19 ≤ <i>h</i> ≤ 19 -13 ≤ <i>k</i> ≤ 10 -32 ≤ <i>l</i> ≤ 32	-30 ≤ <i>h</i> ≤ 30 -20 ≤ <i>k</i> ≤ 18 -27 ≤ <i>l</i> ≤ 27	-15 ≤ <i>h</i> ≤ 10 -25 ≤ <i>k</i> ≤ 25 -18 ≤ <i>l</i> ≤ 19
Reflections collected	81132	62996	72065	69642	28405
Independent reflections	10094 [<i>R</i> (int) = 0.0379]	8506 [<i>R</i> (int) = 0.0457]	8958 [<i>R</i> (int) = 0.0388]	8562 [<i>R</i> (int) = 0.0318]	8003 [<i>R</i> (int) = 0.0676]
Observed reflections	9202	7281	8134	7959	5573
Completeness to θ	100.0%	99.9%	100.0%	100.0%	99.3%
Data / restraints / parameters	10094 / 316 / 771	8506 / 0 / 482	8958 / 0 / 499	8562 / 30 / 502	8003 / 0 / 512
Goodness-of-fit on <i>F</i> ²	1.062	1.071	1.106	1.063	1.031
Final <i>R</i> indices [<i>>2 σ(I)</i>]	<i>R</i> ₁ = 0.0317, <i>wR</i> ₂ = 0.0795	<i>R</i> ₁ = 0.0365, <i>wR</i> ₂ = 0.0946	<i>R</i> ₁ = 0.0351, <i>wR</i> ₂ = 0.0888	<i>R</i> ₁ = 0.0318, <i>wR</i> ₂ = 0.0789	<i>R</i> ₁ = 0.0543, <i>wR</i> ₂ = 0.1318
<i>R</i> indices (all data)	<i>R</i> ₁ = 0.0347, <i>wR</i> ₂ = 0.0812	<i>R</i> ₁ = 0.0442, <i>wR</i> ₂ = 0.0985	<i>R</i> ₁ = 0.0384, <i>wR</i> ₂ = 0.0907	<i>R</i> ₁ = 0.0340, <i>wR</i> ₂ = 0.0801	<i>R</i> ₁ = 0.0856, <i>wR</i> ₂ = 0.1488
Largest diff. peak and hole (e.Å ⁻³)	0.334 and -0.269	0.334 and -0.651	0.318 and -0.482	0.330 and -0.359	0.722 and -0.337

5.2 SC-XRD Data for $[K(18\text{-crown}\text{-}6)][(^h\text{IMesPyO})\text{Ni}(\text{PhCN})]$ (5a)

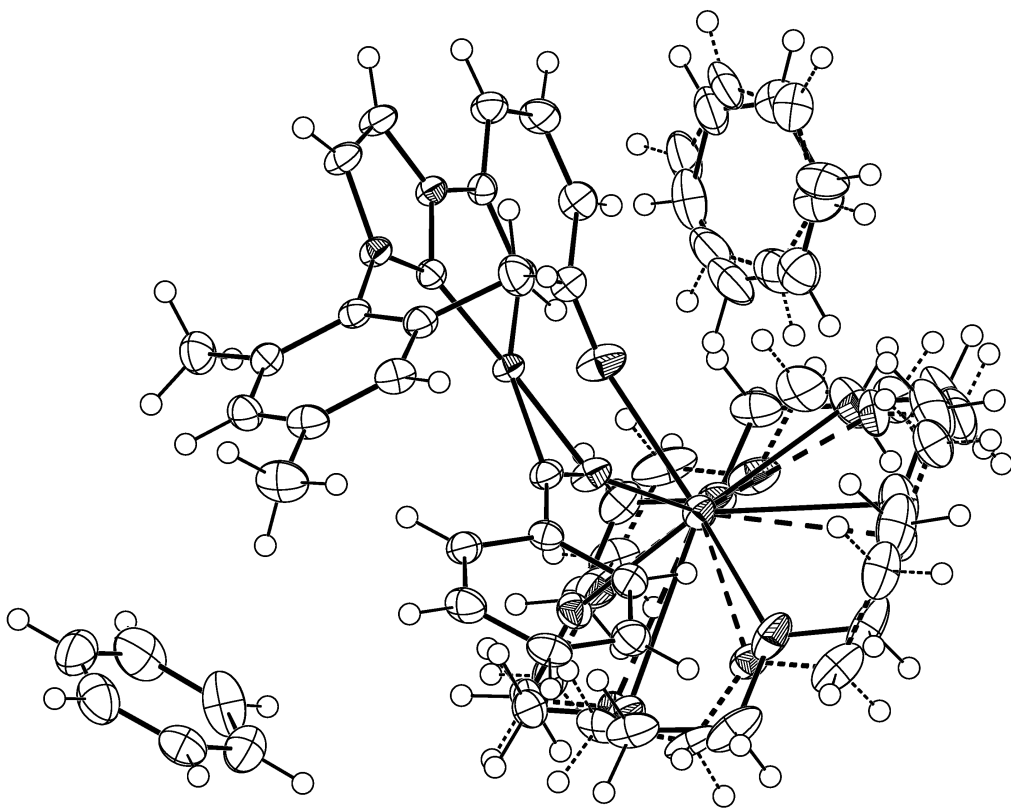


Figure S92. Solid-state structure of **5a**• $2\text{C}_6\text{D}_6$ determined by SC-XRD. Anisotropic displacement ellipsoids drawn at the 50 % probability level. Figure generated with OLEX2.²⁵

Atomic coordinates ($\times 10^4$) and equivalent isotropic displacement parameters ($\text{\AA}^2 \times 10^3$) are listed below for **5a**• $2\text{C}_6\text{D}_6$. U_{eq} is defined as one third of the trace of the orthogonalized U_{ij} tensor.

	x	y	z	U_{eq}
Ni1	3379(1)	2317(1)	5646(1)	18(1)
K1	2769(1)	5649(1)	5420(1)	23(1)
O1	2609(1)	4068(1)	4708(1)	35(1)
N1	3719(1)	-190(1)	5823(1)	20(1)
N2	2926(1)	365(1)	5146(1)	19(1)
N3	2723(1)	2212(1)	4932(1)	19(1)

N4	3388(1)	3785(1)	5944(1)	27(1)
C1	3421(1)	768(1)	5580(1)	18(1)
C2	3422(1)	-1146(1)	5548(1)	26(1)
C3	2924(1)	-795(1)	5124(1)	26(1)
C4	4250(1)	-248(1)	6310(1)	19(1)
C5	3845(1)	-171(1)	6776(1)	23(1)
C6	4362(1)	-318(1)	7244(1)	27(1)
C7	5258(1)	-523(1)	7254(1)	29(1)
C8	5637(1)	-572(1)	6778(1)	28(1)
C9	5148(1)	-434(1)	6301(1)	23(1)
C10	2884(1)	82(1)	6777(1)	32(1)
C11	5812(1)	-670(2)	7764(1)	42(1)
C12	5586(1)	-469(1)	5796(1)	34(1)
C13	2521(1)	1150(1)	4793(1)	19(1)
C14	1989(1)	818(1)	4364(1)	26(1)
C15	1644(1)	1682(1)	4039(1)	30(1)
C16	1844(1)	2772(1)	4150(1)	28(1)
C17	2405(1)	3074(1)	4606(1)	23(1)
C18	3732(1)	3082(1)	6246(1)	22(1)
C19	4111(1)	3110(1)	6796(1)	22(1)
C20	3777(1)	3860(1)	7150(1)	26(1)
C21	4118(1)	3894(1)	7665(1)	30(1)
C22	4796(1)	3182(1)	7839(1)	31(1)
C23	5136(1)	2437(1)	7490(1)	31(1)
C24	4794(1)	2399(1)	6970(1)	25(1)
O2	4197(1)	6357(2)	4869(1)	26(1)

C25	4055(2)	6850(2)	4365(1)	32(1)
C26	3208(2)	6424(2)	4111(1)	32(1)
O3	2503(1)	6831(2)	4386(1)	27(1)
C27	1690(2)	6440(2)	4146(1)	38(1)
C28	970(2)	6809(3)	4462(1)	45(1)
O4	1016(1)	6203(2)	4940(1)	44(1)
C29	337(2)	6508(3)	5259(2)	62(1)
C30	515(2)	5959(3)	5783(2)	61(1)
O5	1298(2)	6428(2)	6024(1)	46(1)
C31	1475(2)	6055(3)	6545(1)	51(1)
C32	2263(3)	6652(3)	6783(1)	50(1)
O6	3003(2)	6296(3)	6525(1)	37(1)
C33	3808(3)	6735(3)	6760(1)	44(1)
C34	4542(2)	6266(3)	6481(1)	38(1)
O7	4470(2)	6652(3)	5952(1)	31(1)
C35	5121(1)	6169(2)	5653(1)	36(1)
C36	5033(2)	6642(2)	5115(1)	35(1)
O2'	3890(6)	6468(8)	4714(4)	37(2)
C25'	3572(10)	6859(10)	4220(4)	39(2)
C26'	2683(11)	6410(10)	4083(4)	49(3)
O3'	2101(7)	6814(7)	4438(3)	39(2)
C27'	1254(9)	6385(12)	4317(5)	48(3)
C28'	674(8)	6753(11)	4725(6)	59(4)
O4'	921(5)	6200(8)	5201(4)	41(2)
C29'	356(7)	6450(14)	5592(6)	56(3)
C30'	717(7)	5970(11)	6100(6)	52(3)

O5'	1504(6)	6518(8)	6255(4)	35(2)
C31'	1847(9)	6180(12)	6756(5)	41(3)
C32'	2718(9)	6747(11)	6883(5)	43(3)
O6'	3307(6)	6385(15)	6527(5)	30(2)
C33'	4186(9)	6662(11)	6653(5)	34(3)
C34'	4743(8)	6197(12)	6266(5)	37(3)
O7'	4514(7)	6676(12)	5771(4)	27(2)
C35'	5062(7)	6366(10)	5377(6)	35(2)
C36'	4739(7)	6870(11)	4876(5)	46(3)
C43	-34(13)	802(18)	6305(7)	39(2)
D43	-487	260	6308	47
C44	479(7)	847(10)	5894(4)	42(2)
D44	387	334	5611	50
C45	1131(7)	1639(11)	5890(4)	51(3)
D45	1470	1680	5596	61
C46	1311(7)	2382(10)	6304(5)	49(2)
D46	1779	2903	6302	58
C47	783(10)	2333(12)	6718(4)	41(2)
D47	881	2837	7004	49
C48	106(15)	1545(19)	6719(7)	39(2)
D48	-258	1521	7003	47
C43'	-107(9)	892(12)	6385(5)	37(1)
D43'	-588	464	6488	45
C44'	235(5)	668(7)	5912(3)	40(1)
D44'	-3	82	5693	48
C45'	931(5)	1309(8)	5757(4)	53(2)

D45'	1176	1154	5435	63
C46'	1265(4)	2173(7)	6075(5)	59(2)
D46'	1719	2638	5965	71
C47'	928(6)	2349(8)	6554(4)	54(2)
D47'	1179	2913	6781	64
C48'	240(10)	1727(13)	6708(5)	42(2)
D48'	6	1871	7035	50
C37	7443(1)	1836(2)	7282(1)	53(1)
D37	7128	2418	7098	63
C38	7578(1)	1876(2)	7818(1)	42(1)
D38	7355	2488	8004	51
C39	8034(1)	1040(2)	8086(1)	41(1)
D39	8113	1065	8457	49
C40	8374(1)	170(2)	7821(1)	48(1)
D40	8705	-394	8008	57
C41	8241(1)	110(2)	7286(1)	54(1)
D41	8471	-502	7103	64
C42	7767(1)	945(2)	7011(1)	57(1)
D42	7667	904	6640	69

5.3 SC-XRD Data for $[K(18\text{-crown}\text{-}6)][(^h\text{IMesPyO})\text{Ni}(1\text{k})]$ (5b)

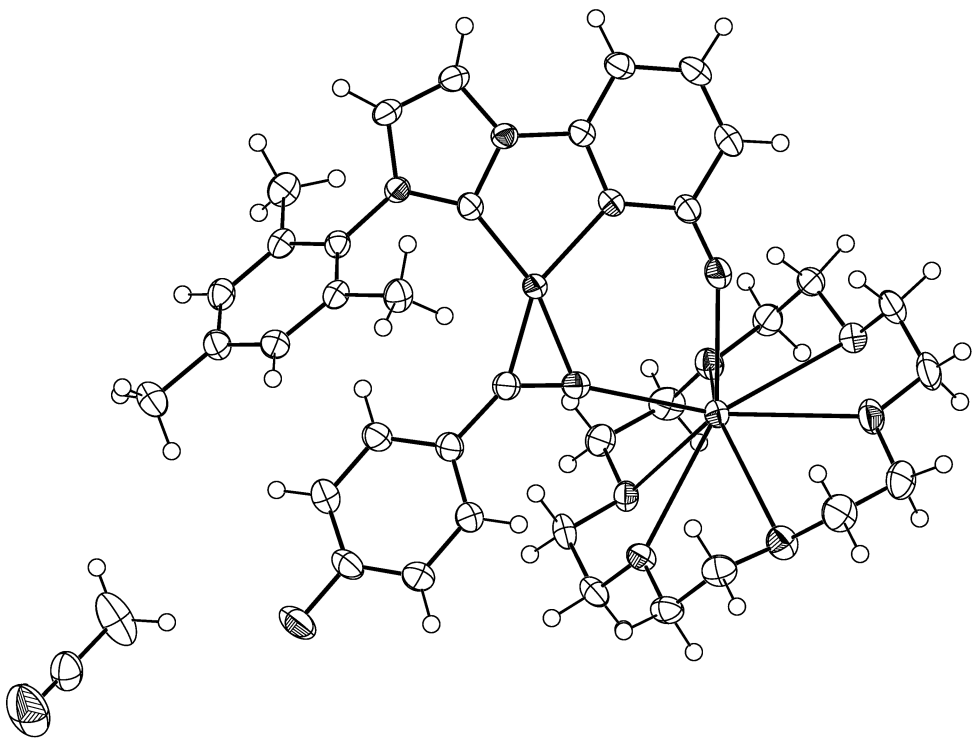


Figure S93. Solid-state structure of **5b**· CD_3CN determined by SC-XRD. Anisotropic displacement ellipsoids drawn at the 50 % probability level. Figure generated with OLEX2.²⁵

Atomic coordinates ($\times 10^4$) and equivalent isotropic displacement parameters ($\text{\AA}^2 \times 10^3$) are listed below for **5b**· CD_3CN . U_{eq} is defined as one third of the trace of the orthogonalized U_{ij} tensor.

Atom	x	y	z	U_{eq}
Ni1	5633(1)	3899(1)	7355(1)	22(1)
K1	6364(1)	3908(1)	3973(1)	24(1)
F1	-346(1)	3008(1)	5337(1)	48(1)
O1	7859(1)	4076(1)	5862(1)	35(1)
O2	6014(1)	4826(1)	3627(1)	28(1)
O3	8336(1)	4533(1)	3233(1)	32(1)
O4	8477(1)	3622(1)	3050(1)	35(1)

O5	6410(1)	3093(1)	2536(1)	33(1)
O6	4243(1)	3404(1)	3060(1)	27(1)
O7	3943(1)	4307(1)	2965(1)	26(1)
N1	5005(1)	3977(1)	9811(1)	22(1)
N2	6722(1)	4205(1)	9467(1)	23(1)
N3	7300(1)	4157(1)	7669(1)	23(1)
N4	5171(1)	3698(1)	5798(1)	33(1)
C1	5661(1)	4019(1)	8924(2)	23(1)
C2	5632(2)	4134(1)	10855(1)	26(1)
C3	6708(2)	4277(1)	10646(2)	27(1)
C4	3796(2)	3809(1)	9684(1)	23(1)
C5	3603(2)	3362(1)	9501(1)	25(1)
C6	2424(2)	3210(1)	9437(2)	28(1)
C7	1461(2)	3485(1)	9546(2)	30(1)
C8	1696(2)	3926(1)	9716(2)	29(1)
C9	2861(2)	4097(1)	9786(1)	25(1)
C10	4627(2)	3058(1)	9368(2)	31(1)
C11	192(2)	3312(1)	9470(2)	41(1)
C12	3075(2)	4577(1)	9970(2)	33(1)
C13	7612(1)	4303(1)	8768(1)	22(1)
C14	8647(2)	4528(1)	9191(2)	28(1)
C15	9423(2)	4620(1)	8386(2)	30(1)
C16	9164(2)	4473(1)	7267(2)	30(1)
C17	8091(2)	4226(1)	6880(2)	25(1)
C18	4361(2)	3650(1)	6404(2)	26(1)
C19	3124(2)	3472(1)	6170(2)	27(1)

C20	2868(2)	3124(1)	5392(2)	33(1)
C21	1702(2)	2965(1)	5113(2)	37(1)
C22	804(2)	3160(1)	5614(2)	34(1)
C23	1011(2)	3501(1)	6386(2)	33(1)
C24	2194(2)	3652(1)	6674(2)	30(1)
C25	6981(2)	5107(1)	3465(2)	33(1)
C26	8145(2)	4892(1)	3961(2)	33(1)
C27	9396(2)	4293(1)	3678(2)	37(1)
C28	9451(2)	3901(1)	2914(2)	38(1)
C29	8445(2)	3245(1)	2330(2)	44(1)
C30	7608(2)	2922(1)	2735(2)	42(1)
C31	5580(2)	2812(1)	2974(2)	33(1)
C32	4331(2)	2983(1)	2591(2)	31(1)
C33	3095(2)	3595(1)	2680(2)	29(1)
C34	3037(2)	4025(1)	3281(2)	30(1)
C35	3896(2)	4725(1)	3485(2)	33(1)
C36	4874(2)	5004(1)	3147(2)	35(1)
N5	5867(2)	2447(1)	6885(3)	83(1)
C37	6553(2)	2711(1)	6839(2)	42(1)
C38	7455(2)	3042(1)	6805(3)	62(1)
D38A	7116	3279	6292	93
D38B	8152	2916	6509	93
D38C	7712	3155	7592	93

5.4 SC-XRD Data for $[K(18\text{-crown}\text{-}6)][(^h\text{IMesPyO})\text{Ni}(\text{CyCN})]$ (5c)

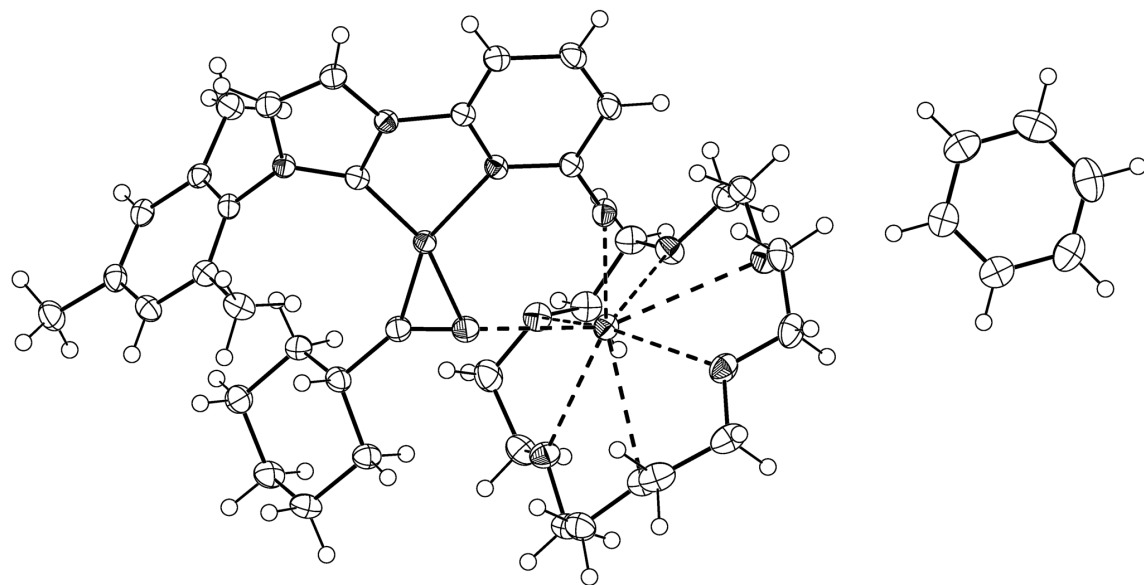


Figure S94. Solid-state structure of **5c**• C_6D_6 determined by SC-XRD. Anisotropic displacement ellipsoids drawn at the 50 % probability level. Figure generated with OLEX2.²⁵

Atomic coordinates ($\times 10^4$) and equivalent isotropic displacement parameters ($\text{\AA}^2 \times 10^3$) are listed below for **5c**• $2\text{C}_6\text{D}_6$. U_{eq} is defined as one third of the trace of the orthogonalized U_{ij} tensor.

Atom	x	y	z	U_{eq}
Ni1	3469(1)	5248(1)	3191(1)	19(1)
K1	5044(1)	7518(1)	4180(1)	22(1)
O1	5656(1)	5812(1)	3581(1)	24(1)
O2	4071(1)	6792(1)	5063(1)	27(1)
O3	5912(1)	6526(1)	5200(1)	26(1)
O4	7145(1)	7335(1)	4583(1)	27(1)
O5	6362(1)	8949(1)	3754(1)	29(1)
O6	4856(1)	10211(1)	3937(1)	26(1)
O7	3676(1)	9091(1)	4542(1)	27(1)

N1	2246(1)	3298(1)	2614(1)	19(1)
N2	3665(1)	3223(1)	2597(1)	19(1)
N3	4676(1)	4528(1)	3071(1)	19(1)
N4	3498(1)	6804(1)	3543(1)	29(1)
C1	3026(1)	3893(1)	2804(1)	19(1)
C2	2401(1)	2294(2)	2304(1)	24(1)
C3	3294(1)	2248(2)	2291(1)	24(1)
C4	1379(1)	3573(1)	2756(1)	19(1)
C5	867(1)	4525(2)	2504(1)	22(1)
C6	5(1)	4708(2)	2629(1)	23(1)
C7	-339(1)	3969(2)	2992(1)	23(1)
C8	212(1)	3064(2)	3253(1)	22(1)
C9	1076(1)	2851(1)	3141(1)	20(1)
C10	1217(1)	5314(2)	2099(1)	28(1)
C11	-1288(1)	4154(2)	3103(1)	30(1)
C12	1679(1)	1896(2)	3436(1)	26(1)
C13	4583(1)	3553(1)	2743(1)	19(1)
C14	5265(1)	2912(2)	2566(1)	22(1)
C15	6144(1)	3299(2)	2765(1)	25(1)
C16	6281(1)	4252(2)	3113(1)	24(1)
C17	5536(1)	4911(1)	3272(1)	20(1)
C18	2728(1)	6415(2)	3406(1)	23(1)
C19	1782(1)	6836(2)	3440(1)	23(1)
C20	1755(1)	8195(2)	3589(1)	24(1)
C21	800(1)	8595(2)	3644(1)	28(1)
C22	410(1)	7810(2)	4045(1)	28(1)

C23	411(1)	6469(2)	3883(1)	28(1)
C24	1360(1)	6033(2)	3828(1)	25(1)
C25	4586(1)	6839(2)	5577(1)	28(1)
C26	5408(1)	6065(2)	5584(1)	27(1)
C27	6798(1)	6033(2)	5266(1)	27(1)
C28	7136(1)	6091(2)	4746(1)	28(1)
C29	7457(1)	7456(2)	4088(1)	29(1)
C30	7302(1)	8745(2)	3897(1)	32(1)
C31	6162(1)	10120(2)	3525(1)	31(1)
C32	5164(1)	10306(2)	3440(1)	33(1)
C33	3932(1)	10538(2)	3901(1)	34(1)
C34	3652(1)	10362(2)	4430(1)	32(1)
C35	3317(1)	8793(2)	5004(1)	31(1)
C36	3238(1)	7421(2)	5027(1)	32(1)
C37	9299(1)	7694(2)	5266(1)	32(1)
D37	8673	7632	5134	38
C38	9831(1)	6658(2)	5315(1)	37(1)
D38	9572	5883	5215	44
C39	10742(2)	6748(2)	5509(1)	43(1)
D39	11111	6037	5541	52
C40	11114(1)	7885(2)	5659(1)	43(1)
D40	11737	7951	5797	51
C41	10579(1)	8914(2)	5608(1)	37(1)
D41	10833	9690	5710	45
C42	9676(1)	8820(2)	5409(1)	32(1)
D42	9310	9534	5370	39

5.5 SC-XRD Data for [^bIMesPyO]Ni(CyHCN(Bpin)₂) (6)

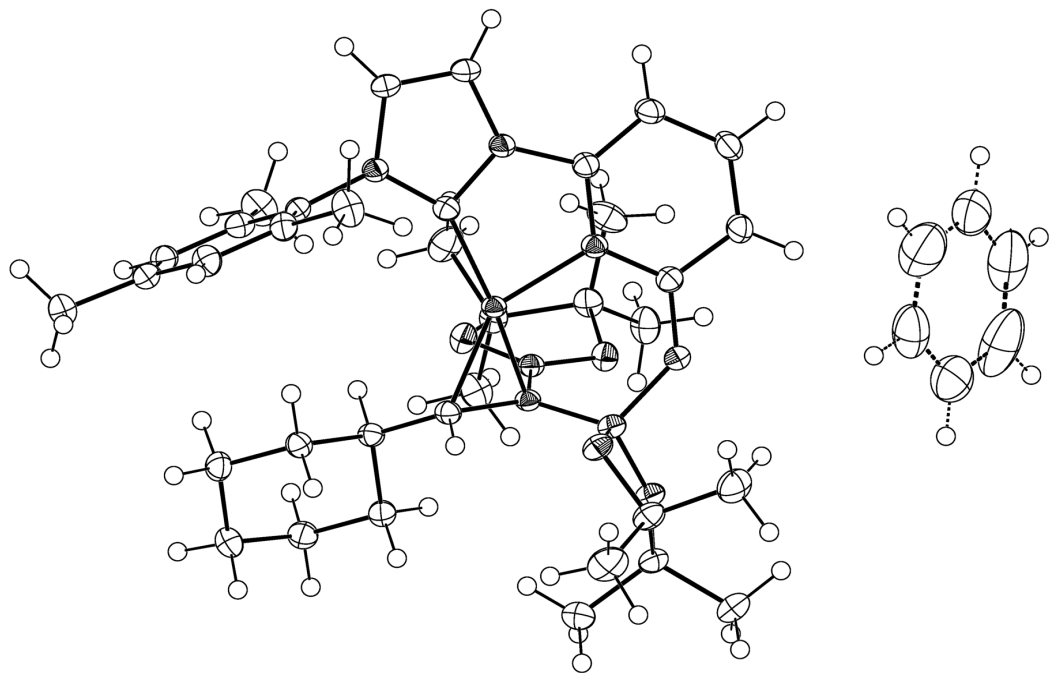


Figure S95. Solid-state structure of **6·½ C₆D₆** determined by SC-XRD. Anisotropic displacement ellipsoids drawn at the 50 % probability level. Figure generated with OLEX2.²⁵

Atomic coordinates ($\times 10^4$) and equivalent isotropic displacement parameters ($\text{\AA}^2 \times 10^3$) are listed below for **6·½ C₆D₆**. U_{eq} is defined as one third of the trace of the orthogonalized U_{ij} tensor.

Atom	x	y	z	U _{eq}
Ni1	7822(1)	6012(1)	6473(1)	16(1)
O1	6867(1)	5016(1)	6900(1)	19(1)
O2	6758(1)	5009(1)	5744(1)	20(1)
O3	6936(1)	3773(1)	6333(1)	20(1)
O4	8733(1)	4752(1)	7225(1)	21(1)
O5	7934(1)	4286(1)	7538(1)	20(1)
N1	8430(1)	7736(1)	6480(1)	18(1)
N2	7922(1)	7459(1)	7136(1)	18(1)

N3	7389(1)	6258(1)	7075(1)	18(1)
N4	7752(1)	4822(1)	6444(1)	16(1)
C1	8077(1)	7134(1)	6613(1)	17(1)
C2	8495(1)	8415(1)	6902(1)	22(1)
C3	8177(1)	8239(1)	7316(1)	22(1)
C4	8694(1)	7718(1)	5953(1)	18(1)
C5	8391(1)	8083(1)	5387(1)	21(1)
C6	8663(1)	8098(1)	4890(1)	24(1)
C7	9220(1)	7771(1)	4957(1)	22(1)
C8	9502(1)	7401(1)	5531(1)	22(1)
C9	9247(1)	7365(1)	6037(1)	21(1)
C10	7795(1)	8463(1)	5314(1)	29(1)
C11	9516(1)	7827(1)	4423(1)	29(1)
C12	9550(1)	6948(1)	6651(1)	31(1)
C13	7526(1)	6990(1)	7392(1)	19(1)
C14	7305(1)	7230(1)	7888(1)	23(1)
C15	6894(1)	6674(1)	8034(1)	26(1)
C16	6730(1)	5938(1)	7701(1)	24(1)
C17	6995(1)	5726(1)	7212(1)	19(1)
C18	7990(1)	5137(1)	5939(1)	17(1)
C19	8575(1)	4855(1)	5863(1)	18(1)
C20	8686(1)	5294(1)	5279(1)	20(1)
C21	9279(1)	5042(1)	5182(1)	23(1)
C22	9336(1)	4084(1)	5137(1)	26(1)
C23	9204(1)	3631(1)	5703(1)	24(1)
C24	8610(1)	3892(1)	5789(1)	21(1)

C25	6299(1)	4424(1)	5469(1)	24(1)
C26	6572(1)	3556(1)	5724(1)	22(1)
C27	5762(1)	4644(1)	5708(1)	32(1)
C28	6154(1)	4521(1)	4755(1)	36(1)
C29	6138(1)	2892(1)	5819(1)	31(1)
C30	6958(1)	3187(1)	5326(1)	30(1)
C31	8954(1)	4378(1)	7849(1)	22(1)
C32	8400(1)	4372(1)	8114(1)	21(1)
C33	9450(1)	4924(1)	8216(1)	32(1)
C34	9172(1)	3498(1)	7746(1)	29(1)
C35	8299(1)	5209(1)	8414(1)	32(1)
C36	8363(1)	3643(1)	8552(1)	28(1)
B1	7075(1)	4659(1)	6334(1)	18(1)
B2	8139(1)	4623(1)	7059(1)	17(1)
C37	5047(6)	6237(7)	7305(4)	80(4)
D37	5053	6801	7158	96
C38	4994(7)	5578(7)	6890(6)	60(2)
D38	4993	5685	6463	72
C39	4943(4)	4765(6)	7087(7)	62(3)
D39	4886	4310	6794	74
C40	4975(6)	4620(8)	7704(6)	87(6)
D40	4929	4061	7844	104
C41	5073(6)	5263(8)	8123(5)	87(5)
D41	5130	5142	8559	104
C42	5090(4)	6088(6)	7934(5)	92(4)
D42	5131	6539	8228	111

5.6 SC-XRD Data for $[K(18\text{-crown}\text{-}6)][(^h\text{IMesPyO})\text{Ni}(7)]$ (8)

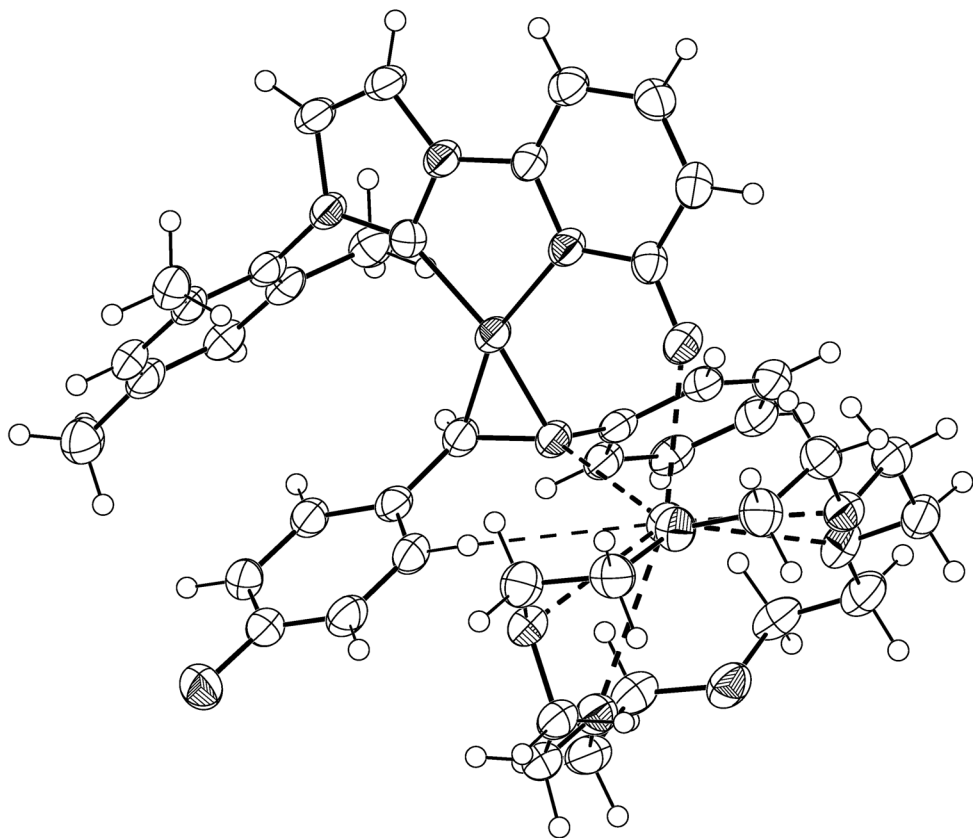


Figure S96. Solid-state structure of **8** determined by SC-XRD. Anisotropic displacement ellipsoids drawn at the 50 % probability level. Figure generated with OLEX2.²⁵

Atomic coordinates ($\times 10^4$) and equivalent isotropic displacement parameters ($\text{\AA}^2 \times 10^3$) are listed below for complex **8**. U_{eq} is defined as one third of the trace of the orthogonalized U_{ij} tensor.

Atom	x	y	z	U_{eq}
Ni1	3148(1)	2982(1)	3985(1)	31(1)
K1	6330(1)	2652(1)	3852(1)	36(1)
F1	4298(2)	4758(1)	562(1)	54(1)
O1	4907(2)	1846(1)	4424(2)	37(1)
O2	7868(2)	3901(1)	4713(2)	45(1)

O3	7613(2)	2681(1)	5431(2)	43(1)
O4	7791(2)	1574(1)	4396(1)	38(1)
O5	6928(2)	1630(1)	2682(1)	38(1)
O6	6526(2)	2799(1)	1890(2)	40(1)
O7	7455(2)	3711(1)	2974(2)	39(1)
N1	735(2)	3212(1)	3588(2)	32(1)
N2	1291(2)	2303(1)	4020(2)	33(1)
N3	3088(2)	2069(1)	4287(2)	32(1)
N4	4409(2)	3446(1)	4332(2)	31(1)
C1	1665(2)	2877(2)	3759(2)	32(1)
C2	-182(2)	2853(2)	3760(2)	36(1)
C3	152(2)	2287(2)	4024(2)	35(1)
C4	688(2)	3855(2)	3317(2)	32(1)
C5	541(2)	3992(2)	2434(2)	34(1)
C6	469(2)	4619(2)	2189(2)	38(1)
C7	536(2)	5108(2)	2781(2)	38(1)
C8	680(2)	4951(2)	3657(2)	36(1)
C9	761(2)	4332(2)	3930(2)	35(1)
C10	484(3)	3472(2)	1782(2)	38(1)
C11	507(3)	5785(2)	2497(3)	47(1)
C12	935(3)	4171(2)	4873(2)	40(1)
C13	2062(2)	1843(2)	4300(2)	32(1)
C14	1769(3)	1255(2)	4558(2)	35(1)
C15	2618(3)	850(2)	4823(2)	38(1)
C16	3672(3)	1048(2)	4789(2)	39(1)
C17	3938(3)	1663(2)	4494(2)	34(1)

C18	3650(2)	3830(2)	3897(2)	33(1)
C19	3845(2)	4061(2)	3012(2)	32(1)
C20	4603(2)	3789(2)	2477(2)	37(1)
C21	4762(2)	4026(2)	1658(2)	40(1)
C22	4157(3)	4536(2)	1379(2)	41(1)
C23	3395(3)	4815(2)	1873(2)	38(1)
C24	3248(2)	4575(2)	2693(2)	35(1)
C25	4602(2)	3575(2)	5215(2)	33(1)
C26	4895(2)	3086(2)	5789(2)	34(1)
C27	5208(3)	3217(2)	6643(2)	39(1)
C28	5214(3)	3829(2)	6950(2)	40(1)
C29	4897(2)	4316(2)	6398(2)	39(1)
C30	4599(2)	4190(2)	5542(2)	35(1)
C31	7503(3)	3787(2)	5557(2)	45(1)
C32	8030(3)	3206(2)	5901(2)	47(1)
C33	8061(3)	2108(2)	5739(2)	43(1)
C34	7500(3)	1576(2)	5278(2)	43(1)
C35	7319(3)	1046(2)	3955(2)	41(1)
C36	7513(3)	1101(2)	3014(2)	44(1)
C37	7019(3)	1683(2)	1775(2)	42(1)
C38	6315(3)	2219(2)	1460(2)	45(1)
C39	7586(2)	3040(2)	1757(2)	40(1)
C40	7631(3)	3702(2)	2075(2)	39(1)
C41	7554(3)	4329(2)	3320(2)	43(1)
C42	7187(3)	4325(2)	4231(2)	45(1)

6. Computational Analyses

6.1 Computational Methods

All electronic structure calculations were performed on the Bluehive computing cluster maintained by the University of Rochester Center for Integrated Research Computing. Density functional theory calculations were performed using Gaussian 16 A.03²⁶ with the ωB97XD level of density functional theory,²⁷ and implicit solvent correction (PCM, MeCN).²⁸ The basis set def2-TZVP was employed for all calculations²⁹ along with the LANL2DZ pseudopotential (for potassium) where relevant.³⁰ Unless stated otherwise, default criteria for geometric and SCF convergence were used. For cases in which frequency calculations were not complete, an in-RAM (Random Access Machine) algorithm for Gaussian was implemented using Int=Acc2E=11 keyword. Stationary points were validated by the presence of all positive eigenvalues for local minima and a single negative eigenvalue for transition state. All reported energies are Gibbs free energies. Natural population analysis was implemented as developed by Weinhold.^{31, 32} All molecular structures were rendered in CYLView.³³ In all cases, the following color-coding scheme applies: H = white, C = grey, N = blue, O = red, B = gold, K = purple.

Sample Gaussian Input File for Geometry Optimization and Frequency Analysis

```
%nprocshared=12
%chk=checkpoint.chk
%Mem=50GB
#n      wb97XD/Gen      Opt      Pseudo=Read      Freq=noramam      Pop=none
SCRF=(solvent=acetonitrile, pcm)

Title

0 1
Ni          0.72647       -0.05270       -0.23974
...
C H N Ni O 0
def2TZVP
*****
B -1
def2TZVP
*****
K 1
LANL2DZ
*****
K 1
LANL2DZ
```

6.2 Anionic Model

Due to the lack of conclusive insight from experimental work alone on the role of pyridone in hydride and boryl delivery, density functional theory (DFT, ω B97XD/def2-TZVP) modeling was pursued. To simplify the computational model, $[\text{K}(18\text{-crown-6})]^+$ was omitted and acetonitrile was used as a model substrate.

Reaction Coordinate Analysis

The local-minimum stationary-state structures for hydride and boryl deliveries were evaluated initially with the aim of distinguishing between hydride delivery through the primary sphere (migratory insertion via a Ni–H), secondary sphere (via ligand-to-ligand H transfer), or outer-sphere $[\text{H}_2\text{BPin}]^-$ (Figure S94). We focused on the first hydride transfer (i.e. nitrile to N-borylimine) with the assumption that the second hydride transfer likely followed an analogous mechanism.

Consistent with experimental observations, acetonitrile and imine adducts **A** and **F** were found substantially lower in energy than HBpin adducts **J** (featuring Ni^0 with a B–H agostic interaction) and **I** (featuring a Ni^{II} hydride boryl). Although an energetically reasonable series of intermediates was identified for B–H oxidative addition through κ^1 -N nitrile adducts **B** (which features a B–H agostic interaction) and **C** (or through **J**, **I**, and **C**), $\eta^2(\text{CN})$ -coordinated intermediates **G** and **H** offered a lower energy alternative, compatible with outer-sphere hydride delivery. However, the model incorrectly predicted that boryl adduct **G** would be preferred (relative to **A**) at equilibrium. As such, a more complete model, including the K^+ countercation, was deemed necessary, and transition state analyses were not pursued on the anionic model.

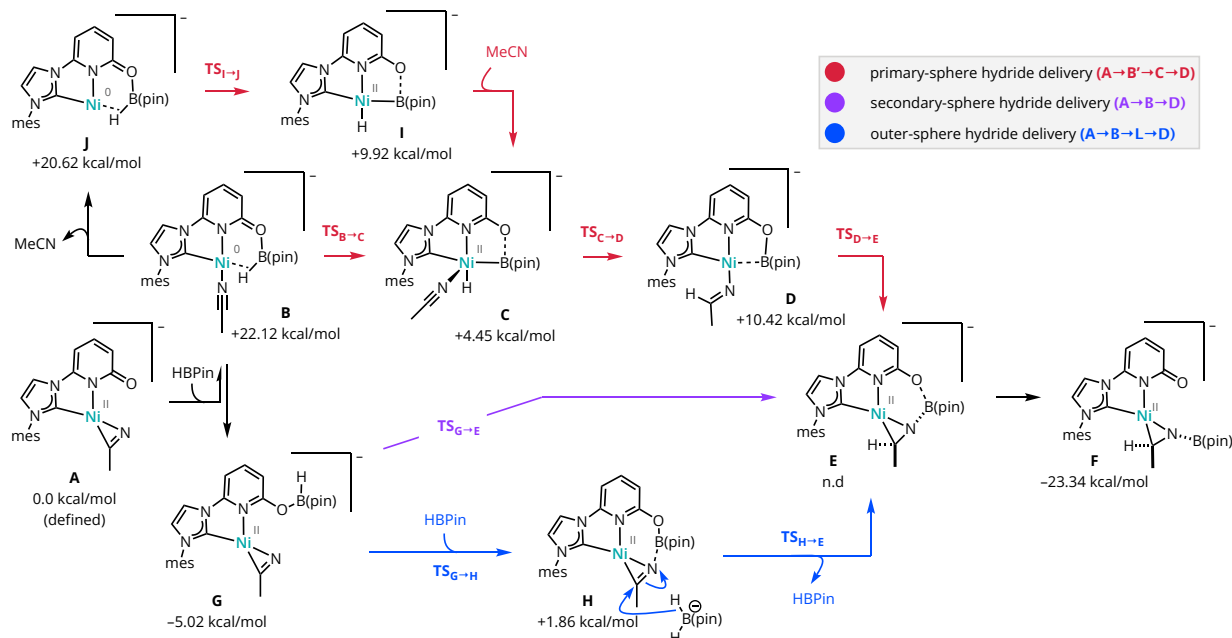


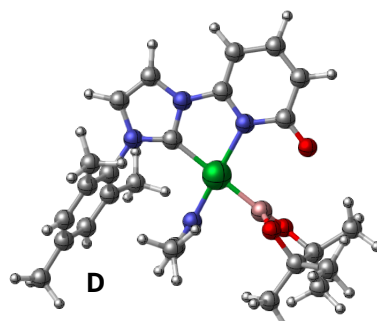
Figure S97. Calculations performed with ω B97XD/def2-TZVP. Gibbs free energies reported in kcal/mol. Mes = 2,4,6-trimethylphenyl.

Natural Bonding Orbital Analysis

Natural Bonding Orbital (NBO) analysis of intermediate **D** revealed an electronic structure intermediate between Ni(0) and Ni(II). The net electron occupancy of Ni-centered d-type natural atomic orbitals (NAOs) was 9.02. Additionally, an NBOs with Ni–B bonding character were located with electron occupancy of 1.80, consistent with the Bpin unit acting as a weak ligand while also involved in secondary-sphere Lewis acid-base interactions with the pyridone oxygen.

Natural atomic orbital occupancies for Ni-centered d orbitals

NAO	Atom	No	lanc	Type(AO)	Occupancy	Energy
216	Ni	13	dxy	Val(3d)	1.47585	-0.09213
217	Ni	13	dxy	Ryd(4d)	0.00237	2.90860
218	Ni	13	dxy	Ryd(5d)	0.00047	2.92430
219	Ni	13	dxy	Ryd(6d)	0.00016	3.74905
220	Ni	13	dxz	Val(3d)	1.95004	-0.14776



221	Ni	13	dxz	Ryd(4d)	0.00273	1.06312
222	Ni	13	dxz	Ryd(5d)	0.00024	1.88785
223	Ni	13	dxz	Ryd(6d)	0.00003	4.55600
224	Ni	13	dyz	Val(3d)	1.92569	-0.14875
225	Ni	13	dyz	Ryd(4d)	0.00342	1.09097
226	Ni	13	dyz	Ryd(5d)	0.00032	1.93734
227	Ni	13	dyz	Ryd(6d)	0.00003	4.53609
228	Ni	13	dx2y2	Val(3d)	1.70367	-0.13252
229	Ni	13	dx2y2	Ryd(4d)	0.00169	2.16586
230	Ni	13	dx2y2	Ryd(5d)	0.00033	2.57277
231	Ni	13	dx2y2	Ryd(6d)	0.00017	4.05919
232	Ni	13	dz2	Val(3d)	1.95239	-0.14305
233	Ni	13	dz2	Ryd(4d)	0.00209	1.50192
234	Ni	13	dz2	Ryd(5d)	0.00018	2.62638
235	Ni	13	dz2	Ryd(6d)	0.00005	4.53207

Natural atomic orbital occupancies for Ni-centered d orbitals

(Occupancy) Bond orbital/ Coefficients/ Hybrids

16. (1.79864) BD (1)Ni 13 - B 40

(48.86%) 0.6990*Ni 13 s(36.61%)p 0.64(23.51%)d 1.09(39.88%)

f 0.00(0.00%)

(51.14%) 0.7151* B 40 s(49.07%)p 1.03(50.61%)d 0.01(0.30%)

f 0.00(0.03%)

6.3 Neutral Model

Because the anionic model did not adequately reproduce experimental findings a revised model including the K^+ counterion was included. The 18-crown-6 was omitted for most computations in an attempt to keep the system size computationally tractable. For all potassium-containing intermediates, a pseudo-potential (LANL2DZ) was used on potassium.

The local-minimum stationary-state structures for hydride and boryl deliveries were re-evaluated with the aim of distinguishing between hydride delivery through the primary sphere (migratory insertion via a Ni–H), secondary sphere (via ligand-to-ligand H transfer), or outer-sphere $[H_2BPin]^-$ (Figure S95). Inclusion of the K^+ counterion resulted in substantial geometric changes to the local-minimum structures, supporting its integral role. Notably, local-minimum structures for **B'** and **C'** could not be identified when K^+ was included. However, the low energies predicted for **G'** (-6.52 kcal/mol) and **J'** (-7.21) relative to **A'** were inconsistent with experimental observations.

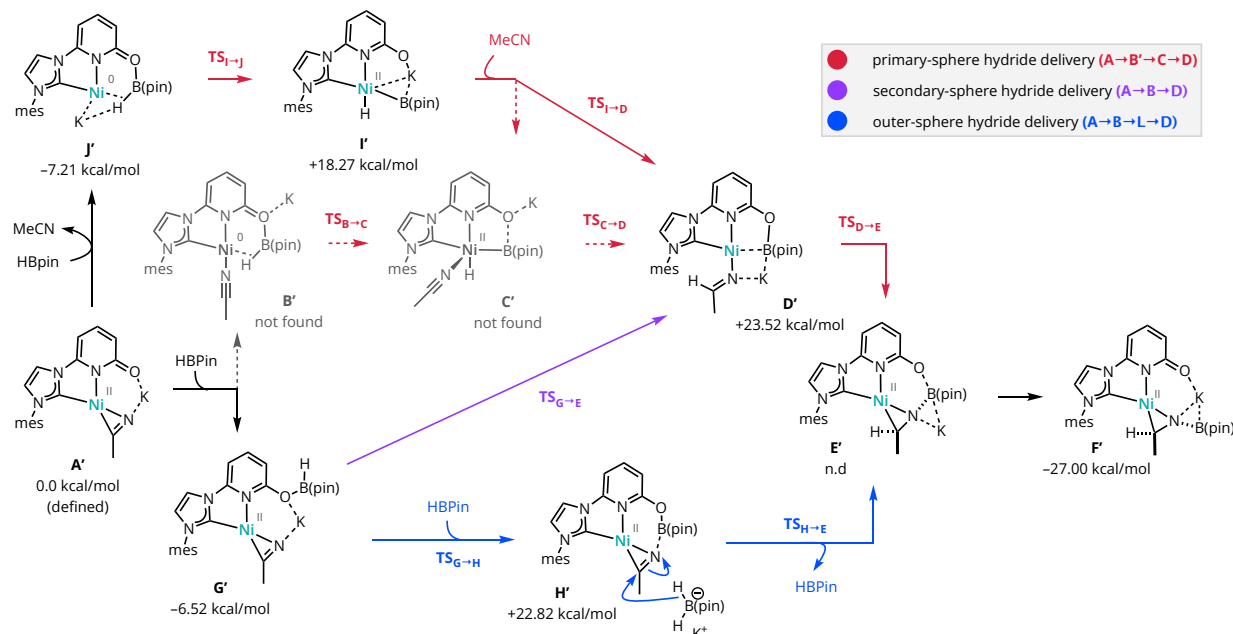


Figure S98. Calculations performed with ω B97XD/def2-TZVP/LANL2DZ(K). Gibbs free energies reported in kcal/mol. Mes = 2,4,6-trimethylphenyl.

In subsequent experiments, inclusion of an implicit solvation model (PCM) in geometry optimizations was found to improve agreement between predicted and observed relative energies of key intermediates, the resulting system was judged too computationally resource intensive to pursue further.

7. References

1. Burger, B. J.; Bercaw, J. E., Vacuum Line Techniques for Handling Air-Sensitive Organometallic Compounds. In *Experimental Organometallic Chemistry*, American Chemical Society: 1987; Vol. 357, pp 79–115.
2. Complete List of Prismacolor Colored Pencils. Jenny's Crayon Collection, <https://www.jennyscrayoncollection.com/2020/04/complete-list-of-prismacolor-premier.html> (accessed 2022-08-20).
3. Krysan, D. J.; Mackenzie, P. B. A new, convenient preparation of bis(1,5-cyclooctadiene)nickel(0). *J. Org. Chem.* **1990**, *55*, 4229–4230. DOI: 10.1021/jo00300a057
4. Huckaba, A. J.; Senes, A.; Aghazada, S.; Babaei, A.; Meskers, S. C. J.; Zimmermann, I.; Schouwink, P.; Gasilova, N.; Janssen, R. A. J.; Bolink, H. J.; Nazeeruddin, M. K. Bis(arylimidazole) Iridium Picolinate Emitters and Preferential Dipole Orientation in Films. *ACS Omega* **2018**, *3*, 2673–2682. DOI: 10.1021/acsomega.8b00137
5. Occipinti, G.; Bjørsvik, H.-R.; Törnroos, K. W.; Fürstner, A.; Jensen, V. R. The First Imidazolium-Substituted Metal Alkylidene. *Organometallics* **2007**, *26*, 4383–4385. DOI: 10.1021/om700590v
6. Afandiyeva, M.; Kadam, A. A.; Wu, X. J.; Brennessel, W. W.; Kennedy, C. R. Synthesis, Structure, and Hydroboration Reactivity of Anionic Nickel(0) Complexes Supported by Bidentate NHC-Pyridone Ligands. *Organometallics* **2022**, *41*, 3014–3023. DOI: 10.1021/acs.organomet.2c00439
7. Pangborn, A. B.; Giardello, M. A.; Grubbs, R. H.; Rosen, R. K.; Timmers, F. J. Safe and Convenient Procedure for Solvent Purification. *Organometallics* **1996**, *15*, 1518–1520. DOI: 10.1021/om9503712
8. Fulmer, G. R.; Miller, A. J. M.; Sherden, N. H.; Gottlieb, H. E.; Nudelman, A.; Stoltz, B. M.; Bercaw, J. E.; Goldberg, K. I. NMR Chemical Shifts of Trace Impurities: Common Laboratory Solvents, Organics, and Gases in Deuterated Solvents Relevant to the Organometallic Chemist. *Organometallics* **2010**, *29*, 2176–2179. DOI: 10.1021/om100106e (doi: 10.1021/om100106e)
9. Craig, S. M.; Malyk, K. R.; Silk, E. S.; Nakamura, D. T.; Brennessel, W. W.; Kennedy, C. R. Synthesis and characterization of Ni(0) complexes supported by an unsymmetric C,N ligand. *J. Coord. Chem.* **2022**, *75*, 1841–1852. DOI: 10.1080/00958972.2022.2117037
10. Saha, S.; Eisen, M. S. Catalytic Recycling of a Th–H Bond via Single or Double Hydroboration of Inactivated Imines or Nitriles. *Acs Catal* **2019**, *9*, 5947–5956. DOI: 10.1021/acscatal.9b01399
11. Geri, J. B.; Szymczak, N. K. A Proton-Switchable Bifunctional Ruthenium Complex That Catalyzes Nitrile Hydroboration. *J. Am. Chem. Soc.* **2015**, *137*, 12808–12814. DOI: 10.1021/jacs.5b08406
12. Kaithal, A.; Chatterjee, B.; Gunanathan, C. Ruthenium-Catalyzed Selective Hydroboration of Nitriles and Imines. *J. Org. Chem.* **2016**, *81*, 11153–11161. DOI: 10.1021/acs.joc.6b02122
13. Dai, H.; Guan, H. Switching the Selectivity of Cobalt-Catalyzed Hydrogenation of Nitriles. *Acs Catal* **2018**, *8*, 9125–9130. DOI: 10.1021/acscatal.8b02645
14. Weetman, C.; Anker, M. D.; Arrowsmith, M.; Hill, M. S.; Kociok-Köhne, G.; Liptrot, D. J.; Mahon, M. F. Magnesium-catalysed nitrile hydroboration. *Chem. Sci.* **2016**, *7*, 628–641. DOI: 10.1039/C5SC03114A
15. Sanagawa, A.; Nagashima, H. Hydrosilane Reduction of Nitriles to Primary Amines by Cobalt–Isocyanide Catalysts. *Org. Lett.* **2019**, *21*, 287–291. DOI: 10.1021/acs.orglett.8b03736
16. Bismuto, A.; Cowley, M. J.; Thomas, S. P. Aluminum-Catalyzed Hydroboration of Alkenes. *Acs Catal* **2018**, *8*, 2001–2005. DOI: 10.1021/acscatal.7b04279

17. Elangovan, S.; Topf, C.; Fischer, S.; Jiao, H.; Spannenberg, A.; Baumann, W.; Ludwig, R.; Junge, K.; Beller, M. Selective Catalytic Hydrogenations of Nitriles, Ketones, and Aldehydes by Well-Defined Manganese Pincer Complexes. *J. Am. Chem. Soc.* **2016**, *138*, 8809–8814. DOI: 10.1021/jacs.6b03709
18. Chen, F.; Topf, C.; Radnik, J.; Kreyenschulte, C.; Lund, H.; Schneider, M.; Surkus, A.-E.; He, L.; Junge, K.; Beller, M. Stable and Inert Cobalt Catalysts for Highly Selective and Practical Hydrogenation of C≡N and C=O Bonds. *J. Am. Chem. Soc.* **2016**, *138*, 8781–8788. DOI: 10.1021/jacs.6b03439
19. Harinath, A.; Bhattacharjee, J.; Panda, T. K. Catalytic Hydroboration of Organic Nitriles Promoted by Aluminum Complex. *Adv. Syn. Catal.* **2019**, *361*, 850-857. DOI: 10.1002/adsc.201801252
20. Schneekönig, J.; Tannert, B.; Hornke, H.; Beller, M.; Junge, K. Cobalt pincer complexes for catalytic reduction of nitriles to primary amines. *Catal Sci Technol* **2019**, *9*, 1779–1783. DOI: 10.1039/C9CY00225A
21. Widegren, J. A.; Finke, R. G. A review of the problem of distinguishing true homogeneous catalysis from soluble or other metal-particle heterogeneous catalysis under reducing conditions. *J. Mol. Catal. A Chem.* **2003**, *198*, 317–341. DOI: 10.1016/S1381-1169(02)00728-8
22. Bage, A. D.; Hunt, T. A.; Thomas, S. P. Hidden Boron Catalysis: Nucleophile-Promoted Decomposition of HBpin. *Org. Lett.* **2020**, *22*, 4107-4112. DOI: 10.1021/acs.orglett.0c01168
23. Sheldrick, G. SHELXT - Integrated space-group and crystal-structure determination. *Acta Crystallogr. A* **2015**, *71*, 3-8. DOI: doi:10.1107/S2053273314026370
24. Sheldrick, G. Crystal structure refinement with SHELXL. *Acta Crystallogr. C* **2015**, *71*, 3-8. DOI: 10.1107/S2053229614024218
25. Dolomanov, O. V.; Bourhis, L. J.; Gildea, R. J.; Howard, J. A. K.; Puschmann, H. OLEX2: a complete structure solution, refinement and analysis program. *J. Appl. Crystallogr.* **2009**, *42*, 339–341. DOI: 10.1107/S0021889808042726
26. Frisch, M. J.; Trucks, G. W.; Schlegel, H. B.; Scuseria, G. E.; Robb, M. A.; Cheeseman, J. R.; Scalmani, G.; Barone, V.; Petersson, G. A.; Nakatsuji, H.; Li, X.; Caricato, M.; Marenich, A. V.; Bloino, J.; Janesko, B. G.; Gomperts, R.; Mennucci, B.; Hratchian, H. P.; Ortiz, J. V.; Izmaylov, A. F.; Sonnenberg, J. L.; Williams-Young, D.; Ding, F.; Lipparini, F.; Egidi, F.; Goings, J.; Peng, B.; Petrone, A.; Henderson, T.; Ranasinghe, D.; Zakrzewski, V. G.; Gao, J.; Rega, N.; Zheng, G.; Liang, W.; Hada, M.; Ehara, M.; Toyota, K.; Fukuda, R.; Hasegawa, J.; Ishida, M.; Nakajima, T.; Honda, Y.; Kitao, O.; Nakai, H.; Vreven, T.; Throssell, K.; Montgomery, J., J. A. ; Peralta, J. E.; Ogliaro, F.; Bearpark, M. J.; Heyd, J. J.; Brothers, E. N.; Kudin, K. N.; Staroverov, V. N.; Keith, T. A.; Kobayashi, R.; Normand, J.; Raghavachari, K.; Rendell, A. P.; Burant, J. C.; Iyengar, S. S.; Tomasi, J.; Cossi, M.; Millam, J. M.; Klene, M.; Adamo, C.; Cammi, R.; Ochterski, J. W.; Martin, R. L.; Morokuma, K.; Farkas, O.; Foresman, J. B.; Fox, D. J. *Gaussian 16, Revision A.03*, Gaussian, Inc.: Wallingford, CT, 2016.
27. Chai, J.-D.; Head-Gordon, M. Long-range corrected hybrid density functionals with damped atom–atom dispersion corrections. *Phys. Chem. Chem. Phys.* **2008**, *10*, 6615–6620. DOI: 10.1039/B810189B
28. Tomasi, J.; Mennucci, B.; Cammi, R. Quantum Mechanical Continuum Solvation Models. *Chem. Rev.* **2005**, *105*, 2999–3094. DOI: 10.1021/cr9904009
29. Weigend, F. Accurate Coulomb-fitting basis sets for H to Rn. *Phys. Chem. Chem. Phys.* **2006**, *8*, 1057-1065. DOI: 10.1039/b515623h
30. Hay, P. J.; Wadt, W. R. Ab initio effective core potentials for molecular calculations. Potentials for K to Au including the outermost core orbitals. *J. Chem. Phys.* **1985**, *82*, 299–310. DOI: 10.1063/1.448975

31. E. D. Glendening; A. E. Reed; J. E. Carpenter; Weinhold, F. *NBO Version 3.1*.
32. Reed, A. E.; Weinstock, R. B.; Weinhold, F. Natural population analysis. *J. Chem. Phys.* **1985**, *83*, 735–746. DOI: 10.1063/1.449486
33. Legault, C. Y. *CYLview, Version 1.0b*, Université de Sherbrooke: Sherbrooke QC, 2009.